The Institute of Paper Chemistry

Appleton, Wisconsin

Doctor's Dissertation

The Rheology of Synthetic Fiber Suspensions

William Thomas Myers, Jr.

June, 1962

Errata sheet for Doctoral Dissertation by W. T. Myers, Jr.

The errors and the corrected forms are as follows:

Equation (2), p. 10, change $V \cdot (\rho\vec{V})$ to $\nabla \cdot (\rho\vec{V})$

Page 10, paragraph 2, line 4, change $\rho(\vec{\underline{V}} \cdot V)\vec{\underline{V}}$ to $\rho(\vec{V} \cdot \nabla)\vec{\underline{V}}$

Page 10, paragraph 2, line 5, change $\mu_o V^2\vec{\underline{V}}$ to $\mu_o \nabla^2\vec{\underline{V}}$

Equation (3), p. 11, change $\gamma V^2\vec{V} = Vp/\rho$ to $\gamma\nabla^2\vec{V} = \nabla p/\rho$

Equation (4), p. 11, change $V \cdot \vec{V} = 0$ to $\nabla \cdot \vec{V} = 0$

Equation (5), p. 11, change $\rho[(\vec{u} \cdot V)\vec{V}] = -Vp/\rho + \gamma V^2\vec{V}$

to $\rho[(\vec{u} \cdot \nabla)\vec{V}] = -\nabla p/\rho + \gamma\nabla^2\vec{V}$

Figure 1, p. 13, change u to H

Page 23, line 14, change 2 rh to $2\pi rh$

Figure 9, p. 43, add +0 to $.3937''$ $-.0005$

Page 99, 8th line from bottom, change fluid to fluids

THE RHEOLOGY OF SYNTHETIC FIBER SUSPENSIONS

A thesis submitted by

William Thomas Myers, Jr.,
B.E. 1957, Yale University
M.S. 1959, Lawrence College

in partial fulfillment of the requirements
of The Institute of Paper Chemistry
for the degree of Doctor of Philosophy
from Lawrence College,
Appleton, Wisconsin

June, 1962

TABLE OF CONTENTS

INTRODUCTION

Rheology (1) is defined as the science of the deformation and flow of matter. A knowledge of the rheological behavior of particles suspended in a viscous medium is essential in the understanding of many commercial operations. In the formation of synthetic latices by emulsion polymerization, the suspension must be continuously sheared under controlled conditions to obtain an acceptable product. The grinding occurring in the initial preparation of pigment dispersions such as clay coatings for paper is accomplished by shear transmission through a viscous vehicle. The ultimate performances of paints and pastes depend on their flow properties after application to a surface. The shear behavior of an ink can limit its use to a specific printing process.

In the paper industry there are numerous operations where the rheological behavior of suspensions plays an important, yet not always clearly understood, part. In the conversion of cooked wood to pulp fiber suspensions, bundles of fibers are subjected to high shearing stresses. The refining process causes fiber suspensions to again undergo shearing stresses to change such properties as fiber surface area and flexibility. The power required to transfer a slurry through a pipe depends on its flow behavior, while the final formation of a fibrous sheet may be changed appreciably by varying the conditions of shear under which the fibers are deposited on the wire of a machine.

Though most of the experimental work in a given industry has been restricted to the study of a particular suspension or related suspensions, there is a remarkable degree of similarity in the rheological behavior of all such suspensions. At concentrations of suspended particles where the flow is Newtonian (defined in this study as the flow region where the shear stress is directly proportional to the shear rate), the viscosity may be used as a parameter in comparing the behavior of suspensions. The viscosity is proportional to the energy dissipated within the flowing fluid or suspension. At very low particle concentrations in a viscous fluid, the flow of the solvent or suspending solution is disturbed by the presence of particles, resulting in an increase in the rate of energy dissipation over that for the fluid under the same flow conditions. Because the particles are sufficiently far apart, the disturbances do not overlap and the total viscosity effect is a summation of all the individual effects of the particles and the effect due to the fluid. In this range the increase in the energy dissipation or the relative viscosity between the suspension and the suspending fluid is proportional to the volume fraction of the particles.

As the concentration of the particles is increased, the hydrodynamic perturbations due to the particles begin to overlap and the viscosity effect is no longer a simple addition of the individual particle effects, but has been shown to depend on higher powers of the volume fraction. At the same time, two and three particle interactions will begin to occur which contribute to the viscosity in a manner similar to the overlapping of the disturbed flow around particles, i.e., proportional to higher powers of the volume fraction. Of course, these interactions would be expected to occur to some extent even at the lowest concentrations, but the contribution to the total viscosity would be insignificant compared to that of the individual particles. Finally, some concentration is reached where the particles become so limited in their motion that structural effects become predominant over the hydrodynamic effects in controlling the rheological behavior of the suspension.

Experimentally, it has been found that the rheological behavior of suspensions is affected by the following factors:

1. The shape, size, and mass of the particles;
2. the flexibility and deformability of the particles;

3. the thermodynamic conditions in the system;
4. the surface forces on the particles;
5. the concentration; and
6. the rate of shear.

Solutions of polymeric electrolytes (2) such as deoxyribonucleic acid are found to exhibit Newtonian behavior only at concentrations less than 0.01% by weight or at shear rates approaching zero. This result is attributed to the presence of surface charges on the particles combined with Brownian motion effects. Colloidal latices (3) may show Newtonian flow up to concentrations of 25% by weight. At higher concentrations, structural properties occur in the suspensions resulting in anomalous flow. Suspensions of printing inks (4) follow non-Newtonian flow behavior as a result of the disturbances of rotating particle clusters and the immobilization of the vehicle in the interstices of such clusters.

During the papermaking process, most operations are performed with suspensions where the shear rates would not be directly proportional to the applied stresses. It is possible that at certain consistencies (less than 0.1%) existing in the headboxes of paper machines Newtonian flow would occur if the fluid flow itself were laminar. The rheological characteristics of these suspensions are attributable to the disturbances of the fluid motion caused by fiber-fluid interaction and fiber-fiber interaction. The properties of the fibers (axis ratios, flexibilities, surface forces, and shapes) enable extremely stable clusters of flocs of fibers to be formed at consistencies of less than 0.1%. As the concentration of a suspension is increased, the flocs become larger, more dense, and are interconnected by thinly dispersed fibers so that the suspension resembles a nonhomogeneous network.

Experimentally, it has been demonstrated that such fiber networks have measurable strength properties. Mason and co-workers (5) showed that a Douglas-fir sulfite pulp slurry of 0.8% consistency had a tensile strength of about 10 dynes per sq. cm. The tensile strength was determined by allowing a suspension of fibers to run slowly through a vertical tube into a reservoir of water moving at the same vectorial velocity. When the weight of the suspended plug of fibers became greater than the forces holding the plug together, failure would occur. Richardson (6) sheared a fiber suspension between two concentric cylinders and determined the shear stress at which the suspension yielded. The part of the suspension under high shear stresses flowed, while the annular ring at the lower stresses remained stationary. From these observations, he was able to determine a yield stress as a function of concentration. A similar study was performed by Head (7), who determined the yield stress as a function of concentration and fiber length.

At this time, the hydrodynamics of dilute pulp fiber suspensions and the mechanical or structural properties of fiber networks formed at higher concentrations have not been quantitatively studied because of the inability to assign definite values to the important fiber variables. This area of study is of interest to the industry because of the desirability for better control of the flow of fiber suspensions prior to and during formation of paper on a machine. Aside from these practical implications, such a study would serve to increase the understanding of fundamental flow phenomena for both Newtonian and non-Newtonian fluids.

Synthetic fiber suspensions differ from pulp fiber suspensions only in degree, not in nature. Therefore, rheological studies of synthetic fiber suspensions would be very important in obtaining an insight into the behavior of pulp fiber suspensions.

Work on the flow behavior of synthetic fiber suspensions in concentric cylinder viscometers was performed by Eirich, et al. (8) in 1936 and by Nawab and Mason (9) in 1958. They showed that Newtonian flow could be obtained in suspensions of glass, silk, and rayon fibers up to concentrations of 3% depending upon the fiber axis ratios. In both studies, the viscosity of a suspension was shown to be a function of the volume concentration and the axis ratio of the fibers. Mason and Nawab indicated that the viscosity contribution of the fibers determined in the earlier study was high due to wall effects. They found that wall effects could be eliminated by using very small fibers in a relatively large annulus viscometer. In neither study was there any mention of corrections for viscometer end effects. Lindsey and Fischer (10) have shown that such effects can be appreciable for viscometers with large annulus widths, such as those used in the fiber suspension studies. The work of Nawab and Mason also showed that the viscosity contribution of fibers suspended in a castor oil solution could be increased by soaking the fibers in water before placing them in suspension. The increase was attributed to fiber bending under fluid stresses, but it is possible that part of the increase was due to changes in the surface properties of the fibers.

Studies of the structural properties of networks composed of synthetic fibers have been only of exploratory nature up to this time. Mason (11) indicated that initial attempts to apply the tensile strength technique to suspensions of synthetic fibers were unsuccessful because small fluid disturbances caused a disruption of the networks. At M.I.T. (12), suspensions of kraft pulp fibers were set in rotatory motion in a cylindrical container and allowed to slow down. Upon stopping, the fibers would counterrotate, indicating that elastic strains had been set up in the network. Wilder (13) repeated these measurements with nylon fiber suspensions and observed a similar but less pronounced effect. Daily and Tsuchiya

(14) observed that nylon fibers having a large axis ratio (greater than 200) underwent plug flow in pipes at consistencies as low as 0.1% by weight, indicating network structure.

ANALYSIS OF THE PROBLEM

In the Introduction, it was indicated that industrial processes rely on a knowledge of rheology to properly use and prepare suspensions. Therefore, by increasing this knowledge, a better insight into the process variables may be obtained. A particular void exists in the understanding of the rheological behavior of fiber suspensions. Only a limited amount of data has been obtained for the Newtonian region of fiber slurry flow. Even less data exist for the region of suspension flow where networks are present. Experimental data for these types of suspensions accompanied by both phenomenological and theoretical interpretations of the data would constitute a significant contribution to the knowledge of rheology. Such a contribution is the expressed purpose of this study.

A fundamental study of the flow of fiber suspensions can only be performed when fiber properties such as length, diameter, density, and flexibility and the suspension consistency can be assigned definite values. Therefore, an approach such as that employed by Eirich, et al. (8) where synthetic fibers were used would be very profitable. The study should seek to show how the above variables affect the flow (or viscosity) of a suspension. The present theory (see Theoretical) of the flow of suspensions of cylindrical fibers would provide a good foundation for an analysis of the data. Apparatus effects, such as wall and end effects, should be accounted for before applying the theory. Upon completion of this phase of the study, other fiber variables such as irregular shapes and different surface properties could be introduced into the system and studied.

No theory exists at this time for the behavior of networks in fiber suspensions subjected to shear stresses. By considering a network of randomly oriented fibers, the initial analysis of this problem would be simplified. After obtaining data on the stress-strain behavior of synthetic fiber networks, modifications could be made in the original theory.

Based on the work of Wilder (13), Mason (11), and Daily and Tsuchiya (14), a study of fiber networks would appear to require an instrument capable of exerting very low shear stresses on the networks. Ferry and Parks (15) have shown that elastic or structural effects in polyisobutylene may be determined in a concentric cylinder viscometer. Therefore, such an apparatus should be applicable for this study if it were designed so that frictional forces would not interfere with the recovery of strained networks. Furthermore, the feature of low stresses would mean low shear rates in a flow experiment and thus permit the apparatus to be used in the study of suspension flow. Such an apparatus would also be useful in other rheological studies of such substances as polyelectrolytes (2), inks (4), and colloidal latices (3).

THEORETICAL

Two concentration regions of suspension behavior will be considered. These are: (1) the extremely dilute suspension where the viscosity is the sum of the contributions of all the particles and (2) the concentrated suspension where structural effects are present. Because of the complexity of interaction forces, little theoretical or experimental work has been done in the concentration region where hydrodynamic and physical interactions of the suspended particles are of paramount importance. For this reason, no theory of interaction will be presented. The theories discussed not only help to analyze experimental data but also define the conditions under which meaningful experiments may be carried out. It is not intended to present a detailed mathematical analysis of dilute suspension flow, but rather to outline the physical bases so that certain mechanisms of fiber behavior become apparent. The reader is referred to the original papers of Jeffery (16) and Burgers (17) for a more detailed presentation.

THE FLOW OF DILUTE FIBER SUSPENSIONS

The theoretical studies of the flow of solutions and suspensions have been greatly implemented by the ability to use phenomenological equations of fluid motion. Were an application of the molecular theory of flow to be attempted, one would be limited by the inherent complexity of the mathematics. The phenomenological approach consists of applying the hydrodynamic equations of motion to a volume of an incompressible fluid having a velocity $\vec{\underline{V}}$ and a density ρ. The state of flow of the volume increment may be expressed by the Navier-Stokes equation:

$$\rho\left[\frac{\partial\vec{V}}{\partial t} + (\vec{V}\cdot\nabla)\vec{V}\right] = \rho\vec{f} + \mu_o\nabla^2\vec{V} - \nabla p \qquad (1)^a$$

and the equation of continuity

$$\frac{\partial\rho}{\partial t} + V\cdot(\rho\vec{V}) = 0 \qquad (2)$$

where

$\vec{f}$ = the body forces per unit mass of fluid,

p = the pressure,

μ_o = the Newtonian viscosity coefficient, and

t = time.

Complete specification of flow is obtained when the boundary conditions are chosen.

In an experimental measurement of the viscosity of a solution or suspension, conditions are selected so that steady flow occurs ($\partial\rho/\partial t = 0$, $\partial\vec{V}/\partial t = 0$) and the body forces do not enter into the calculations ($\vec{f} = 0$). If the Stokes approximation is used, i.e., the inertial forces, $\rho(\vec{V}\cdot V)\vec{V}$, are negligible compared with the frictional term, $\mu_o V^2\vec{V}$, Equations (1) and (2) reduce to:

---

[a] $$\nabla\cdot\vec{V} = \frac{\partial u}{\partial x} + \frac{\partial v}{\partial y} + \frac{\partial w}{\partial z}$$

$$\nabla p = \frac{\partial p}{\partial x}\vec{i} + \frac{\partial p}{\partial y}\vec{j} + \frac{\partial p}{\partial z}\vec{k}$$

$$\nabla^2\vec{V} = \left(\frac{\partial^2 u}{\partial x^2} + \frac{\partial^2 u}{\partial y^2} + \frac{\partial^2 u}{\partial z^2}\right)\vec{i} + \left(\frac{\partial^2 v}{\partial x^2} + \frac{\partial^2 v}{\partial y^2} + \frac{\partial^2 v}{\partial z^2}\right)\vec{j} + \left(\frac{\partial^2 w}{\partial x^2} + \frac{\partial^2 w}{\partial y^2} + \frac{\partial^2 w}{\partial z^2}\right)\vec{k}$$

$$\gamma \nabla^2 \vec{V} = \nabla p/\rho \tag{3}$$

$$\nabla \cdot \vec{V} = 0 \tag{4}$$

where γ is the intrinsic viscosity $= \mu_o/\rho$. Oseen (18) showed that the fluid motion at a distance from a suspended particle resulting from the presence of the particle may be better approximated by the equation

$$\rho[(\vec{u} \cdot \nabla)\vec{V}] = -\nabla p/\rho + \gamma \nabla^2 \vec{V} \tag{5}$$

where $\vec{u}$ is the undisturbed fluid velocity existing in the absence of the particle.

Jeffery (16) used Equations (3) and (4) in analyzing the motion of an ellipsoidal fiber in a shear field. Oseen (18) determined the motion of a fluid under the influence of given forces from Equations (4) and (5). Burgers (17) then used Oseen's equations for the motion of the fluid in the presence of external forces to obtain an approximate representation of the disturbances created by cylindrical fibers in a shear field. The assumptions employed by Jeffery (16) and Burgers (17) in their theoretical work and the explanations for making the assumption are listed below.

Assumption	Reason
1. Viscous flow.	1. The Navier-Stokes equations are linear, allowing a simpler solution.
2. Fiber diameters large compared to the mean free path of the solution molecules.	2. No slip at the particle surfaces satisfying one boundary condition to be used in solving the Navier-Stokes equations.
3. Fibers small with respect to the apparatus dimensions.	3. a. No wall effects. b. No "inertial" effects due to the particles.
4. Fibers rigid.	4. The exact fiber geometry may be specified.
5. Low concentrations.	5. No interaction between fibers or their flow fields, thus simplifying the boundary conditions to be used in solving the Navier-Stokes equation.

Jeffery's equations for the motion of the ellipsoidal fibers were quite complex, but Burgers showed that for ellipsoids of large axis ratios they reduce to the forms shown in the following discussion. Consider a cylindrical fiber placed in a shear field (see Fig. 1) defined by $\underline{u} = \underline{G_o y}$, $\underline{v} = \underline{w} = 0$, where $\underline{G_o}$ is the undisturbed shear gradient and $\underline{u}$, $\underline{v}$, and $\underline{w}$ are the undisturbed fluid velocities in the $\underline{x}$-, $\underline{y}$-, and $\underline{z}$-directions. The velocity of the fluid in the direction of the $\underline{x}$-axis at some point $\underline{B}$ on the fiber may be resolved into three components. If the fiber center is at the origin, $\underline{O}$, of the co-ordinate system, then $\underline{\ell}$ is the distance to the point from $\underline{O}$. One component,

$$u_{\phi} = G_o \ell \sin\theta \cos^2\phi \qquad (6),$$

perpendicular to the meridian plane, $\underline{zOB}$, causes the angle, ϕ, to increase. The component, $\underline{u_\theta}$, in this meridian plane perpendicular to the fiber axis causes the angle, θ, to increase. The magnitude of this velocity component is:

$$u_{\theta} = G_o \ell \sin\theta \cos\theta \sin\phi \cos\phi \qquad (7).$$

The third component, $\underline{u_{\shortparallel}}$, of magnitude,

$$u_{\shortparallel} = G_o \ell \sin^2\theta \sin\phi \cos\phi \qquad (8),$$

is directed along the axis of the particle.

The angular velocity of the component in the meridian plane may be determined from Equation (7) and is found to be:

$$\frac{d\theta}{dt} = G_o \sin\theta \cos\theta \sin\phi \cos\phi \qquad (9)$$

while the angular velocity of the meridian plane about the $\underline{z}$-axis obtained from Equation (6) is:

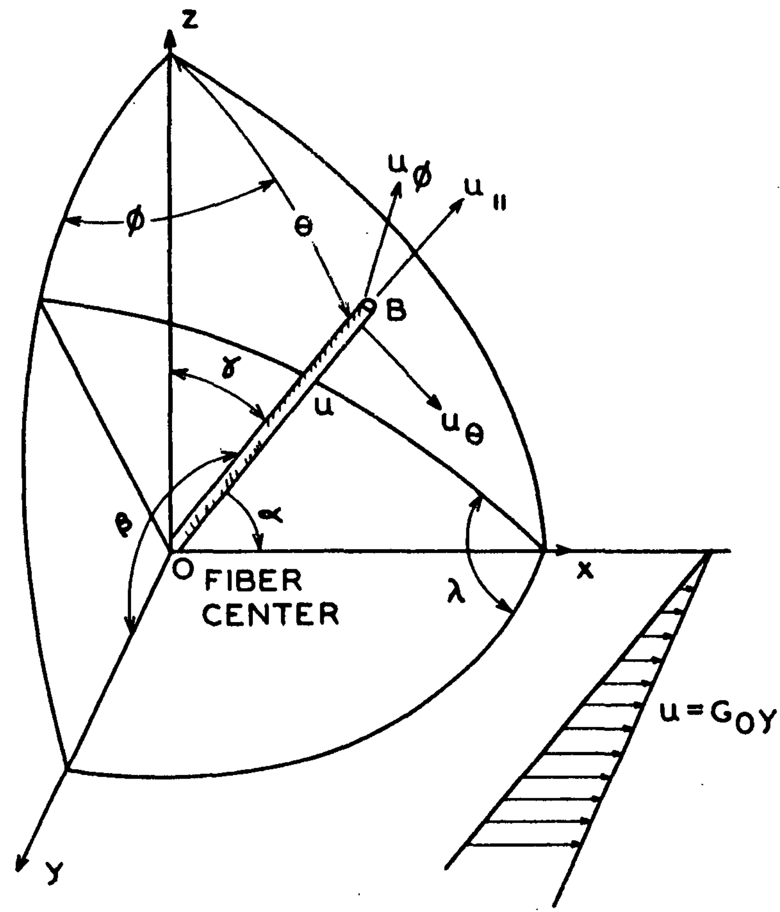

Figure 1. Schematic Representation of a Fiber in a Laminar Flow Field

$$\frac{d\phi}{dt} = G_o \cos^2\phi \tag{10}$$

Upon integration, this equation becomes:

$$\tan\phi = G_o t \tag{11}$$

where t is the time the particle has rotated in the field. Integration of the ratio of Equations (9) and (10) gives:

$$\tan\theta \cos\phi = \cot\lambda = C' \tag{12}$$

where C' is a constant of integration and λ is the angle between the plane OHx and the x-y plane.

These equations predict the motion of a particle in a laminar shear field. When the meridian plane is perpendicular to the direction of flow, $\phi = 0°, 180°$, the angular velocity of the plane is a maximum. The minimum velocity is obtained when the fiber is parallel ($\phi = -90°, +90°$) to the flow direction. After a long period of time, the fiber should become oriented parallel to the direction of flow. [See Equation (11).] However, because of the finite thicknesses of the fibers used in experimental studies, this orientation would never be achieved. The fluid velocity on one side of the fiber will always be greater than the velocity on the other side, thus exerting a shearing motion on the fiber, even when it is perfectly aligned with the x-axis.

If the fiber follows the motion of the liquid as described by the components u_θ and u_ϕ, then there should be no disturbance, although for a fiber of finite thickness, this statement is not rigorously correct. Because the surface of the fiber cannot follow the motion of the velocity component, $u_{\parallel}$, directed along its axis and since the fluid is required to adhere to the fiber surface, a disturbance of the fluid motion, u', parallel to the x-axis will result. There will also be a disturbance of the fluid in the y- and z-directions, but this disturbance is proportional to the diameter of the fiber. Burgers assumed that the fiber was very thin, so that the magnitude of the disturbance which was a function of the diameter was negligible.

The disturbance of the fluid will exert either tension or compression forces on the fiber depending on its position with respect to the direction of flow. Burgers (17) assumed that these forces, $f(\ell)$, were distributed along the axis of a cylindrical fiber of length L in such a manner that the relative velocity of the fluid to the fiber at the fiber surface was zero. Oseen (18) solved the Navier-Stokes equation [Equation (5)] and the equation of continuity [Equation (4)] for the velocity components u', v', and w' at any point in an infinite viscous fluid produced by a force acting on a small volume of the fluid. For a system of forces distributed along the axis of a fiber, the equation representing the disturbance u_s' at the fiber surface is:

$$u_s' = \int_{-1/2L}^{+1/2L} \frac{f(\ell)d\ell}{8\pi\mu_o} g(L, d, \ell) \tag{13}$$

where d is the fiber diameter, ℓ is the distance from the fiber center to a point on the axis, and the function $g(L, d, \ell)$ describes the geometry of the point with reference to a co-ordinate system. A solution of this equation was obtained when $f(\ell)$ was expressed as a power series function of ℓ/L, i.e.:

$$f(\ell) = -8\pi\mu_o G_o [A_1 \left(\frac{\ell}{L}\right) + A_2\left(\frac{\ell}{L}\right)^3] \sin^2\theta \sin\emptyset \cos\emptyset \tag{14}$$

where A_1 and A_2 are adjustable coefficients. The values of the coefficients A_1 and A_2 were determined from the solution of Equation (13) under the condition that u_s' was equal to the velocity component of the fiber in the direction of flow.

This system of forces acting along the fiber axis produces a doublet[a], M, of strength

$$M = \int_{-1/2L}^{+1/2L} f(\ell)\ell \, d\ell \tag{15}$$

[a]Two forces of opposite and equal magnitude, F, acting at points a short distance from one another along a straight line constitute a doublet of strength $M = Fe$, where e is the distance between the points of application of the forces.

acting along the fiber axis. If the relationship for $f(\ell)$ in terms of the known coefficients A_1 and A_2 is substituted into Equation (15) and an integration is performed, the following value of M is obtained:

$$M = -\frac{4\pi\mu_o(L/2)^3G_o}{3(\ln\frac{2L}{d} - 1.80)}\sin^2\theta\,\sin\phi\,\cos\phi \qquad (16)$$

Burgers (17) showed that the x-component of the velocity disturbance of a fluid resulting from the presence of a doublet of strength M is:

$$u' = -\frac{M}{8\pi\mu_o}\frac{x}{r^3}\left(1 - \frac{3P^2}{r^2}\right) \qquad (17)$$

where

$r^2 = x^2 + y^2 + z^2$, and

$P = x\cos\alpha + y\cos\beta + z\cos\gamma$ (see Fig. 1).

The total flow disturbance due to a fiber is simply the disturbance given by Equation (17) summed over all space. Consider the physical picture shown in Fig. 2. Two imaginary planes with co-ordinates y_1 and $-y_2$ have been introduced into the space where a fluid is undergoing shear described by $u = G_oy$, $v = w = 0$. If no particles are present in the fluid, the flow velocities in the planes are $u_1 = G_oy_1$ and $u_2 = -G_oy_2$, respectively. When an incremental volume, $dxdydz$, of the fluid containing $Ndxdydz$ fibers, where N is the number of fibers per unit volume, is introduced between the planes at a point, $x_fy_fz_f$, the total flow disturbance Δ_1 at the point, $E_1(x = 0, y_1, z = 0)$, is:

$$\Delta_1 = Ndy\int_{-\infty}^{+\infty}\int u'dxdz \qquad (18a),$$

or, substituting for u' and integrating,

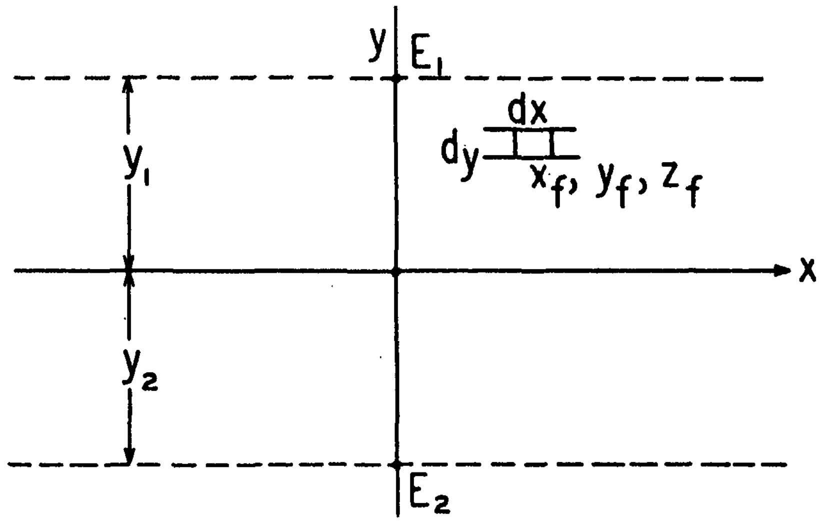

Figure 2. Schematic Representation of Two Imaginary Vertical Planes in a Laminar Flow Field

$$\Delta_1 = \frac{MN}{2\mu_o} \cos\alpha \cos\beta \, dy \tag{18b}$$

where cosα cosβ accounts for the position of the doublet with respect to the coordinate system. Likewise, at the point $\underline{E}_2$ in plane $-\underline{y}_2$, there is a flow disturbance, Δ_2:

$$\Delta_2 = -\frac{MN}{2\mu_o} \cos\alpha \cos\beta \, dy \tag{19}$$

Therefore, the total relative disturbance between the two planes due to the fibers is:

$$\Delta_1 - \Delta_2 = \frac{MN}{\mu_o} \cos\alpha \cos\beta \, dy \tag{20}$$

or between the inner and outer walls of the concentric cylinder viscometer of annulus width $\underline{D}$:

$$\Delta = \int_0^D \frac{MN}{\mu_o} \cos\alpha \cos\beta \, dy \tag{21a}$$

$$= \frac{MN}{\mu_o} (\cos\alpha \cos\beta) D \tag{21b}$$

Because this velocity disturbance, Δ, caused by the fibers is superimposed on the original motion of the suspending fluid, the frictional forces between vertical planes of flow being constant, the velocity gradient, G_f, of the suspension will be

$$G_f = G_o + \frac{MN}{\mu_o} \cos\alpha \cos\beta \qquad (22).$$

If the value of M defined by Equation (16) is substituted into Equation (22) and the cosines of α and β are transformed into functions of θ and ϕ, the following equation results:

$$G_f = G_o + \frac{\pi(L/2)^3 G_o N}{3(\ln \frac{2L}{d} - 1.80)} \sin^4\theta \sin^2 2\phi \qquad (23)$$

Because the tangential stress across planes y = constant was held constant for the suspension and the suspending liquid, that is:

$$\tau_o = \mu_o G_o = \mu_f G_f \qquad (24),$$

the relative viscosity, μ_r, of the suspension may be written as:

$$\mu_r = \frac{\mu_f}{\mu_o} = 1 + \frac{\pi(L/2)^3 N}{3(\ln \frac{2L}{d} - 1.80)} \sin^4\theta \sin^2 2\phi \qquad (25),$$

or, in terms of the volume fraction, $C = N\pi \frac{d^2}{4} L$, of the fibers,

$$\mu_r = 1 + \alpha_o C \qquad (26)$$

where $\alpha_o = \dfrac{(L/d)^2}{6(\ln \frac{2L}{d} - 1.80)} \sin^4\theta \sin^2 2\phi.$

The problem of determining a representative value of $\sin^4\theta \sin^2 2\phi$ may be solved in the following manner. Jeffery's (16) rigorous equations for the motion of an ellipsoidal particle in a laminar shear field indicate that the ends of a rotating ellipsoid describe a spherical ellipse on an imaginary spherical surface around the particle. Therefore, the angles θ and ϕ (see Fig. 1) are continuously changing. This means that $\sin^4\theta$ and $\sin^2 2\phi$ are also changing. From a consideration of the motion of an ellipsoid in a laminar shear field, Jeffery determined the average value of $\sin^4\theta \sin^2 2\phi$ for a particular orbit. Burgers (17) showed that Jeffery's exact equation for the average goniometric factor for a single particle reduces to the following equation for very thin fibers ($L/d \gg 1$):

$$\overline{\sin^4\theta \sin^2 2\phi} = \frac{1}{(L/d)} \frac{2C'}{\sqrt{C'^2 + 1}} \qquad (27).$$

Furthermore, it was shown previously [Equation (12)] for $L/d \gg 1$ that $C' = \cot\lambda$ and so Equation (27) may be written as:

$$\overline{\sin^4\theta \sin^2 2\phi} = \frac{2\cos\lambda}{(L/d)} \qquad (28).$$

In order to determine the mean goniometric term for all fibers in a suspension, an average value of $\cos\lambda$ based on the initial orientation of the fibers must be found. If the fibers are oriented at random, then $\overline{\cos\lambda} = 2/\pi$. For fibers oriented in a horizontal plane, $\lambda = 0$ and $\overline{\cos\lambda} = 1$. Therefore, for these two cases of fiber orientation, the coefficient α_o in Equation (26) may be expressed by the respective equations:

$$\alpha_o = \frac{2L/d}{3\pi(\ln \frac{2L}{d} - 1.80)} \qquad (29a)$$

and

$$\alpha_o = \frac{L/d}{3(\ln \frac{2L}{d} - 1.80)} \qquad (29b).$$

When Equation (29b) is used in conjunction with Equation (26), a maximum viscosity contribution due to the fibers is predicted.

THE SHEAR STRESS-STRAIN BEHAVIOR OF A FIBER NETWORK

The work in this section will be mostly of a qualitative nature. It is not intended to make a rigorous mathematical analysis of the problem, but rather by dimensional and geometric means to indicate certain fiber and network properties which might be important in determining the shear behavior of a fiber network. An analysis of the general case of a fiber suspension sheared between two parallel planes will be considered first. The results of this analysis will then be applied to the shear of a network between two cylinders of greatly different radii.

The approach to the problem will be to consider a network of simplified geometry. The fibers in such a network will be randomly oriented. Strain in the network will be a result of simple bending of the fibers. Twisting, extension, and slippage of fibers will be ignored. Furthermore, the strain in the network will be so small that a simple beam equation may be used to represent the deflection of the individual fibers. The gross behavior of the network will be assumed to be Hookean, so that it may be represented by an equation of the form $\underline{S} = \tau_o/\underline{G}$, where $\underline{S}$ is the shear strain, τ_o the shear stress, and $\underline{G}$ the modulus of elasticity in shear.

Consider the schematic picture (Fig. 3) of a fiber network sheared between two planes of area $\underline{A}'$ and a distance apart $\underline{h}'$. A force $\underline{F}$ will cause the network to undergo a deformation $\Delta\underline{x}$. Because the deformation is small and the material is Hookean, the strain, $\Delta\underline{x}/\underline{h}'$, over the section is:

$$\frac{\Delta x}{h'} = \frac{F}{A'G} \qquad (30).$$

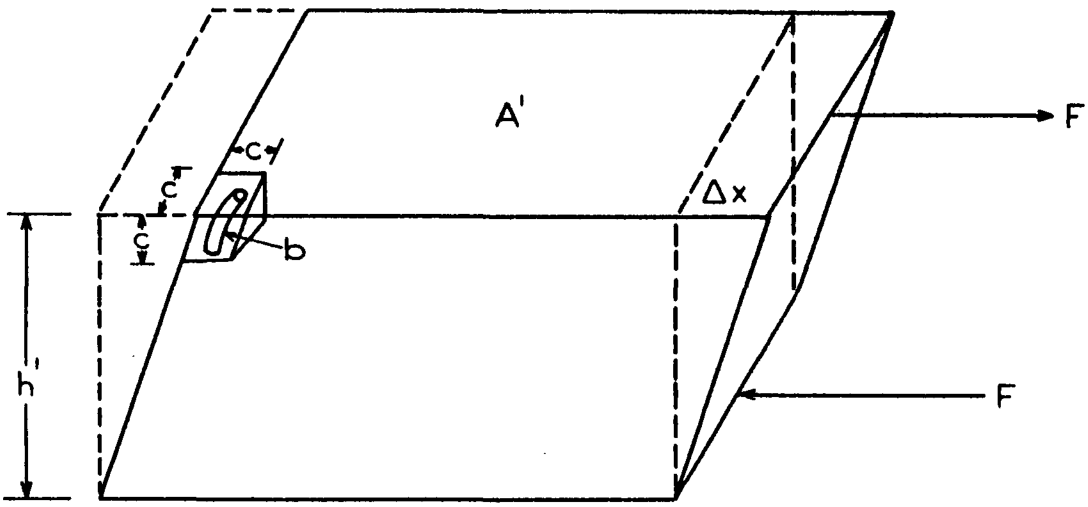

Figure 3. Schematic Representation of a Fiber Suspension in Shear

It was previously assumed that the deflection in a network was a result of the deflection y' of individual fibers. Considering the fibers to be supported at the ends and centrally loaded with a force, f, the deflection of the fiber may be represented by the following equation:

$$y' = kfb^3/EI \tag{31}$$

where

E = modulus of elasticity of beam material,

I = moment of inertia of beam cross section with respect to a centroidal axis,

b = average length of beam between supports, and

k = some statistical average coefficient which accounts for the fact that the points of contact are not regularly spaced along a fiber length and the forces do not necessarily alternate in direction.

The bending within a network will be considered to occur in small cubical elements with a volume of c^3. This element will be representative of the average volume occupied by a bending element, b. Because of the assumption of random orientation, c may be approximated by b/2 (see Appendix I). The total deflection Δx should be proportional to the sum of the deflections of each cubical element, or

$$\Delta x \sim \frac{h'}{c} y' \tag{32}$$

Also, the force, f, acting on the surface of an element will be the total force, F, acting on the surface, A', divided by the number of elements, or:

$$f = \frac{F}{A'/c^2} \tag{33}$$

$$= \frac{Fb^2}{A'4}$$

It should be mentioned here that the average force at a contact point might be a controlling factor in the breakdown of a fiber network under shear. If this were the case, then the yield stress of a network would be expected to be a function of the variables shown in Equation (33). This will be discussed more thoroughly in a later section of the report (see section on the Study of the Stress-Strain Behavior of Fiber Suspensions).

If Equation (33) is substituted for f in Equation (31), the beam deflection becomes:

$$y' = \frac{kFb^3c^2}{EIA'} \tag{34}$$

Substituting for y' and c in Equation (32), the following equation for the total deflection is obtained:

$$\Delta x \sim \frac{khFb^4}{2EIA'} \tag{35}$$

Comparing this relationship for Δx with that expressed by the stress-strain equation, Equation (30), the shear modulus may be shown to be:

$$G = k' \frac{EI}{b^4} \qquad (36),$$

where k' is a coefficient including all of the statistical and numerical terms.

For the case of a network under shear between two concentric cylinders, the physical picture is shown in Fig. 4. The angular deflection, $\Delta\Omega$, across an increment, Δr, will be equal to $\Delta x/r$. The change in angular strain in this increment may be expressed as

$$\frac{\Delta\Omega}{\Delta r} = \frac{1}{r}\frac{\Delta x}{\Delta r} \qquad (37).$$

Using the assumptions that the network is Hookean and the deflections are very small, the strain, $\Delta x/\Delta r$, is equal to τ_o/G and Equation (37) becomes:

$$\frac{\Delta\Omega}{\Delta r} = \frac{1}{r}\frac{\tau_o}{G} \qquad (38).$$

The force, F, at any radius r is related to the applied torque, T, by $F = T/r$. The area of a cylindrical surface at this radius is 2 rh where h is the height of the suspension in the annulus. Therefore, the shear stress at r is

$$\tau_o = \frac{T}{2\pi r^2 h} \qquad (39).$$

If the change in angular deflection with a change in radius is allowed to become very small, Equation (38) may be replaced by a differential equation of the form

$$\frac{d\Omega}{dr} = \frac{1}{r}\frac{T}{2\pi r^2 hG} \qquad (40)$$

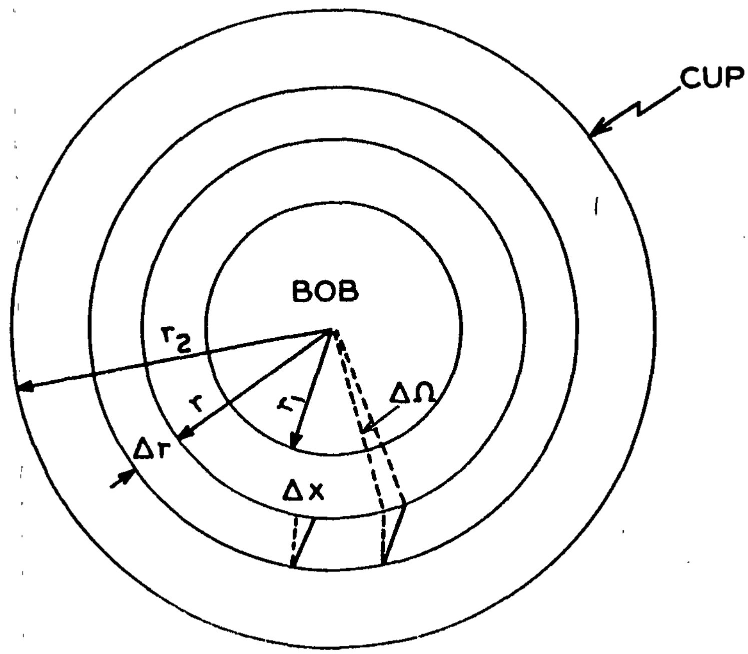

Figure 4. Schematic Representation of a Fiber Network Sheared Between Two Concentric Cylinders

where the shear stress, τ_o, was replaced by the right-hand side of Equation (39). The angular deflection, $\Omega_{\underline{r}}$, at any radius, $\underline{r}$, may be determined by integrating the above equation between the proper limits, or:

$$\int_{o}^{\Omega_r} d\Omega = \frac{T}{2\pi hG} \int_{r_2}^{r} \frac{dr}{r^3} \qquad (41).$$

Upon integration and substituting for $\underline{G}$ from Equation (36), the angular deflection is:

$$\Omega_r = \frac{Tb^4}{k4\pi hEI}\left(\frac{1}{r^2} - \frac{1}{r_2^{\,2}}\right) \qquad (42).$$

Van Wyk (19) used a statistical method (see Appendix II) of determining the length $\underline{b}$ between points of support in terms of the suspension and fiber properties. The result was $\underline{b} = 0.54\ \underline{d}/\underline{C}$ where $\underline{C}$ was the volume fraction of fibers and $\underline{d}$ was the fiber diameter. Substituting for $\underline{b}$ in Equation (42) and rearranging, the final equation is:

$$\nu_r = K \frac{d^4 T}{hEIG^4} \left(\frac{1}{r^2} - \frac{1}{r_2^2}\right) \qquad (43),$$

where $\underline{K}$ includes the numerical and undetermined statistical coefficients.

Thus, the fiber properties, $\underline{E}$, $\underline{I}$, and $\underline{d}$, and the suspension volume fraction, $\underline{C}$, are important in determining the rheological behavior. It is quite probable that other dimensionless groups including the fiber length, $\underline{L}$, and diameter, $\underline{d}$, would enter into a more rigorous analysis of the behavior.

FIBER SELECTION AND CHARACTERIZATION

In the Introduction and Theoretical sections, certain fiber properties were either shown or implied to be important in affecting the viscosity or network behavior of a suspension. The theory showed that the length and diameter are the most important variables in determining the viscosity of a dilute suspension of cylindrical fibers. A knowledge of both is also required in determining the geometry of a fiber network. Experimentally, the bending modulus has been observed to greatly influence suspension behavior both in the dilute and concentrated regions. One assumption made to simplify the solution of the Navier-Stokes equations was that no body forces acted on a particle in suspension. Therefore, a knowledge of the fiber density is required to eliminate gravitational forces on the fibers by suspending them in a fluid of equal density.

Nylon fibers were chosen for the major portion of the study for convenience and the ability to assign definite values to the above variables. Through the courtesy of the Du Pont company, these fibers were obtained in three different diameter ranges (13-15, 44-46, and 75-77 microns) and a high and low modulus range. A small part of the study involved the use of glass fibers, which were kindly made available by R. L. Jones (20), and spruce kraft pulp fibers procured from Mr. John Peckham of the Institute.

The experimental techniques for characterizing and preparing the fibers are described below, while the results of these experiments are listed in the first section of Results and Discussion.

FIBER DIAMETER DISTRIBUTIONS

The samples of the nylon fiber obtained from Du Pont were in the form of yarns containing 1 to 34 individual filaments. A preliminary study indicated that the filaments within a given sample varied in diameter but that any given filament was essentially uniform in diameter. An exception to this are the filaments in Sample P-1643-67-2, where large variations (ca. ±10%) in diameter were noted for a single strand.

The diameter distributions were determined microscopically. A 25X eyepiece equipped with a micrometer scale and a 100X oil immersion objective lens were used in determining the diameters up to values of 50 microns. For larger diameters, a 43X objective was substituted for the 100X objective. The unswollen diameter was measured by placing the fiber on a glass slide and immersing it in an oil of 1.49 index of refraction. This fluid was used in order to increase the contrast between the fiber and the background. A control experiment indicated that if swelling was occurring, it could not be detected at the magnifications used. All the filaments in a yarn were measured.

Because a solution of tetrachloroethane and mineral oil was used to suspend the fibers in the major portion of the flow studies of dilute suspensions, the effect of this solution on the fiber diameter was studied. After soaking the samples in the solution for 12 hours, no swelling could be detected.

A sucrose solution (ca. 1.14 sp. gr.) was employed in one series of runs in the flow study and all the work on network deformation. It has been established (21) that moisture swells nylon, so it was necessary to also determine the magnitude of this swelling. The swollen diameter distribution was measured in a manner similar to that described above except that a 1.14 sp. gr. sucrose solution was utilized as the immersion liquid. The fibers were allowed to soak in the liquid for at least one hour before the measurements were made. Load-elongation measurements of fibers soaked in the solution showed that all changes taking place in the fiber were complete after one hour. All the filaments in a given yarn were measured, since these values were incorporated into the calculation of the swollen densities of the fibers. Measurement precision of 3% or better could be expected for the lower range of diameters. In the intermediate and high ranges, the precision was about 1%. The unswollen average diameters of the samples are presented in the Results and Discussion, Table III.

FIBER DENSITY DETERMINATION

The densities of the fibers were initially determined in air to obtain an estimate of the densities of the solutions required to prevent the fibers from floating or settling. A solution of this density was prepared and a small quantity (ca. 0.01% by weight) of fibers was placed in the solution and the mixture was deaerated for one hour. In all cases, the fibers had a greater density than the solution so the specific gravity was increased until no settling or floating of the fibers could be observed over a 6-hour period. The densities of the 1.0-1.2 sp. gr. solutions at 73°F. were determined with a hydrometer. For solutions with specific gravities greater than 1.2, a Westphal balance was employed for the determination.

MODULUS OF ELASTICITY DETERMINATIONS

The forces exerted on a fiber in the shear field of a fluid in laminar flow or in a network deformed under a shear stress cause the fiber to undergo bending. Therefore, the correct modulus value to use in comparing the reactions of two fiber systems to such forces is the bending modulus. For an isotropic material, the bending modulus should be the same as the modulus determined under tensile loading. However, Wakelin, et al. (22) have shown that nylon has a greater modulus in bending than in extension. They attributed this behavior to anisotropy in the fiber caused by the drawing process.

Since the fibers probably are not isotropic, it would be presumptive to use a fiber modulus of elasticity determined by an extension technique as the true modulus of the fibers. The bending modulus of the fibers may be determined by a resonance frequency technique (23) which assumes that the fibers behave as cantilever beams vibrating in resonance with an external source of vibration. This method not only determines the bending modulus but eliminates time-dependent changes in the fiber structure. However, the decrease in the elastic modulus of a nylon fiber (21) with increased humidity would mean that the bending modulus as determined in air at 73°F., 50% R.H., would not be representative of the modulus of the fibers in suspension. Furthermore, it would be very difficult to use the resonance frequency technique to determine the bending modulus of a liquid-saturated fiber. Studies (20) with a static bending technique showed that because of a permanent set in the fibers no significant modulus could be determined in this manner.

Therefore, the following method was used to estimate the actual modulus of a fiber in either an aqueous or an organic fluid suspension. The bending moduli of the fibers were first determined by the resonance frequency technique and a load-elongation technique in a 73°F., 50% R.H. atmosphere. Then the moduli of the fibers were determined in the sucrose solution (ca. 1.14 sp. gr.) and the organic solution (ca. 1.14 sp. gr.) by a modified load-elongation technique. From the change of the extension modulus of a fiber caused by immersion in a given fluid, the change in the modulus in bending of a fluid-saturated fiber could be estimated.

RESONANCE FREQUENCY TECHNIQUE

The equation which describes the behavior of a cantilever beam vibrating in resonance with an external source of vibration is (24):

$$E_b = \frac{W_\ell \omega_o^2}{gIm^4} \tag{44}$$

where

E_b = modulus in bending,

W_ℓ = weight per unit length of fiber,

ω_o = $2\pi f$, f being the resonance frequency,

m = constant depending on the free length L of the beam and the mode of vibration produced,

g = gravitational constant, and

I = moment of inertia of fiber cross section.

A major error in determination of the bending modulus is the effect of air damping. Kärrholm and Schröder (25) analyzed this effect both theoretically and experimentally and showed that the air damping can be minimized by a judicious choice of fiber lengths. Table I shows the fiber lengths for each diameter range at which the maximum effect was less than 3% as determined from Kärrholm and Schröder's equations. These lengths were employed in the determination of the bending modulus of the fibers used in this study.

Lochner (23) used the sound field of a loud-speaker, a disk recorder cutting head, and an electromagnet to excite quartz fibers to resonance. The moduli of the fibers determined by the three methods were nearly equivalent. In this study, a disk recorder cutting head technique was used because of its simplicity. A phonograph record cutter, Astatic Model X-26 with a twisting type piezoelectric crystal excited the fiber directly. Removable steel pins with machined flat surfaces parallel to the pin axis were constructed for insertion into the head. The fibers were glued to the pin either with a casein glue or an epoxy resin. The results using both glues were equivalent, but the casein glue was preferred because it was easily removable from the pin.

TABLE I

FIBER LENGTH RANGE YIELDING MINIMUM AIR DAMPING IN THE BENDING MODULUS DETERMINATION BY THE RESONANCE FREQUENCY TECHNIQUE

Diameter Range, μ	Fiber Length Range, cm.
14-17	0-0.25
40-50	0-0.90
60-70	0-1.30

The crystal was mounted on the stage of a horizontal microscope pictured schematically in Fig. 5. This arrangement enabled the vibrating end of the fiber to be centered with respect to the microscope lens. The output from a Hewlett-Packard oscillator model 200J was amplified with a Knight Amplifier-model 14E and a small Kenyon transformer type T104. Illumination of the fiber was provided by a 100-watt microscope lamp. A copper sulfate solution cell placed between the lamp and the fiber minimized heat effects.

Because the length is raised to the fourth power in the equation for the modulus [Equation (44)], it must be determined accurately. A micrometer was mounted so that it contacted the flat surface of the horizontal beam of the microscope stage. By raising or lowering this beam, the hairline in the microscope eyepiece could be aligned either with the point where the fiber emerged from the glue on the pin or with the end of the fiber. By taking the difference between the micrometer readings at these two stage settings, the length of the

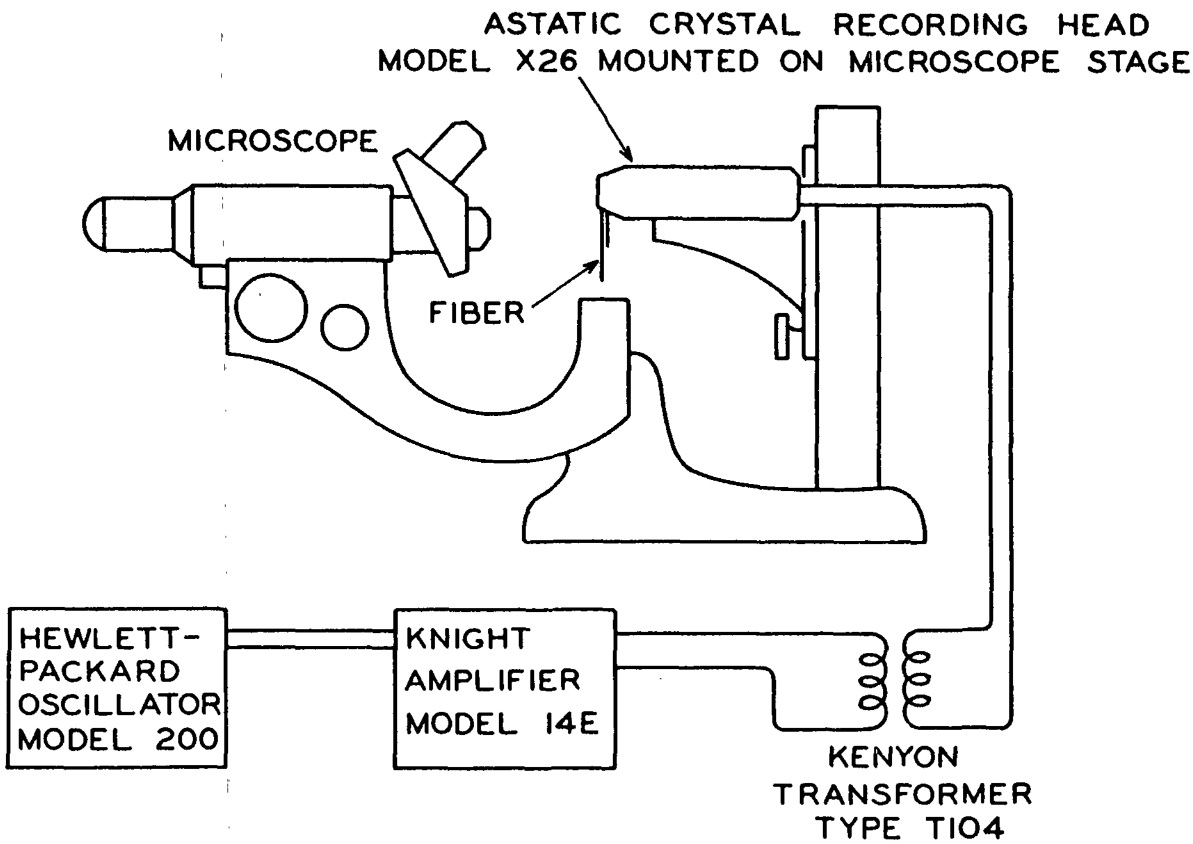

Figure 5. Apparatus to Measure Fiber Bending Modulus of Elasticity with Resonance Frequency Technique

fiber could be determined to the nearest 0.001 cm. A small clamp weighing ca. 0.2 g. held the fiber straight during the measurements. The results of the resonance frequency determinations are presented in Table III in the Results and Discussion section.

LOAD-ELONGATION TECHNIQUE

Modulus of Fiber in a 50% R.H. and 73°F. Atmosphere

The modulus in tension or Young's modulus is defined by the following equation:

$$E = \frac{P'/A}{\Delta L/L} \qquad (45)$$

where

$\underline{E}$ = modulus of elasticity, g./sq. cm.,

$\underline{P}'$ = load, g.,

$\underline{A}$ = fiber cross-sectional area, sq. cm.,

$\Delta\underline{L}$ = extension of the sample, cm., and

$\underline{L}$ = initial length of the sample, cm.

The moduli were determined from the linear portions of the load-elongation curves obtained with the Instron testing instrument, Model TM.

The use of this instrument as a means of determining various stress-strain properties of fibers is described in Du Pont Bulletin X-82 (21). The Instron apparatus applies a constant rate of straining to a specimen held between two jaws. The lower jaw moves downward at a constant, adjustable rate. The stationary upper jaw is connected to one of a series of load cells, depending upon the magnitude of the maximum load applied. The signal from the load cell is amplified and activates a pen on a recording chart. In these experiments, a rate of straining of 2.5% per minute was used while the full-scale deflection load on the chart was adjusted to 10 grams or less. Chart speeds of 5 and 10 inches per minute were used, depending on the fiber's reaction to the loads.

In order to mount the fibers in the instrument, a special technique was employed. Actual clamping of the fibers between various surfaces (steel, aluminum, and paper) caused either damage to the fiber or slipping during the load application. By gluing the fibers to aluminum tabs which could be clamped in the instrument, the above complications were eliminated.

The actual procedure for mounting the fibers is represented schematically in Fig. 6. This procedure is a slightly modified form of that used and described by Jones (26). In part (a), Fig. 6, the fiber is shown glued to the aluminum tabs, 3/4 by 5/16 in., with epoxy resin. The tabs are glued 4 inches center to center to aluminum foil folded over a 9 by 16-inch index card. To place the fibers in the jaws of the instrument, the ends of the index card were cut off, leaving the tabs mounted on the folded foil. This provided enough rigidity to use the special jaw alignment rig (27). After clamping the tabs [see part (b), Fig. 6], the foil was carefully unfolded to prevent any fiber damage and cut along the dotted line shown in part (c), Fig. 6. No slippage of the fibers was noticed up to loads of 10 grams.

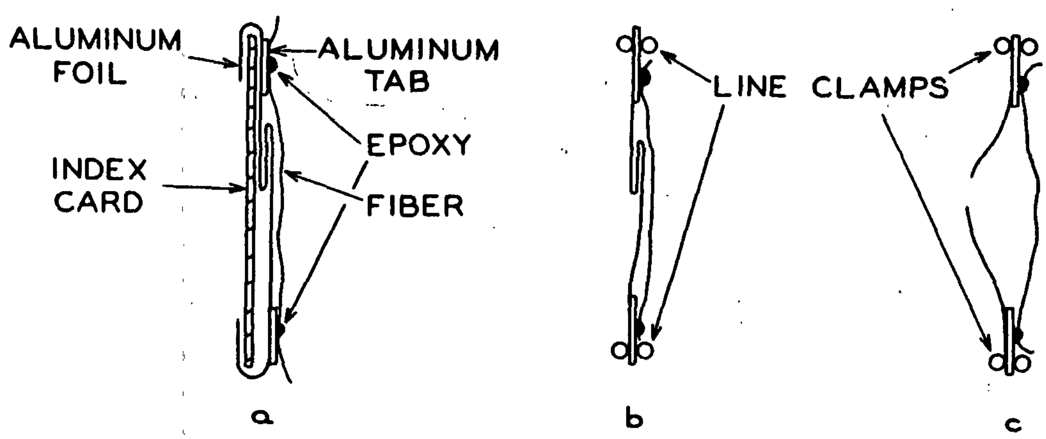

Figure 6. Procedure for Mounting Fibers in the Instron Tensile Tester

The ratio, $\underline{P}/\Delta\underline{L}$, in Equation (45) was determined from the slope of the initial linear portion of the stress-strain curve. The cross-sectional area was determined from the microscopic measurements of the fiber diameter. In order to determine the initial length, $\underline{L}$, the slack in the fiber was added to the span length of the instrument and the clamp-line-to-glue-line distance was substracted from this sum.

Modulus of a Fiber Immersed in a Fluid

Single fibers were placed in a glass cell filled with the fluid and this cell was mounted in the Instron instrument in the manner depicted schematically in Fig. 7. The fibers were again secured to the aluminum tabs with epoxy resin. The upper tab was cut in the shape of a "T" so that it would rest on top of the 4 by 1/2-inch diam. cell. A hole punched in the tab enabled it to be attached to the "A" load cell of the Instron instrument. The lower tab was rectangular, 7/16 by 1-1/4 in. It extended through a cork so that the side holding the fiber was immersed in the solution while the other side could be clamped in the lower jaw of the instrument.

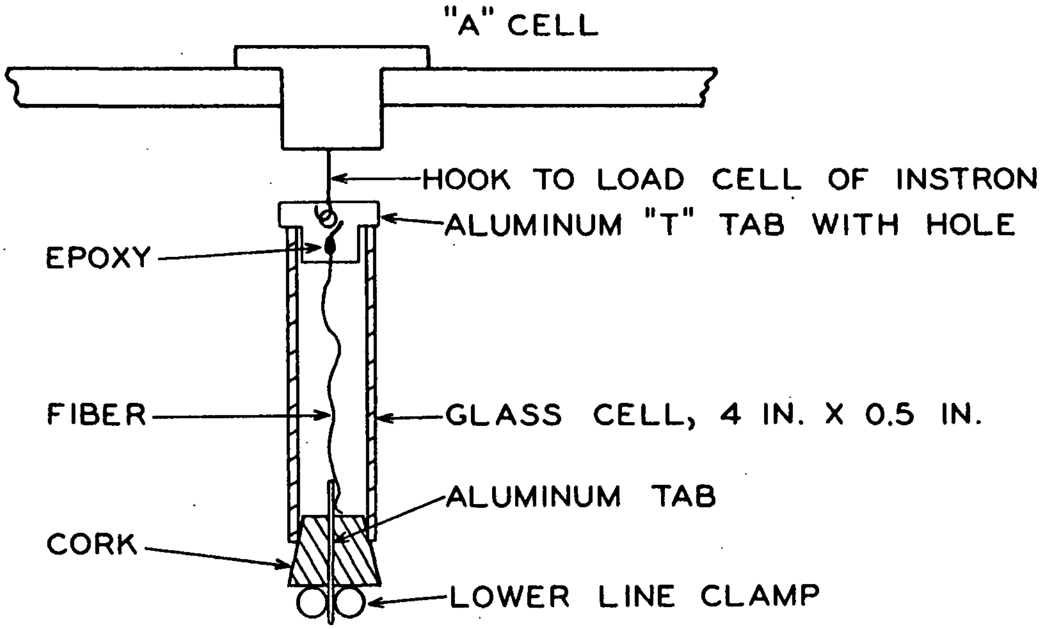

Figure 7. Cell for Determining Modulus of a Fiber Immersed in a Fluid

The fiber was immersed in the solution for at least 1 hour before subjecting it to a load-elongation run. Preliminary work showed that the modulus was essentially constant after this time interval, indicating complete saturation of the fiber. The modulus was calculated in a manner similar to that described for a fiber strained at 50% R.H. and 73°F. These results are given in Table III in the Results and Discussion section.

PREPARATION AND CHARACTERIZATION OF FIBERS WITH A SMALL LENGTH DISTRIBUTION

The fibers were supplied by Du Pont in the form of continuous filaments or yarns wound on bobbins. To cut fibers to uniform lengths, the yarns were rewound on a circular wheel about 2 feet in diameter so that the strands were approximately parallel. The circular skein of fibers was cut once and laid out flat on a solid surface covered with chipboard.

Razor blades held rigidly in parallel array by drill rods and spacers were forced through the skein by a hydraulic press. Variation in fiber length was obtained by changing either the number or the size of the washers between the blades. This technique was similar to that developed by Estridge (28).

To obtain the necessary axis ratio range for the smallest diameter fibers, it was necessary to cut fibers shorter than could be conveniently cut with the razor blade technique. In this case, the skein of fibers was embedded in a Fischer Tissuemat Wax (m.p. 60-63°C.) to form a rigid rectangular bar. The desired lengths of fiber were then cut using a microtome apparatus in which a razor blade was substituted for the regular blade. The wax was removed from the fibers by extracting them in a Soxhlet with hexane overnight. Tensile modulus determinations on fibers treated in this manner indicated little or no change in the physical properties.

The fiber length distributions were determined by the semiautomatic measuring method (29) developed by the Finnish Pulp and Paper Research Institute. The apparatus employed in this technique projects the images of fibers magnified 50X onto a ground-glass screen. At least 200 fiber lengths were measured to the nearest 0.02 mm. in each sample. The results of these determinations are listed in Table IV in the Results and Discussion.

EXPERIMENTAL EQUIPMENT

DESIGN CONSIDERATIONS FOR AN APPARATUS TO STUDY THE BEHAVIOR OF FIBER SLURRIES SUBJECTED TO SHEAR STRESSES

The conditions under which the theoretical analyses of the flow of dilute fiber slurries and the stress-strain behavior of more concentrated slurries were made, suggested the following criteria for the design of an apparatus to study these systems:

1. The geometry of the apparatus should be such that the data obtained can be compared with theory.
2. Laminar flow conditions should exist in the apparatus.
3. Extraneous effects due to the apparatus structure should either be very small or at least be such that corrections for the effect can be made.
4. The apparatus should be sensitive enough to determine accurately small changes in the behavior of fiber slurries at low consistencies.
5. The instrument should be capable of producing stresses below the yield stresses of any structures existing in relatively concentrated slurries.
6. The rates of shear in the dilute fiber slurries should be low enough that fiber bending is not produced by the fluid forces.

A concentric cylinder viscometer appeared to satisfy all these requirements. Therefore, nylon fiber slurries (fiber diameter 44.85 μ, axis ratio 56.3) varying in consistency from 1 to 3% by volume were subjected to a range of shear stresses from 0.2 to 1.0 dynes per sq. cm. in a concentric cylinder viscometer. This viscometer was similar to the commercial Stormer model (30). Torques from 10 to 100 dyne-cm. were applied to the inner bob. The bob and inner surface of the cup were covered with a rough material (see Fig. 13) to make contact with the networks in the apparatus. Some elastic properties were observed, but friction and inertial effects in the apparatus masked a large proportion of the effect. These data indicated that commercial viscometers were not feasible for the study. Not only are such viscometers incapable of producing such low shear stresses, but also the frictional effects in the cylinder suspension systems would be appreciable in this low stress range. The minimum residual frictional torque of the finest ball bearing assemblies is about 10 dyne-cm. (31). Of course, a torsion wire suspension would eliminate the friction, but then the measurement of the elastic recovery of strained structures in the slurries would be very difficult.

These considerations required that a concentric cylinder viscometer be designed in which shear stresses in the range of 0.01 to 10 dynes per sq. cm. could be applied to the inner cylinder mounted so that frictional forces were very small. Furthermore, the apparatus had to be flexible enough in design to permit dimensional alteration either to eliminate wall effects, etc. or to determine them accurately. The final apparatus design included a viscometer with an air bearing suspension system for the bob and an eddy current clutch-type torque-sensing mechanism.

The purpose of lubrication in a bearing is to replace the friction between sliding or rolling surfaces with the lesser friction in a mobile fluid between the surfaces. The friction in a liquid is proportional to the viscosity, so bearings lubricated with low viscosity fluids would exhibit less friction than if higher viscosity liquids were used. For this reason, air with a viscosity of about one per cent that of water has been used as a lubricant in special bearings. For instance, a precision torque-measuring instrument designed and constructed at M.I.T. (32) includes an air bearing with a residual friction of 10^{-3} dyne-cm.

The small forces observed in fiber networks required that such a bearing be used in this study. The main features of the bearing constructed were two concentric cones separated by a thin air film.

Because a torsion wire was eliminated from the design, some other method of measuring the torque applied to the system had to be found. This problem was solved by using the system of an eddy current drive. This particular method is quite versatile because either the outer or the inner cylinder may be rotated and the torque produced may be measured accurately. A magnetic field rotating above a conducting nonferromagnetic disk causes eddy currents to be set up in the disk which oppose the movement of the field through the disk. This action produces a net torque on the disk. The torque produced is a function of the magnetic field in the rotor, the distance between the rotor and the disk, the speed at which the field is rotated and the material from which the disk is constructed. By proper adjustment of these variables, a desired low torque range may be obtained.

The air bearing and the eddy current torque producer are the main features of the apparatus. These components were mounted in such a way that different bob and cup combinations could be used. Because of the critical features of the air bearing and the eddy current drive and their relative importance to the study, detailed dimensions are given.

EDDY CURRENT DRIVE

A schematic diagram of the eddy current torque-producing device is pictured in Fig. 8. This part of the apparatus is supported on a separate frame from the cylinders and the air bearing assembly in order to eliminate any vibration from the rotation.

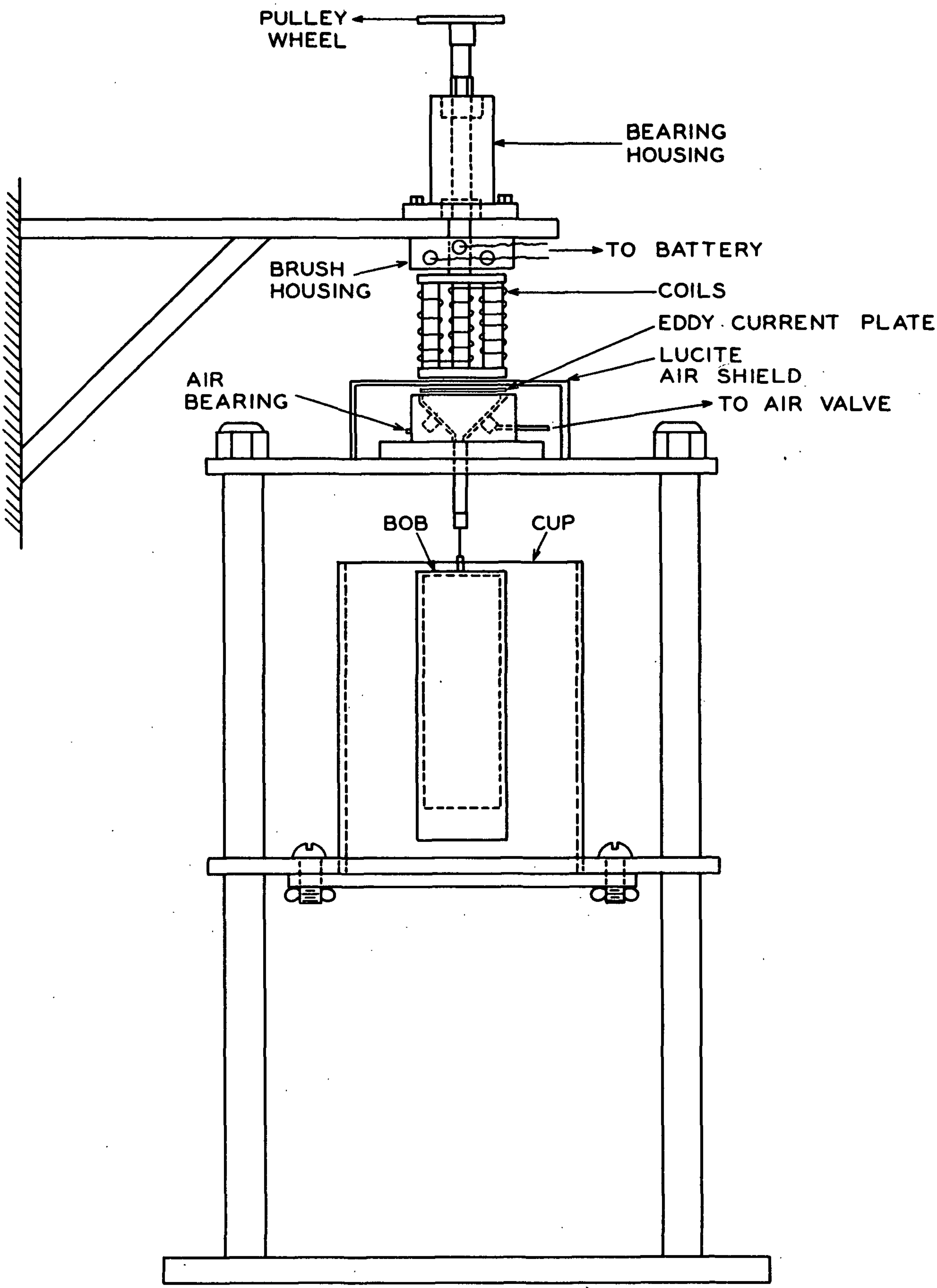

Figure 8. Concentric Cylinder Viscometer

The bearing housing and the shaft for the rotor are drawn to scale in Fig. 9. The coil rotor shaft was positioned in the housing by two New Department angle contact ball bearings, no. QOLOO. A 0.053-in. wide shoulder on the shaft rode against the lower bearing, while the upper part of the shaft was threaded so that a 5/16 - 18 nut could be secured against the upper bearing. A 2-in. diameter pulley wheel on top of the shaft enabled the rotor to be driven by a Bodine 1800 r.p.m. synchronous motor, type NSY-55. The speed of the rotor could be varied by adjusting the ratio of the pulley diameters.

Two coin silver slip rings[a] were attached to the shaft--one on the 0.50-in. diameter section and the other on the 0.3725-in. diameter section. The ring on the larger section was grounded to the shaft, while the ring on the smaller section was insulated from the shaft by a Teflon gasket. Three graphalloy brushes[a] (Grade H9434) spaced 120° apart were used in conjunction with each ring. They were held by brush holders[a] (no. 11509-1) set in the brush housing pictured in Fig. 10. The proper compression of the brushes against the slip rings was maintained by connecter springs[a] (no. 127-9).

The rotor section was constructed as follows: Six 3/8-in. diameter, 2 1/2-in. long Armco magnet iron rods were spaced at 60° intervals around a 1.5-in. diam. circle between two 1/4-in. thick, 2-in. diam. magnesium disks. Shoulders (0.0625 in. wide) on the rods held them securely in place when the two end plates were tightened by screwing the shaft into the bottom plate until the shaft shouldered on the top plate. Each rod was wound with 103 turns of magnet wire (25 gauge). These coils were connected in series with one end grounded to the shaft and the other end soldered to the insulated slip ring.

[a]Materials manufactured by the Graphite Metallizing Corp.

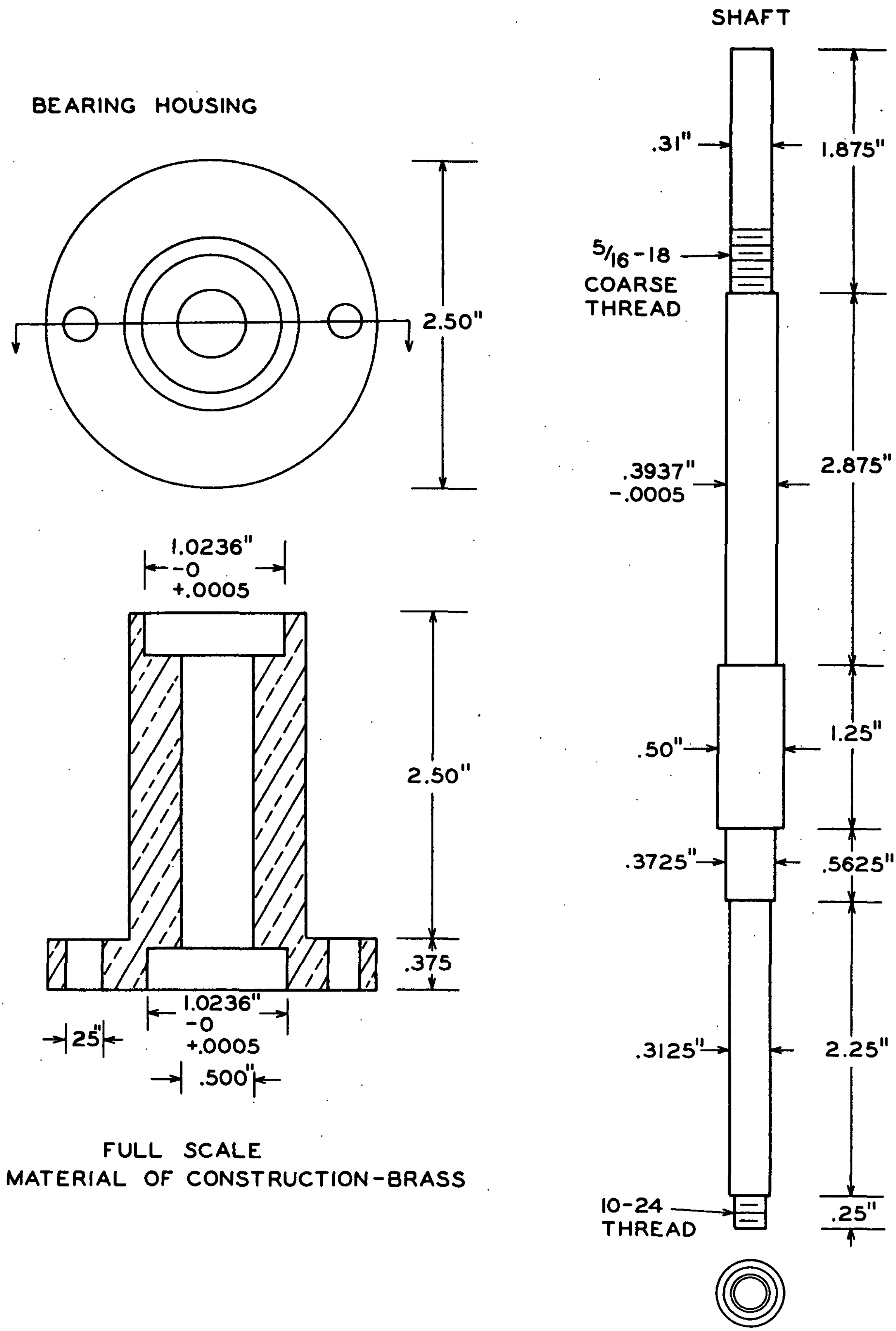

Figure 9. Coil Shaft and Bearing Housing

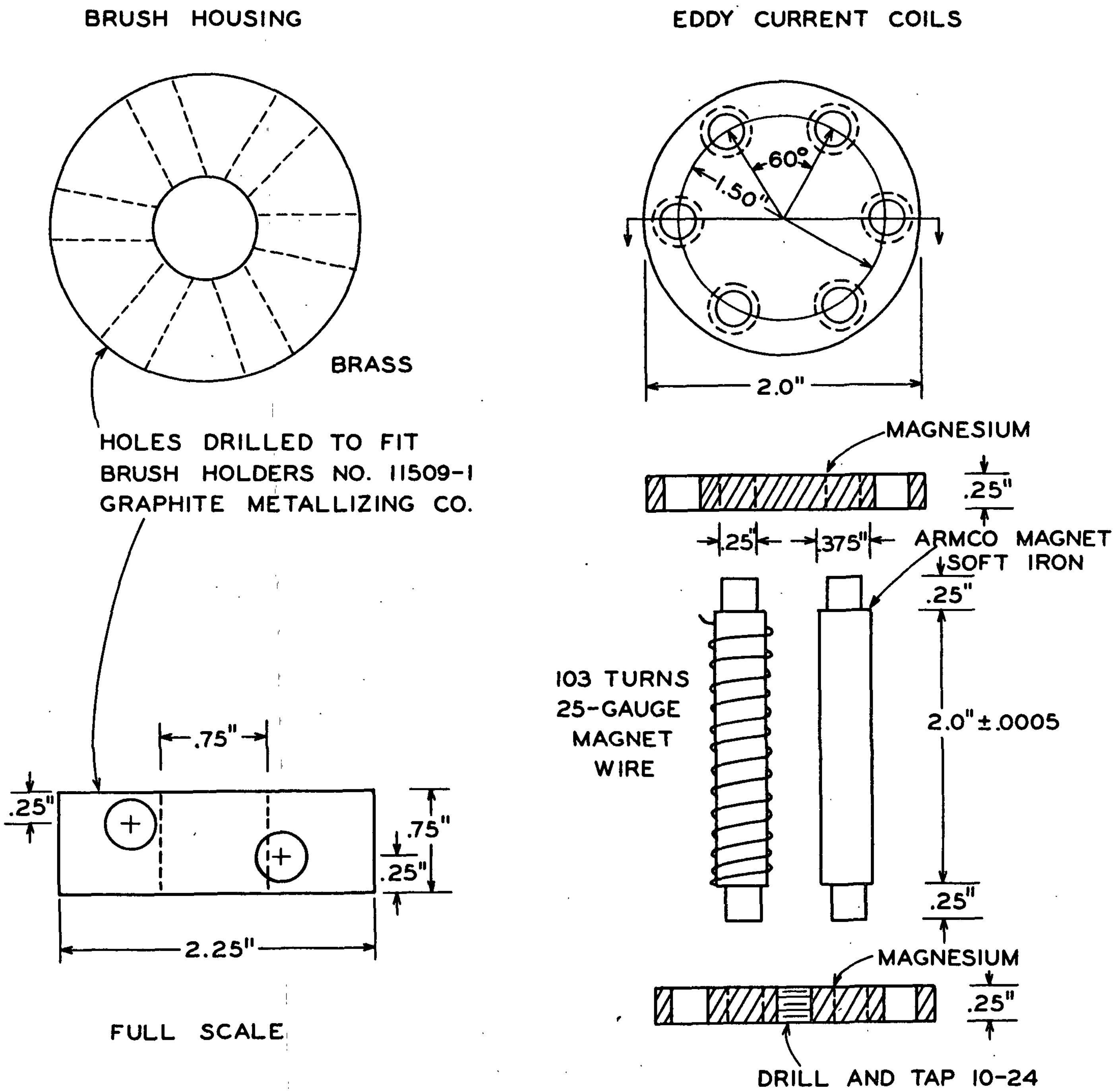

Figure 10. Components of Eddy Current System

A 1/8-in. thick, 2.0-in. diam. magnesium eddy-current disk was used in the study. A 1/4-in. diam. cylindrical section on the bottom of the disk allowed it to be mounted 1/16 in. above the male section of the air bearing. It was spaced 1/8 in. below the bottom of the rotor. At this distance, small variations in the position of the plate did not noticeably affect the torque output.

Torques of 1 to 80 dyne-cm. were obtained by varying a d.c. current through the coils from 0.05 to 2.0 amp. when the rotor was turning at a speed of 900 r.p.m. The electrical system for controlling the current is pictured in Fig. 11. The voltage from a 6-volt Delco storage battery was varied by means of a Milvay rheostat (model 67680, 20 ohms, 4.1 amp.). The current passing through the coils was measured by a Polyranger d.c. ammeter. In order to prevent the iron cores from becoming permanently magnetized, an a.c. current was passed through the coils after each run where d.c. current was used. The maximum value of the a.c. current was 2.6 amp. This current was obtained by stepping down the 115-volt line voltage to 6 volts with a Jefferson Electric transformer (cat. no. 637-251).

Higher torques may be obtained with the apparatus by increasing the speed of the rotor or by using heavier magnet wire so that larger currents may be applied. Lower torque necessitates a more sensitive current-measuring device. This could be accomplished with a voltmeter in conjunction with a precision resistor.

AIR BEARING SUSPENSION

The air bearing consists of brass conical male and female sections drawn to scale in Fig. 12. The male section is a frustrum of 90° cone, bounded by two circular surfaces perpendicular to the cone axis having diameters of .3125 in.

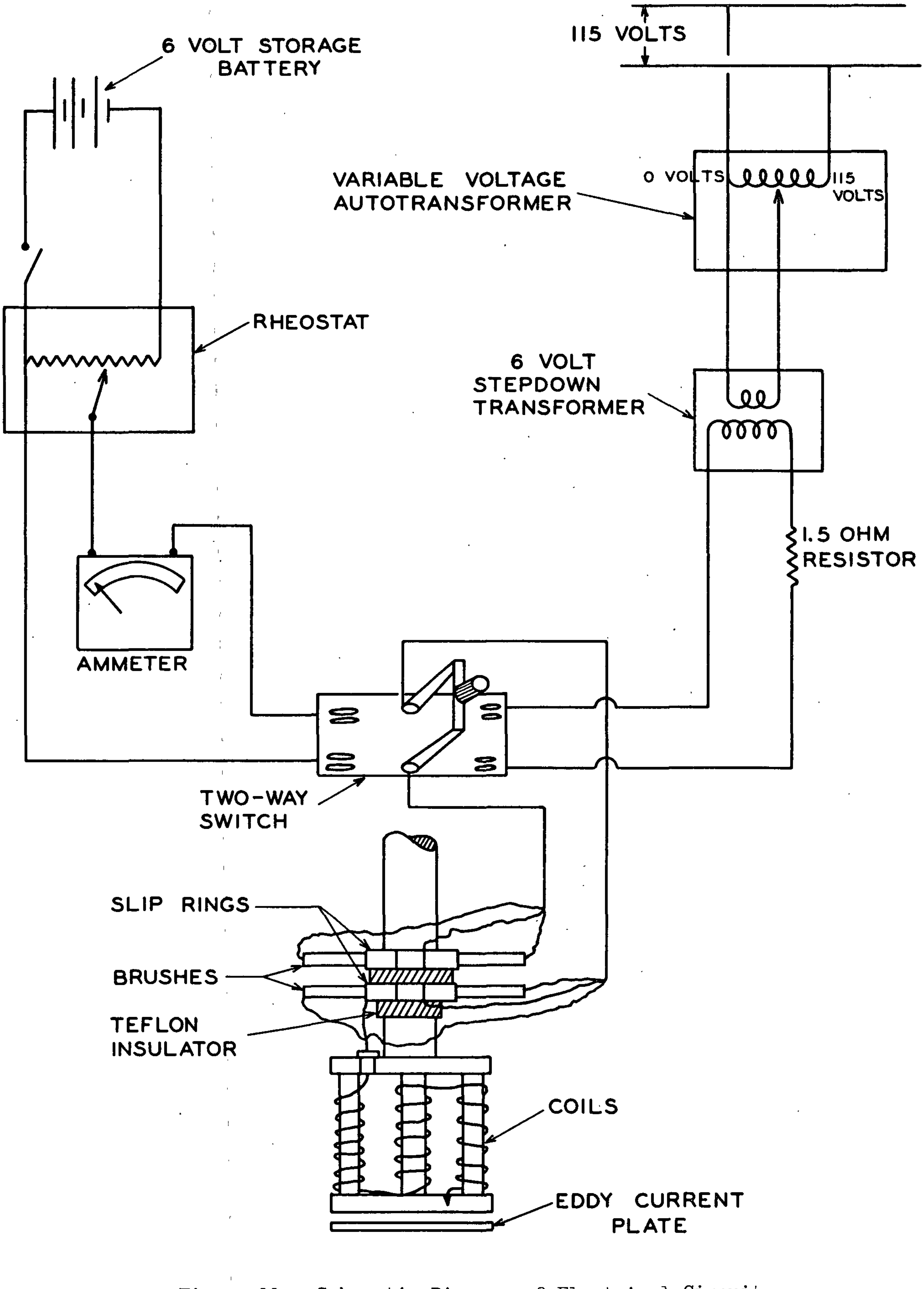

Figure 11. Schematic Diagram of Electrical Circuit of the Eddy Current Drive System

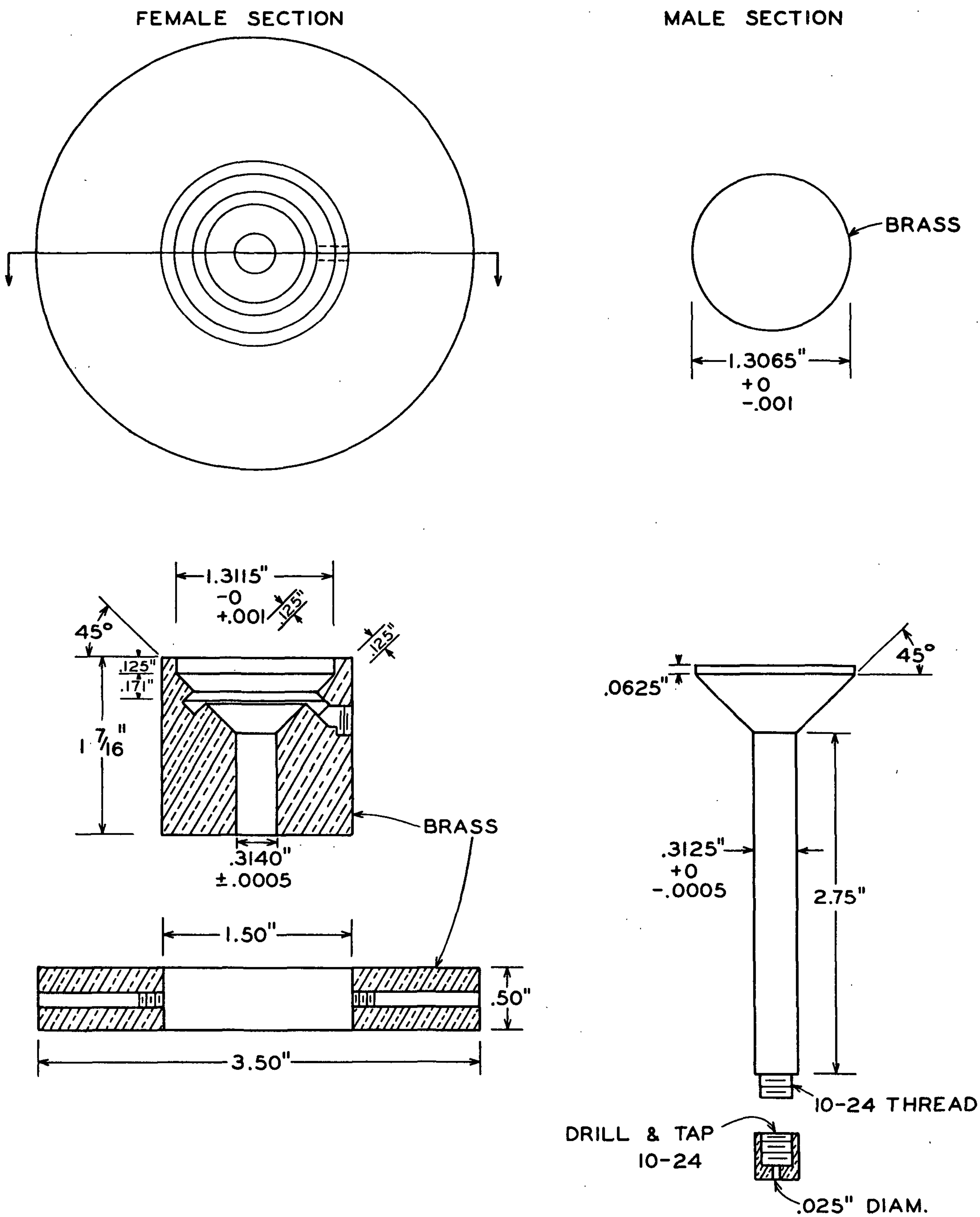

Figure 12. Air Bearing

and 1.3065 in. A 1/16-in. high, 1.3065-in. diam. cylindrical section extends from the top of the conical section. A 0.3125-in. diam., 2 3/4-in. long shaft extends from the lower part of the conical section. The end of this shaft is threaded with a 10-24 thread to enable the bob to be attached to the bearing. Either a solid shaft or a flexible cable may be attached to the shaft at this junction. It is essential that the solid shaft be very straight (less than 0.001-inch variation in concentricity over its length).

The conical section of the female part of the bearing has the same dimensions as the conical section of the male part of the bearing. Both of these parts were turned off the same lathe with the settings unchanged in order to obtain a precision fit. The top cylindrical section has a height of 0.125 in. and a diameter of 1.3115 in. The lower cylindrical section is concentric with the shaft and has a diameter of 0.3140 in. The dimensions and tolerances are shown in Fig. 12.

A 1/8 by 1/8-in. rectangular groove extends around the inner surface of the female section of the bearing. The center of this groove lies 0.296 in. from the top surface of the bearing. Air is fed into the groove through a 1/8-in. diameter channel[a] from a Conaflow Corp. flow valve (no. 5). The output range is 0-125 p.s.i.g. A U-tube manometer using tetrabromoethane as the fluid was placed between the valve and the bearing to measure the air pressure to the bearing. Water and dirt were removed from the air by a Norgren air filter (type 11200-4). The entire bearing was enclosed in a cylindrical Lucite shield (see Fig. 8) to prevent dirt and air drafts from disturbing the bearing operation.

---

[a]The air feed channel must be perpendicular to the circumference of the groove in order to eliminate any torque due to air impingement.

The operation of the bearing was checked initially by grounding one lead of an ohmmeter to the female section and dipping the other lead in a conducting solution in which the shaft of the male section was immersed. By adjusting the air pressure to the bearing, the male section was suspended on a cushion of air. If the bearing is operating correctly, the male section should not rotate and the ohmmeter should indicate infinite resistance.

BOB AND CUPS

Two bob-and-cup combinations were employed in the study. For the calibration of the instrument and for the measurement of absolute viscosities of various liquids, a 6.017-in. high, 1.961-in. diam. brass bob was used in conjunction with a 6.75-in. high, 2.191-in. diam. precision glass cup. The same bob was used with an 8-in. high, 3.75-in. diam. glass cup in the study of the flow behavior of the fiber slurries.

The bob is shown in Fig. 13, a, b, and c. It was turned out of a solid brass rod to insure uniformity. The center of the bob was hollow, leaving a wall thickness of 1/16 in. extending down 4-9/16 inches from the bob top. A 1-in. deep inverted conical section formed the bottom of the inner cavity. The brass cap and bob were threaded (24 threads per inch) and formed a leakproof fit. The nylon cable connecting the bob and the male section of the air bearing was attached to the bob by forcing it through a 0.0025-in. diam. hole in the cap. The bob and cap weighed 650 g. For use in denser liquids (sp. gr. > 2.1 g./cc.), additional weight could be added to the inner cavity of the bob.

In the study of the structural effects of concentrated slurries, a material[a] from which nylon fiber loops protruded (see Fig. 13, c) was placed around the

[a]This material is sold commercially as a synthetic garment zipper.

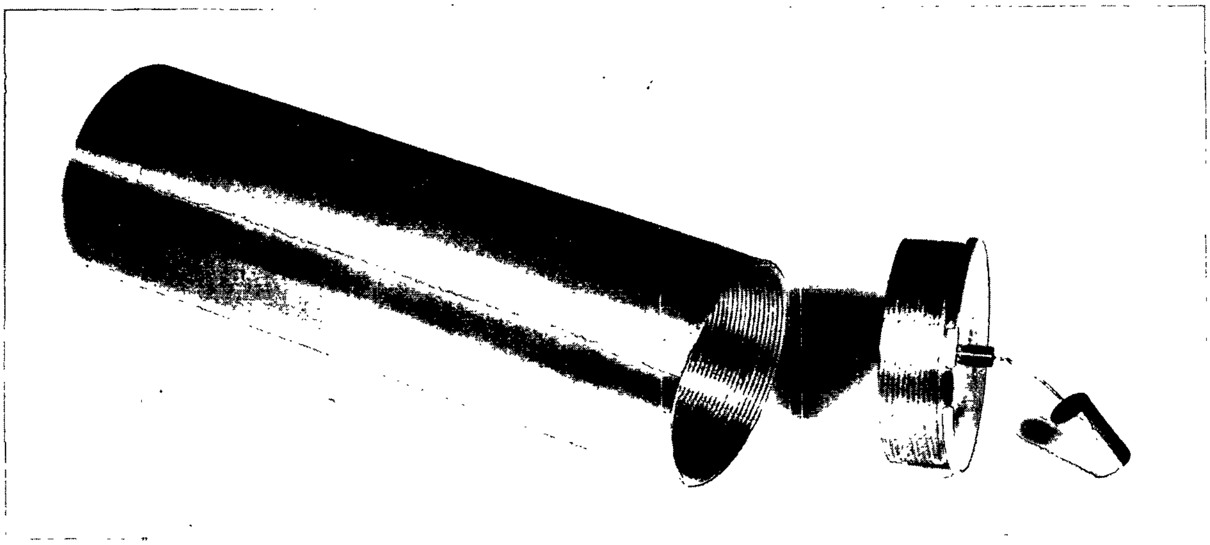

a. Bob and Cap

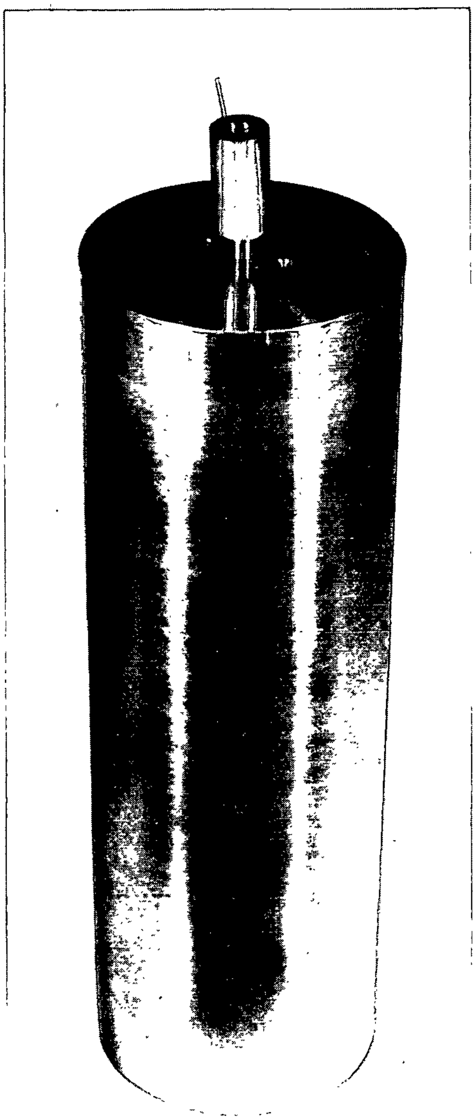

b. Bob and Cap Assembled

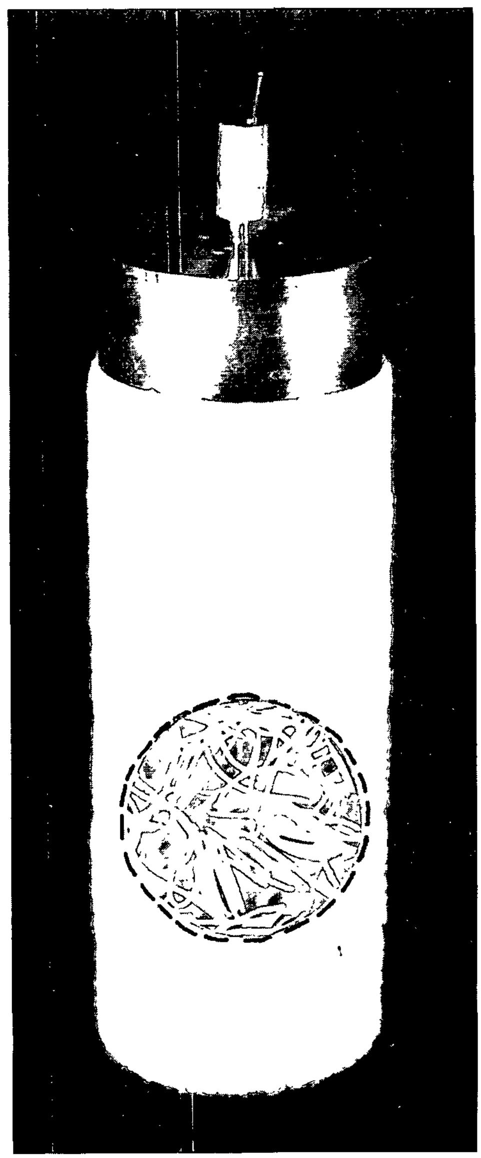

c. Bob Covered
With Nylon Loop Material

Figure 13. Viscometer Bob

outer surface of the bob and inner surface of the cup. Each loop was a nylon fiber, the diameter of which was about 55 μ. The material increased the radius of the bob by about 2 millimeters. The appearance of the surface of the material is shown in Fig. 13, c. It was hoped that the fibers in the slurries would become enmeshed in this material and slippage at the boundaries of the network would be eliminated.

The small cup (Fig. 14) was constructed by gluing with epoxy resin a right cylinder section of precision glass tubing to a flat section of Lucite. The cup was aligned concentrically with respect to the bob by means of two holes in the Lucite base which fitted over threaded pins in the frame of the instrument (see Fig. 8). The large cup shown in Fig. 14 consisted of a glass cylindrical section of precision tubing and a brass base and top. The bottom glass of the cylinder fitted over a shoulder in the base. The base was connected to the top ring by two 1/8-in. brass rods. Teflon gaskets on the top and bottom surfaces of the cylinder prevented any loss of fluid. The alignment procedure was the same for the large cup as for the small cup.

In the study of the shear stress-strain behavior of a fiber slurry, a 5-in. i.d. glass cylinder was used as the cup. It was glued to a brass plate which could be centered with respect to the bob.

OPTICAL AND ELECTRICAL SYSTEMS USED IN MEASURING THE MOVEMENT OF THE BOB

The deflection of the bob in a slurry of fibers in which structural effects were observed was obtained with an optical system shown in Fig. 15. A small mirror on the axis of the bob reflected a beam of light from a source onto a curved scale. The sensitivity of the measurement could be adjusted by varying

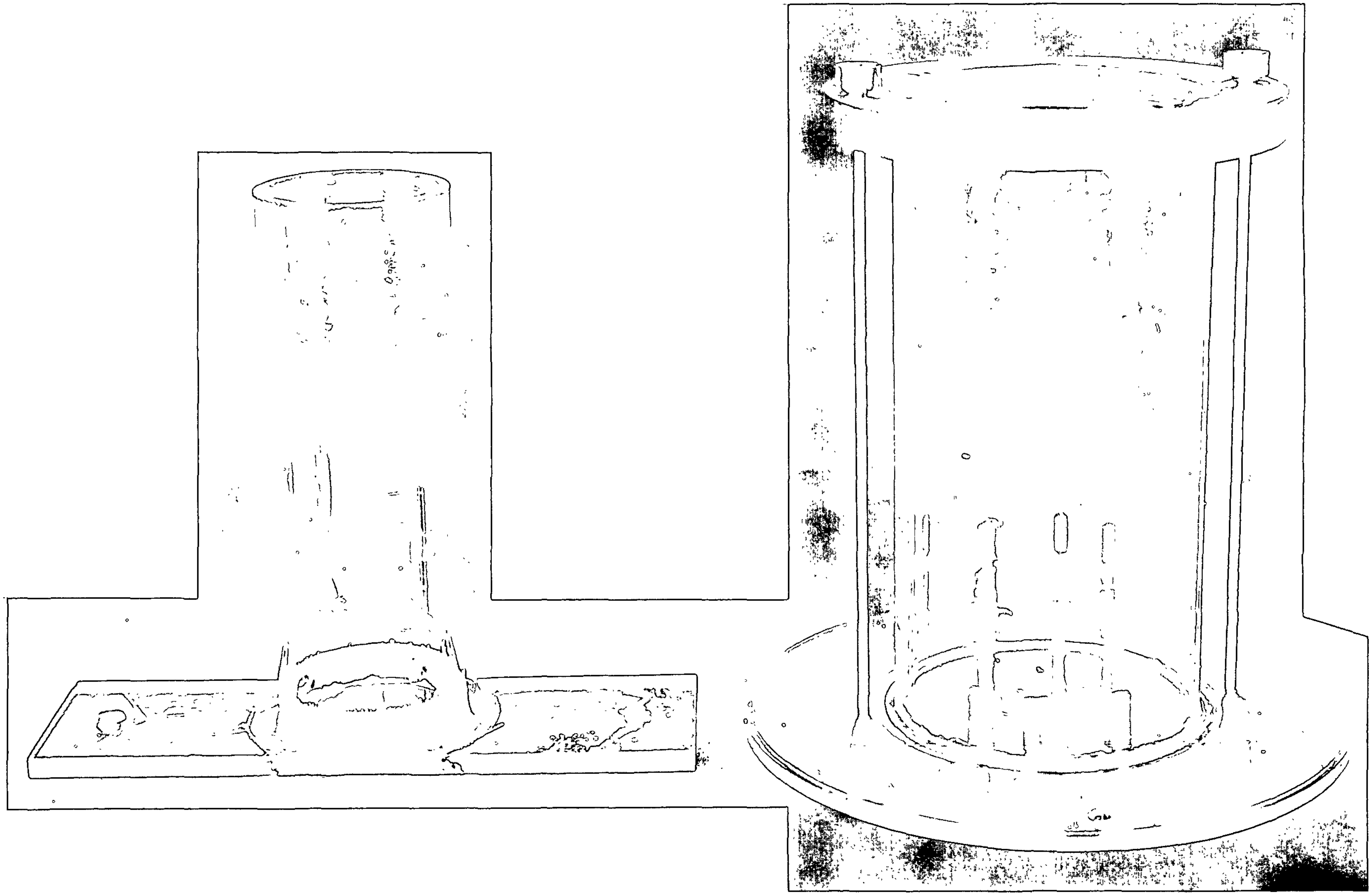

Figure 14. Viscometer Cups

the distance from the scale to the mirror. For most of the measurements, the distance was 10 inches, but for very small deflections, the distance was about 100 inches.

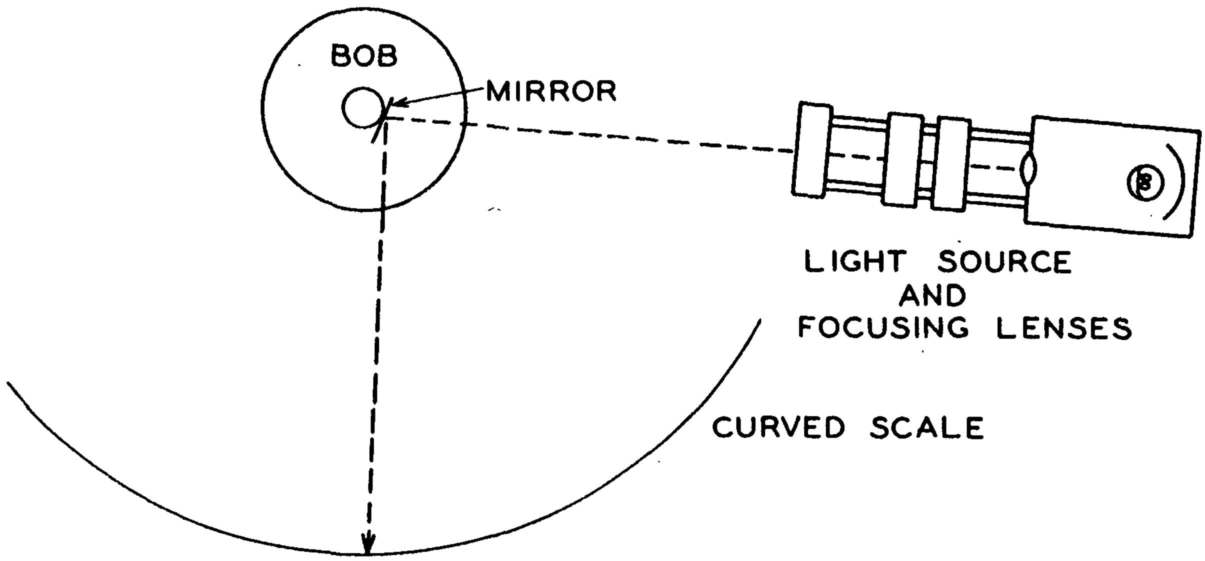

Figure 15. Optical System for Measuring Small Deflections of the Bob Under Applied Torques

It was necessary to measure the angular velocity of the bob during the study of the flow of fiber slurries with accuracy. This was accomplished by the electrical system shown in Fig. 16. A beam of light reflected from the mirror on the bob axis striking the phototube (R.C.A. 928) caused an electrical impulse to be fed to the Esterline-Angus recorder no. 84756. This resulted in a pip on the recorder chart. The time for the bob to complete one revolution could either be measured from the chart or determined with a stopwatch. With this arrangement, it was possible to determine the bob angular velocity to within 0.1%.

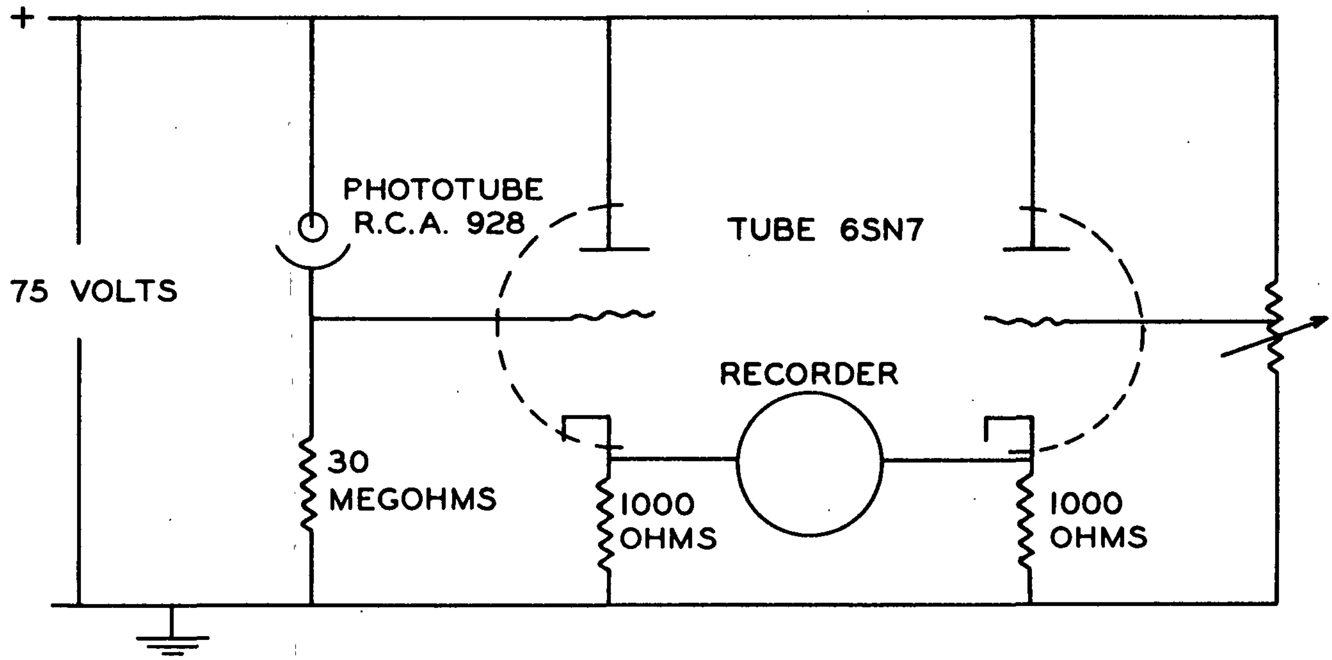

Figure 16. Circuit Used in Determining the Angular Velocity of the Bob During the Study of Fluid or Suspension Flow

EXPERIMENTAL PROCEDURES

CALIBRATION OF THE EDDY CURRENT DRIVE

The relationship between the torque output of the eddy current effect and the input current to the coils was initially determined by a static technique. A Lucite pulley wheel (1.361 cm. diameter) was fitted on the lower section of the air bearing shaft to which the bob was attached (see Fig. 17). A 45 μ diameter nylon filament was wrapped around this pulley. The free end of the filament passed through a loop in the end of another filament which was anchored to a vertical surface. Small weights were hung from the pulley filament and the current in the rotating coils was adjusted so that the bob remained at equilibrium at a position where the supporting filament formed a 45° angle with the shaft. In this position, the force due to the eddy currents was exactly equal to that exerted by the weights.

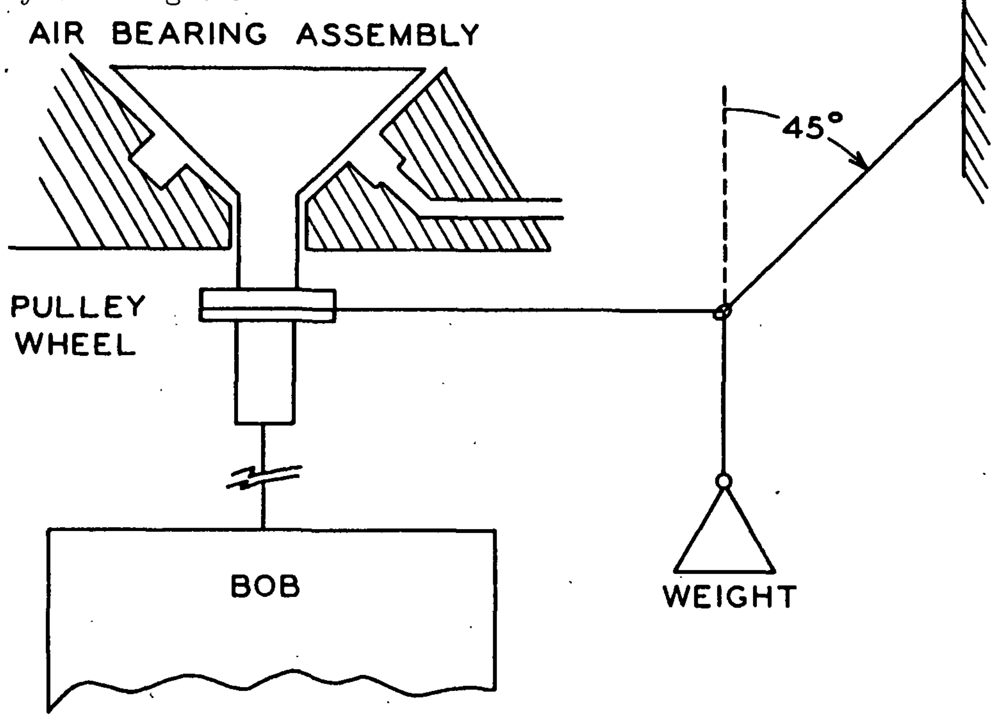

Figure 17. Static Method of Calibrating the Eddy Current Drive

Because the coils were rotated at a high rate of speed (>900 r.p.m.), it was believed that at very low bob speeds (<10 r.p.m.) the static calibration curve would apply. In order to check this hypothesis, a dynamic determination of the current torque relationship was made. The small glass cup was filled with distilled water at 73°F. The equilibrium velocities of the bob were determined for a series of coil currents. By assuming that laminar flow occurred in the annulus and that the end effects were negligible, the following equation could be used (33):

$$T = \frac{4\pi\mu_o h\omega_b}{1/r_1^2 - 1/r_2^2} \tag{46}$$

where

T = torque exerted by eddy current drive, dyne-cm.,

ω_b = bob angular velocity, rad./sec.,

μ_o = viscosity coefficient, g./cm.-sec.,

h = bob height, cm.,

r_1 = radius bob, cm., and

r_2 = cup radius, cm.

The data from these determinations are shown in Fig. 19 in the Results and Discussions, and tabulated in Table X in Appendix II. The good agreement between the two techniques showed that the assumption was correct that at low bob speeds the static and dynamic techniques were equivalent.

DETERMINATION OF THE FLOW BEHAVIOR OF FIBER SLURRIES

After the densities of the fibers had been determined by the procedure discussed in the Fiber Selection and Characterization section, a given volume of the organic solution was prepared with the same density as the fiber sample to be studied. Enough fibers were weighed out and placed in the solution to yield the highest concentration desired for study. The suspension was then deaerated for an hour and poured into the annulus formed by the bob and the 3.75-in. diameter cup. Care was taken to prevent air bubbles from entering the slurry during this procedure. The fibers were distributed throughout the annulus by a small stirrer constructed by soldering a 3/8-in. diameter brass propeller on the end of a speedometer cable sheathed in Tygon tubing. This stirrer permitted the slurry to be thoroughly mixed while it was in the annulus. One-half hour was allowed for the fluid eddy currents to subside and then a very low torque was applied to the bob. As soon as the bob reached an equilibrium velocity, the applied current, the temperature in the chamber, and the time per bob revolution were recorded. The torque level was then increased by a given amount and after the bob had reached a constant velocity, the above data were recorded again. This procedure was repeated until the desired range of torques had been covered. Initially, as many as 15 torques were used to make one run, but after it had been established that the flow in the annulus was Newtonian at the low consistencies, only two or three torque values were required.

The consistency was changed by withdrawing a known volume of slurry from the annulus, filtering off the fibers, and deaerating the filtrate which was returned to the annulus. The volume of the suspension in the annulus was kept constant by the addition of fresh solution to replace the volume of the fibers and solution lost in the filtration process. The slurry was then stirred and the procedure was begun again. The viscosity of the solution was checked in an Ostwald viscometer between runs at the different consistencies. Only when the suspension had been left overnight were any changes observed. The viscosity of the solution increased. This increase was felt to be a result of evaporation of some of the tetrachloroethane. In making calculations of the relative viscosities of suspensions, the change in Ostwald viscosity was used to correct the viscosity of the pure solution.

Some preliminary experiments showed that the organic solution could be removed from the fibers by washing them with carbon tetrachloride. Two liters of carbon tetrachloride were used to wash 2 grams of fiber. Most of the carbon tetrachloride was removed from the pad by filtration. The fibers were then spread out in a weighing dish and allowed to equilibrate with a 73°F., 50% R.H. atmosphere.

DETERMINATION OF THE STRESS-STRAIN BEHAVIOR OF FIBER SLURRIES EXHIBITING STRUCTURAL EFFECTS

The slurry preparation was exactly the same as that used for the flow studies except that a sucrose solution was used instead of the organic solution. This solution was placed in the space between the bob and the cup, both of which had been covered with the nylon material with loops. Large flocs were broken up by the stirring procedure. Then a torque was exerted on the bob and the instantaneous deflection was observed. After increasing the torque by a small amount, the instantaneous deflection was again recorded. This procedure was carried out until the network yielded completely and the bob turned freely in the slurry. When recovery runs were made, the torque was reduced in steps and the resulting recovery was measured. In those runs in which the bob would not move under any torque or would turn freely when a small torque was placed on it the run was halted. The slurry was then restirred and the stress-loading procedure was started again.

RESULTS AND DISCUSSION

INTRODUCTION

The objectives of this thesis are such that it is convenient to divide the Results and Discussion into three sections. The first section deals with the performance of the special viscometer. This includes the variables affecting its performance, the stability of flow in the instrument, and the range of shear stresses and shear rates attained with it. The next section is concerned with the use of this apparatus for the determination of the flow behavior of fiber suspensions. This behavior is discussed initially from a phenomenological viewpoint. The phenomenological data and the visual observations of the behavior of the fiber phase are then employed to develop a theory for the actual flow behavior of the fluid phase. Where possible, the data are compared to existing theories (16, 17) of suspension flow. The last part of the Results and Discussion evaluates the techniques used in determining the shear stress-strain behavior of concentrated slurries of synthetic fibers which exhibit structural properties. Data are presented for comparison with the relationships developed in the Theoretical Considerations.

PERFORMANCE OF THE CONCENTRIC CYLINDER VISCOMETER

OPERATION VARIABLES

The two variables which were felt to be most important in governing the operation of the viscometer were:

(1) The air pressure to the gas bearing, and

(2) The relative speed between the coils and the eddy current plate.

By increasing the pressure to the gas bearing above that necessary to support the suspended weight, an increase in the torque on the bob was observed. If the air inlet to the bearing were perpendicular to the surface of the male section of the bearing and if this section were concentric about the vertical axis, there should be no torque due to the air jet. However, in the construction of the apparatus, slight deviations from the ideal design occurred resulting in the air jet torque.

If the pressure to the bearing was adjusted to just raise the male section of the bearing so that it did not contact the female section (see Experimental Equipment), the air torque was minimized. However, the lower limit of the operating range of the instrument was restricted by this "air drive." This effect made it extremely difficult to calibrate the instrument accurately at low torques (less than 2 dyne-cm.). Also, at very low bob velocities, the torque due to the air appeared to be dependent upon the speed. However, the effect did not limit the usefulness of the instrument because all significant data were taken at torques greater than 2 dyne-cm. and relatively high velocities (>0.1 rad./sec.) where the effect was considered negligible. In order to keep the torque due to the air at a minimum the pressure just necessary to support a given weight was determined for a series of weights encompassing the range of interest.

Figure 18 shows the relationship between the suspended weight and the pressure required to freely support the weight. This relationship was used as a guide throughout the experiments. The data are tabulated in Appendix IV, Table IX.

The effect of the relative velocity between the coils and the eddy current disk was evaluated during the calibration procedure. If changes in the bob angular velocity over the range of velocities employed in this work (0.1-2 radian

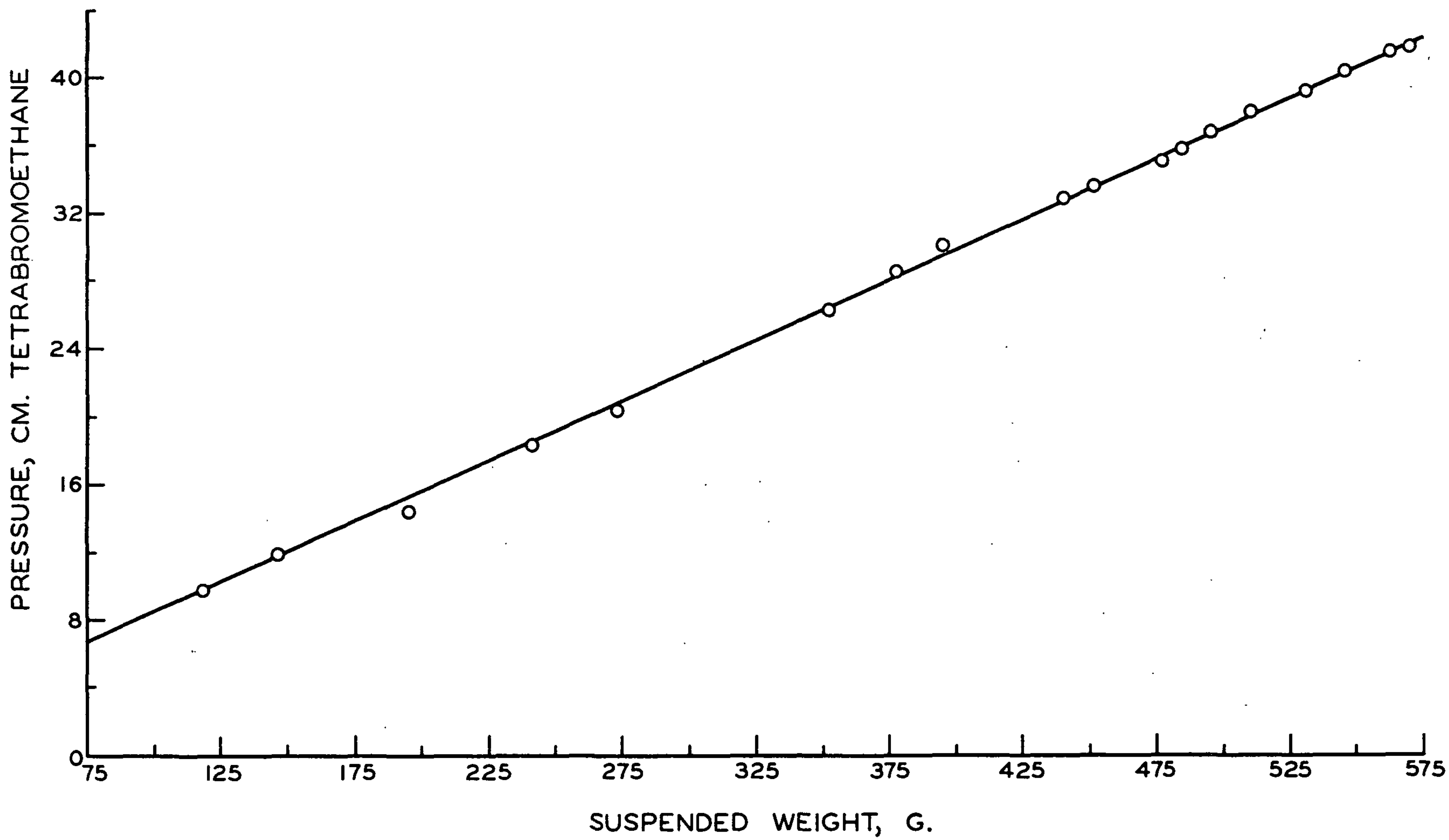

Figure 18. Air Pressure in Bearing Required to Support a Given Weight

per second) caused a subsequent change in the current-torque relationship for the instrument, then the static and dynamic calibrations would have been different. This was not the case, as is evidenced by the data in Fig. 19 (see Appendix IV, Table X).

This relationship also shows that the instrument may be used as an absolute viscometer for liquids having viscosities in the centipoise range. The end effect appears to be very small (less than 0.5%) and this is in agreement with the results of Lindsey and Fisher (10) for a narrow annulus viscometer with a long bob, the bottom of which is at least 1 cm. from the bottom of the cup. Even better accuracy would be expected if the bottom of the bob were constructed so that the flow near this region could be specified more exactly. Eisenberg (31) used a large-angle conical bottom on his viscometer and indicated how it was accounted for theoretically.

REPRODUCIBILITY OF DATA

Various liquids which were employed at one time or another in the work were studied in the apparatus. The torque-angular velocity relationships for water and for sucrose solutions (33 and 38% sucrose by weight) were determined in the small annulus viscometer. The reproducibility of the measurements was ± 0.20%. The viscosity of water calculated from the dimensions of the apparatus and employing the static torque-current relationship was less than the value reported in the literature (34) by only 0.30%. The viscosity of the sucrose solution as measured in the small annulus viscometer agreed with the viscosity calculated from measurements with an Ostwald viscometer to within + 3%. The larger variation observed in the study of the sucrose solution was felt to be due to cumulative errors in the use of the Ostwald viscometer and the preparation of the "standard"

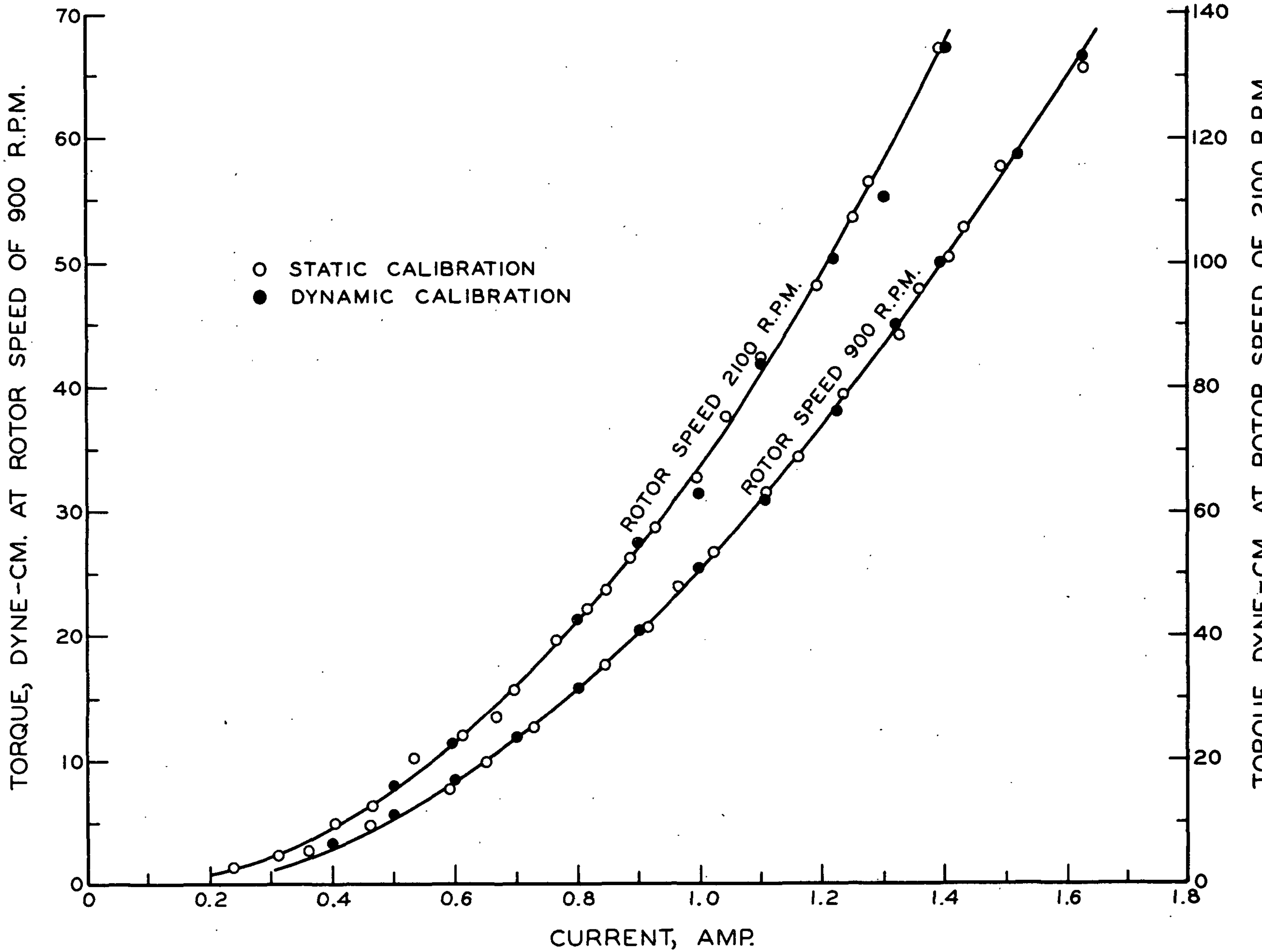

Figure 19. Calibration Curve for Eddy Current Drive

1.15 sp. gr. sucrose solution. The torque-angular velocity relationships for water and the sucrose solution in the narrow annulus viscometer are respectively shown in Fig. 20 and 21. The linearity of the plots indicates laminar flow over the designated velocity ranges.

The reproducibilities of the torque-angular velocity relationships in the 3.75-in. diameter cup for the low-viscosity liquids (water, tetrachloroethane and the tetrachloroethane-tetrabromoethane-mineral oil solution) were $\pm$ 1.5, $\pm$ 0.6, and $\pm$ 1.5%, respectively. The relationships are represented in Fig. 22 and 23. The higher deviations encountered in the determinations for the first two liquids resulted from the necessity of employing low torques (and thus low angular velocities) to cover the laminar flow region. It has already been noted that the instrument calibration is subject to error in this range. The reproducibility of the runs with the higher viscosity solutions--the tetrachloroethane-mineral oil solution (see Fig. 25) and the sucrose solution (see Fig. 24)--was $\pm$ 0.13%, for three determinations with each solution. Laminar flow was observed over the range of angular velocities studied. The experimental data for the runs with the pure liquids are listed in Appendix IV, Tables XI, XII, XIII, XIV, and XV.

The deviation from linearity of the $\underline{T}$-$\omega_{\underline{b}}$ data at low torques (Fig. 21, 22, and 24) probably results from the air torque in the bearing and the errors in the calibration procedure in this torque range. However, there were some indications that the sucrose solutions did not exhibit a flow behavior consistent with that of the other liquids. Such behavior could also contribute to the deviation of the data from nonlinearity. The observations of the behavior of the sucrose solutions are discussed in more detail in Appendix III.

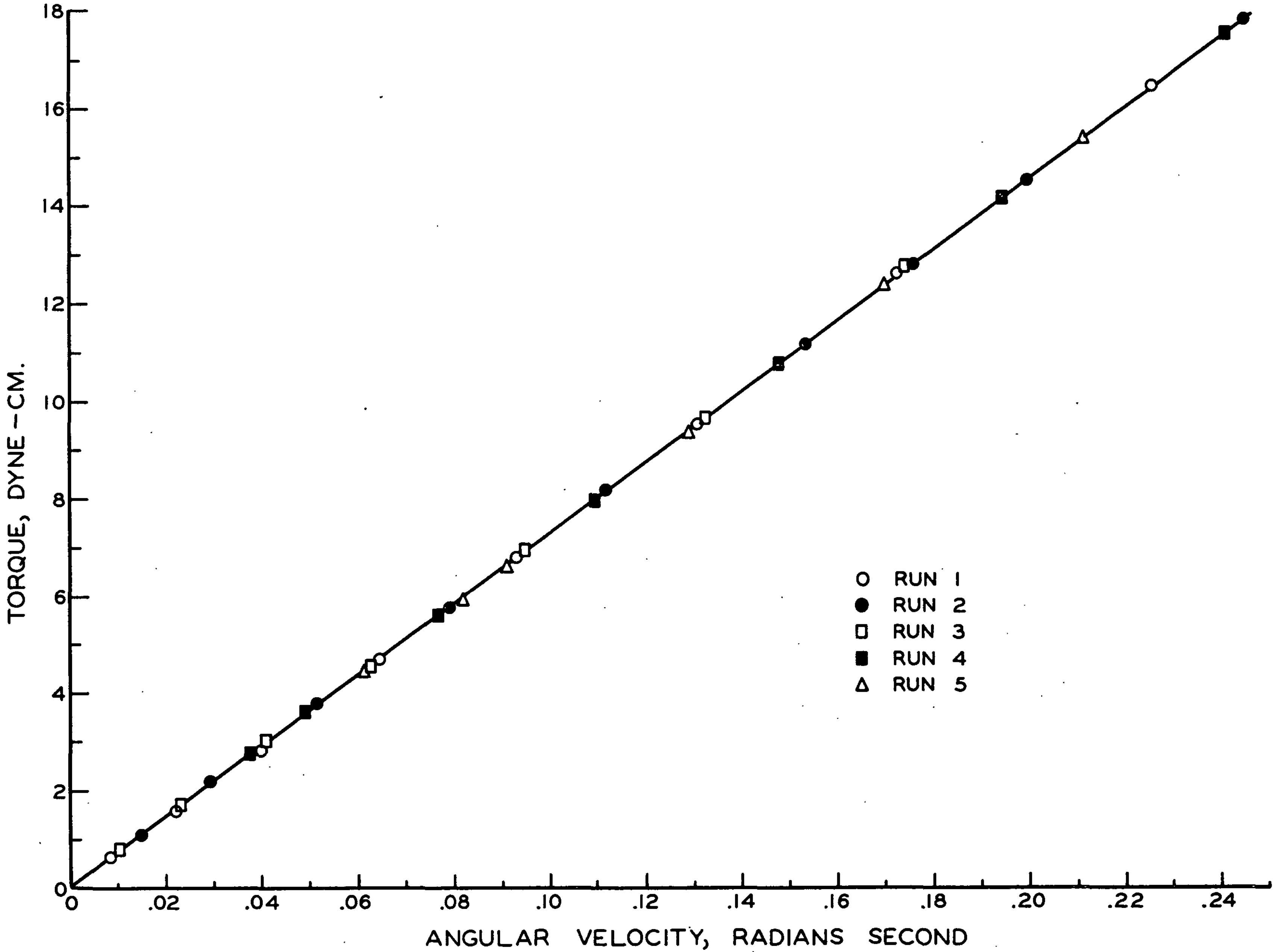

Figure 20. Torque-Angular Velocity Relationship for Water in the Small Annulus Viscometer

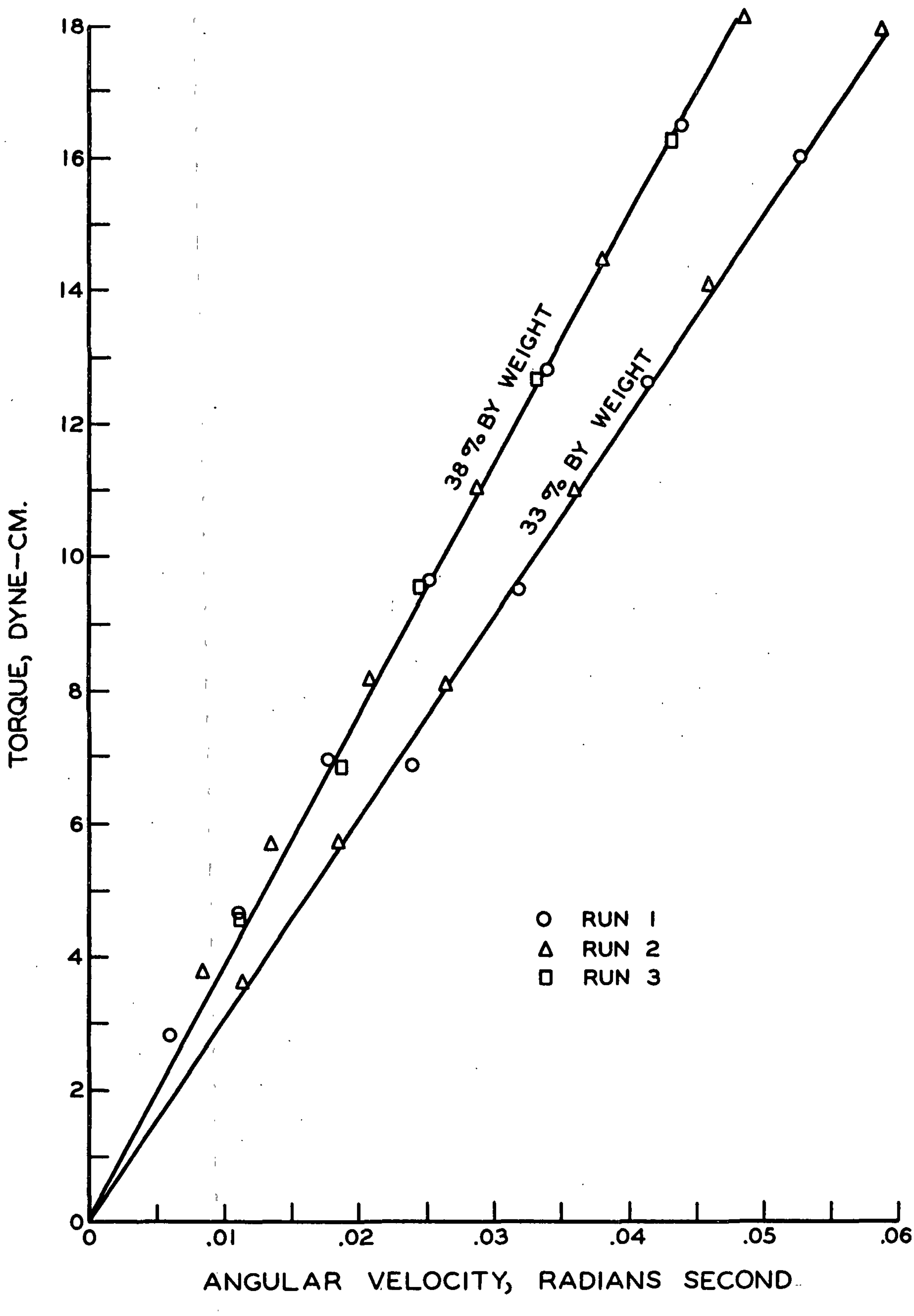

Figure 21. Torque-Angular Velocity Relationships for Sucrose Solutions in the Small Annulus Viscometer

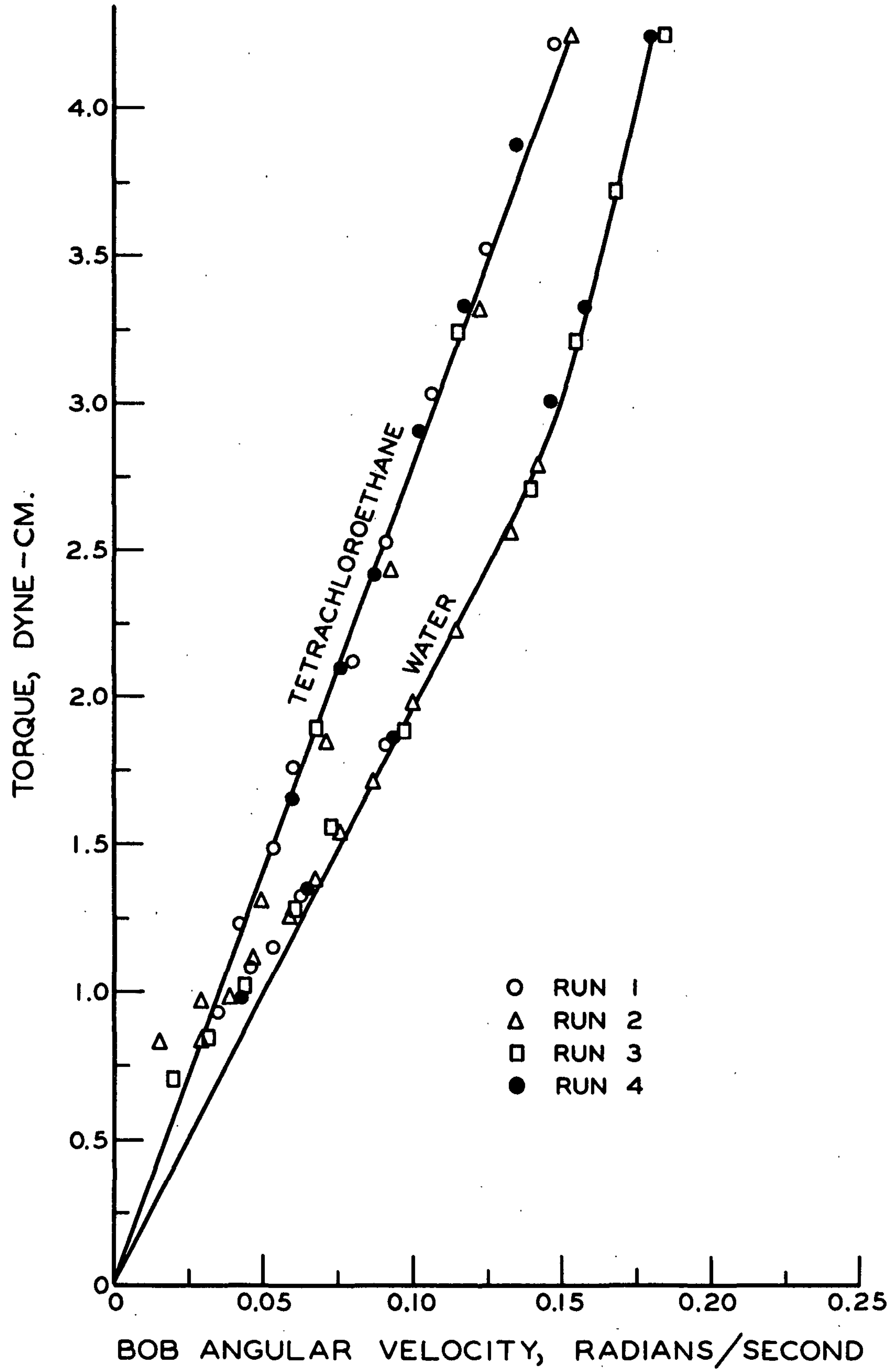

Figure 22. Torque-Angular Velocity Relationship for Low Viscosity Liquids in the Large Annulus Viscometer

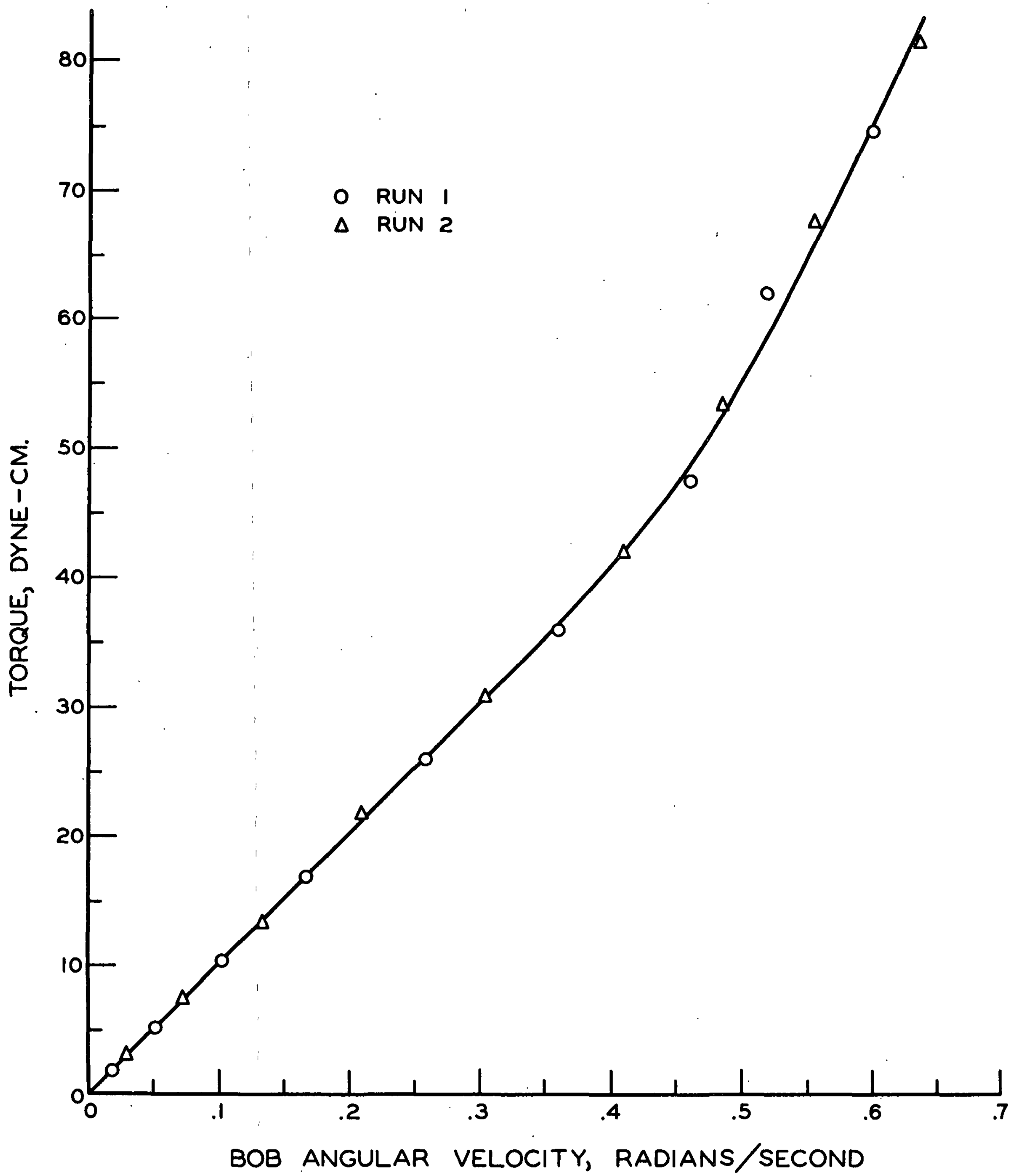

Figure 23. Torque-Angular Velocity Relationship for a Solution of Tetrachloroethane, Tetrabromoethane and Mineral Oil (sp. gr. ca. 2.60) in the Large Annulus Viscometer

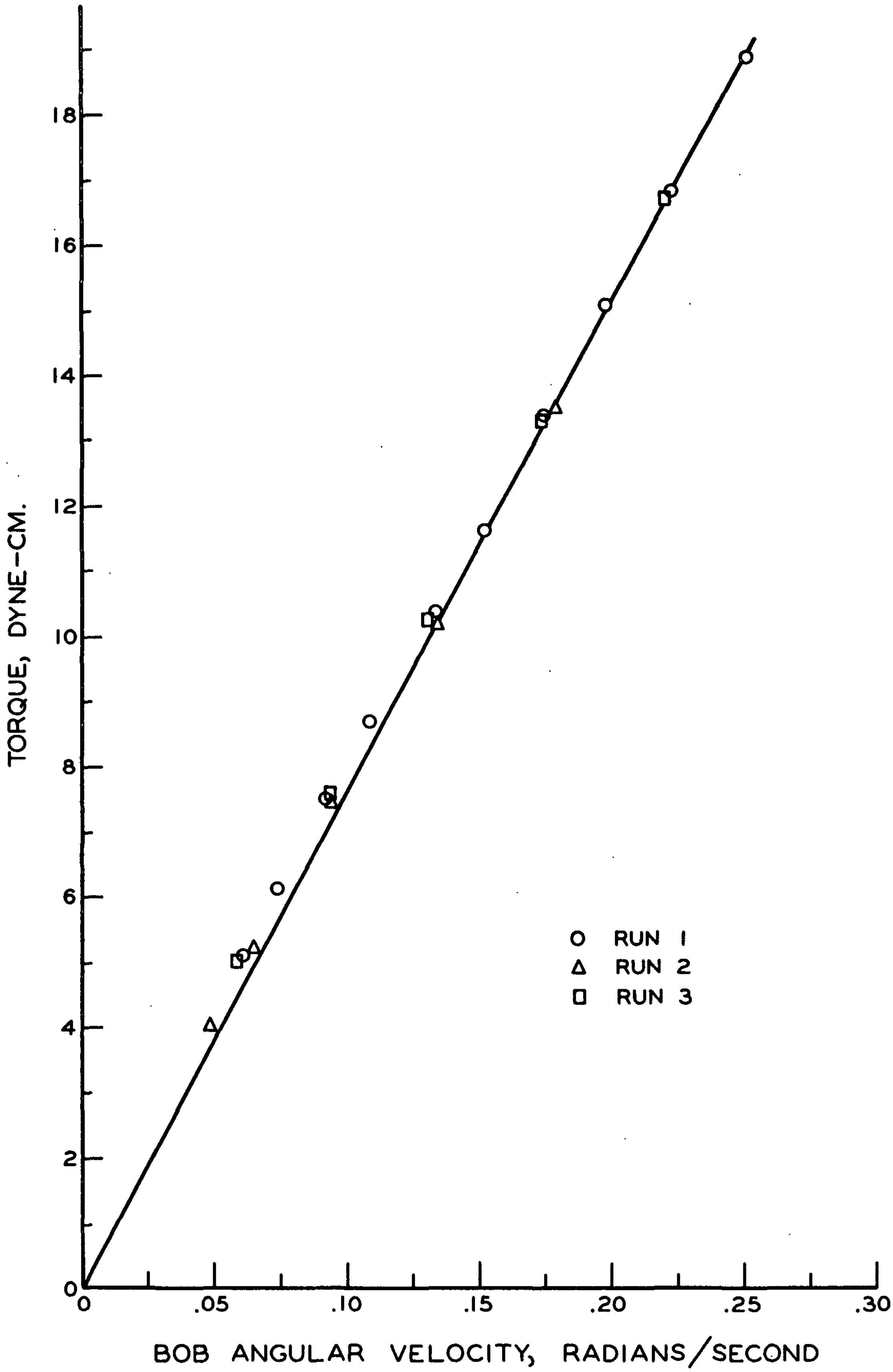

Figure 24. Torque-Angular Velocity Relationship for a Sucrose Solution (ca. 1.14 sp.gr.) in the Large Annulus Viscometer

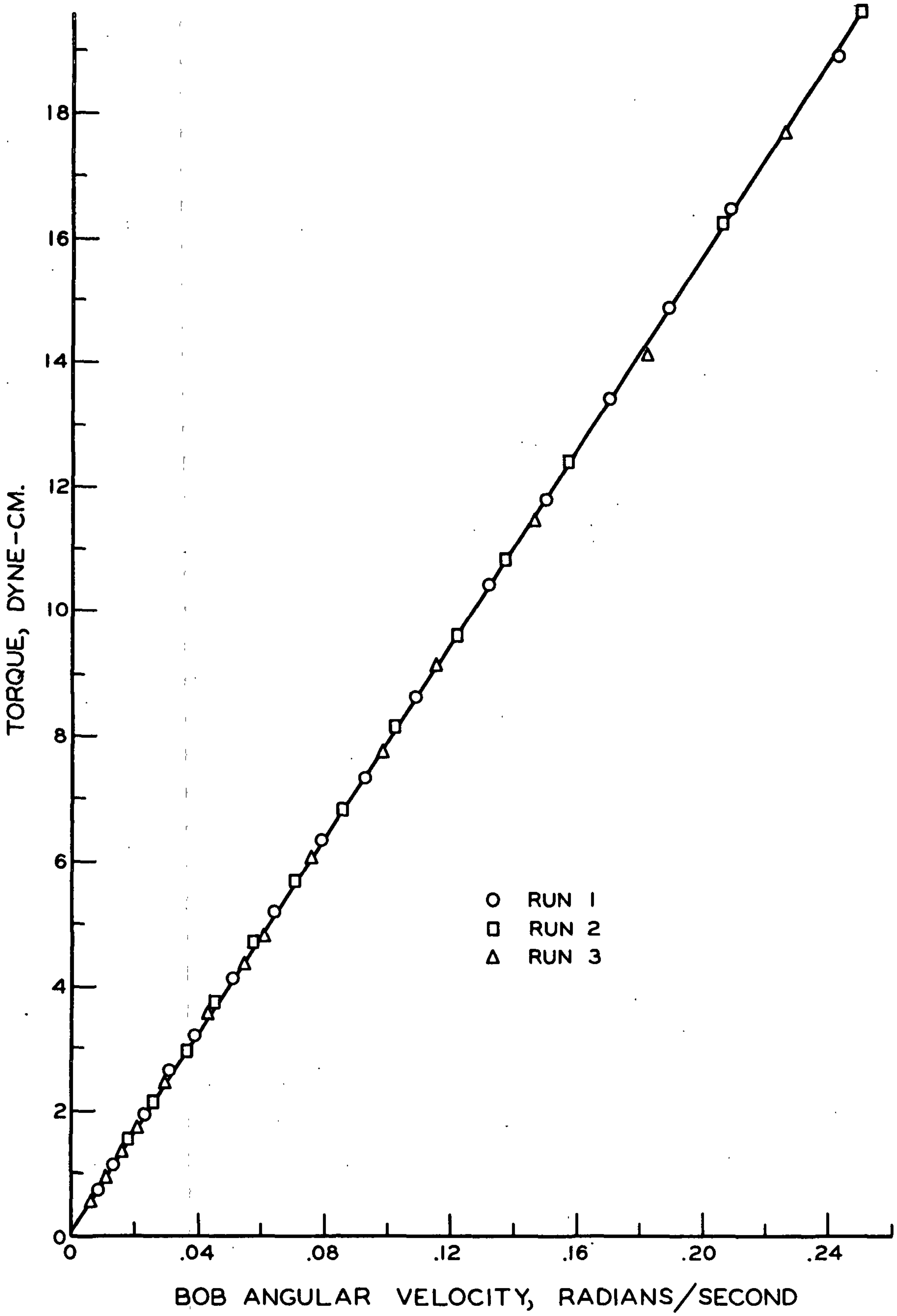

Figure 25. Torque-Angular Velocity Relationship for a Solution of Mineral Oil and Tetrachloroethane (ca. 1.14 sp.gr.) in the Large Annulus Viscometer

STABILITY OF FLOW IN THE INSTRUMENT

Taylor (35) has treated the flow between rotating concentric cylinders both theoretically and experimentally. His equation for the angular velocity, ω_b, of the inner bob, at which instability occurs in the annulus, is as follows:

$$\omega_b = \sqrt{\frac{\frac{1}{2}(r_1 + r_2)\mu_o^2}{r_1^2 D^2 \rho^2} \times \frac{\pi^4 f_o}{0.0571 f_o^2 + 0.00056}} \qquad (47)$$

where

$\underline{r}_1$ = radius of inner cylinder,

$\underline{r}_2$ = radius of outer cylinder,

$\underline{D}$ = annulus width, $\underline{r}_2 - \underline{r}_1$,

$\underline{f}_o$ = $1 - 0.652(\underline{D}/\underline{r}_1)$,

μ_o = fluid viscosity, and

ρ = fluid density.

This equation was derived by assuming that $\underline{D}/\underline{r}_1$ was small. However, Lewis (36) showed that it holds up to an annulus width-bob radius ratio of 0.71. Whether or not the flow in a viscometer follows the above equation would be an indication of the precision in the construction and alignment of the apparatus. If the cylinders are not accurately formed and mounted concentrically and if the bob length-to-radius ratio is not sufficiently large, instability will occur at a much lower velocity than predicted by the above equation.

The critical bob angular velocity data obtained in this study for the various liquids in the two different diameter cups are reported in Table II. For viscous flow in the annulus of a concentric cylinder viscometer, the torque is directly proportional to the bob angular velocity [see Equation (46)]. When turbulent flow occurs, inertia forces become appreciable. By analogy with the flow in pipes, these forces should be nearly proportional to the fluid velocity squared. Therefore, when unstable flow involving inertia forces occurs in a viscometer annulus, the relationship between the torque $\underline{T}$ and the angular velocity ω would be expected to be nonlinear. Such nonlinearity above a given $\omega_{\underline{b}}$ is shown by the data in Fig. 22 and 23. The bob angular velocities (Table II) at which the inertia forces became appreciable in the various liquids were taken as the velocity value between the last angular velocity where the ratio $\underline{T}/\omega_{\underline{b}}$ was constant and that where $\underline{T}/\omega_{\underline{b}}$ increased by an amount greater than that due to experimental error. The data were taken over small enough angular velocity intervals so that an accurate value of the critical velocity was obtained.

TABLE II

ACTUAL AND PREDICTED CRITICAL VELOCITY

Liquid	Cup Diameter, in.	Liquid Density, g./cc.	Liquid Viscosity, poise	Critical Angular Velocity, radians/second	
				Predicted	Observed
Water	2.20	1.000	0.00933	2.13	2.17
Water	3.75	1.000	0.00933	0.13	0.142
Sucrose soln.	2.20	1.140	0.0389	7.78	0.35[a]
Sucrose soln.	3.75	1.140	0.0389	0.476	0.469
Tetrachloroethane	3.75	1.583	0.0163	0.145	0.147
Tetrachloroethane-mineral oil soln.	3.75	1.140	0.0702	0.859	0.794[a]
Tetrachloroethane-tetrabromoethane-mineral oil soln.	3.75	2.600	0.0510	0.264	0.262
Tetrachloroethane-tetrabromoethane-mineral oil soln.	3.75	2.75	0.0628	0.318	0.286[a]
Tetrachloroethane-tetrabromoethane-mineral oil soln.	3.75	2.83	0.0705	0.351	0.360

[a]The values represent the maximum angular velocities attained during the experiments. The flow was observed to be stable at least up to these values.

The agreement between the experimental results and those predicted by Taylor's equation is felt to be very good. The data appear to indicate that Taylor's equation is valid up to an annulus width-bob radius ratio of 0.75. The fact that the observed velocities came very close to the predicted velocities indicates that the apparatus was properly designed and precisely constructed.

When the inner cylinder of a concentric cylinder apparatus is rotated, the flow does not immediately become completely turbulent when instability occurs, but goes into another mode of laminar motion. Taylor (35) injected dye into the annulus of his viscometer and photographed the resulting flow patterns. During laminar flow, the dye formed a colored layer around the bob. A few seconds after instability had occurred, this layer was broken up into films whose planes were perpendicular to the axis of rotation. These planes of colored liquid were separated by a distance equal to the width D of the annulus (see Fig. 26).

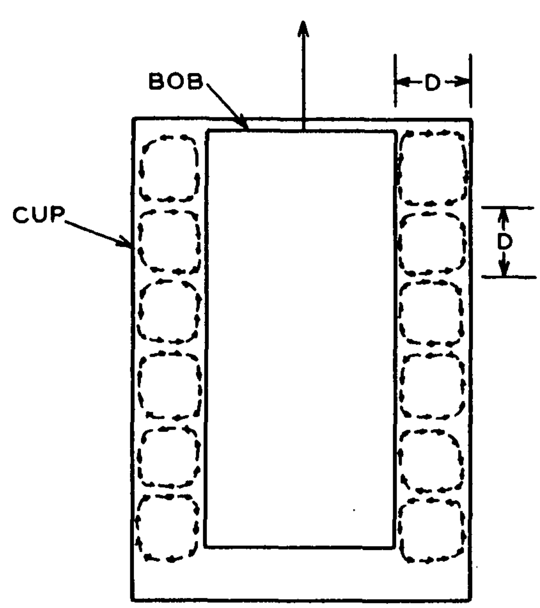

Figure 26. Flow Pattern at Onset of Instability in a Concentric Cylinder Viscometer When the Inner Cylinder is Rotated (Cross Section Bob and Annulus)

During the initial studies of the flow of fibers suspended in a sucrose solution, a similar pattern of flow was observed. The fibers became extremely oriented in the horizontal planes of flow bounding cells of fibers which were randomly oriented. These horizontal bands were so distinct that it was possible to measure the distance between them, thus reconfirming Taylor's observation that the distance was equal to the annulus width.

THE FLOW BEHAVIOR OF FIBER SUSPENSIONS

PHYSICAL CHARACTERISTICS OF THE FIBERS

The diameter, density, and elastic modulus of the fibers used in the flow study are summarized in Table III. The lengths and axis ratios of the fibers are listed in Table IV. The precision of the determinations in Table III was better than 3%. Therefore, the values in parentheses represent fairly accurately the variation in the properties of the fibers within the same yarn. Enough fibers were characterized so that the uncertainty in the mean value of a property given in Tables III and IV was less than 2%.

The organic solutions in which the fibers were suspended had only a slight effect on the physical properties. The study of the modulus change of Sample 680 brought about by immersion showed an increase of approximately 7% in the modulus. This increase was probably caused by dehydration of the fiber by the solution. The diameter determinations of fibers soaked in the organic solution showed a 0.2% decrease under the diameters measured at 73°F., 50% R.H. However, as indicated later in the section on the flow of fiber slurries, the use of the modulus data for interpreting the results is quite limited. Actually, only an order of magnitude of the modulus was required for the analysis. The data could be of greater

TABLE III

PHYSICAL CHARACTERISTICS OF FIBERS USED IN FLOW OF FIBER SLURRIES STUDY

Manufacturer's Code Number	No. of Fibers in Yarn	Diameter, microns	Density, g./cc.	Modulus of Elasticity, dynes/sq. cm. x 10^{-10} Tensile 73°F., 50% R.H.	Tensile In Solution	Bending 73°F., 50% R.H.
Nylon						
11925	34	14.98 (0.95)[a]	1.202	0.77 (0.13)	--	2.66 (0.33)
260-1-17-7-300	17	44.85 (2.74)	1.146	4.25 (0.13)	1.12[c] (0.05)	5.27 (0.31)
680	34	16.79 (0.62)	1.150	3.89 (0.20)	4.20[d] (0.20)	4.72 (0.54)
P-1643-67-2	34	14.95 (1.28)	1.206	1.18 (0.70)	--	1.85 (0.54)
P-1643-67-3	10	43.86 (4.31)	--	0.91 (0.07)	--	2.16 (0.16)
P-1643-67-6	1	75.45 (1.17)	1.142	3.50 (0.30)	--	4.81 (0.26)
Glass						
O.C. 13.35[b]	--	12.86 (0.94)	2.56	72.70 (1.28)	--	--

[a]Numbers in parentheses represent standard deviation of measurements.

[b]Data obtained by R. L. Jones (17).

[c]In a 1.14 sp. gr. sucrose solution.

[d]In a 1.14 sp. gr. tetrachloroethane-mineral oil solution.

TABLE IV

FIBER LENGTHS AND AXIS RATIOS OF FIBERS USED IN FLOW OF FIBER SLURRIES STUDY

Sample No.	Weighted Mean Length, mm.	Axis Ratio
11925-2.5	2.73 (0.12)	182.2
11925-2.0	1.700 (0.11)	113.5
(P-1643-2)-1	0.98 (0.08)	65.6
260-6	6.08 (0.27)	135.6
260-4	4.23 (0.38)	94.3
260-2.42	2.53 (0.08)	56.4
260-1.5	1.69 (0.10)	37.7
260-0.9	1.00 (0.13)	22.3
680-2.5	2.73 (0.12)	162.6
680-2.0	1.70 (0.11)	101.3
680-1.0	0.98 (0.08)	58.4
680-0.6	0.60 (0.08)	35.7
680-0.4	0.39 (0.11)	23.2
(P-1643-6)-2.5	2.73 (0.12)	36.2
(P-1643-6)-1.5	1.70 (0.11)	22.5
(P-1643-3)-2.5	2.73 (0.12)	62.2
O.C. 13.35	0.98 (0.08)	76.21

Note: Numbers in parentheses represent standard deviation of measurements.

importance if the results of this work are compared with the results of an extension of the flow study to such systems as pulp fiber slurries.

The fiber length data in Table IV indicated that the use of the razor blade cutters provided a method of obtaining a sample of fibers with a very narrow length distribution. Because a razor blade was employed in the microtoming procedure, the relatively high deviation in the length determinations for Samples 680-.6 and 680-.4 were observed. The blade would visibly bend as it passed through the embedded fibers, cutting at an angle rather than perfectly horizontal. For these two samples, at least 500 fibers were measured, so the average tabulated is felt to be representative.

The appearance of typical samples of the high-modulus fibers is shown in Fig. 27. The short fibers of Samples 680-.6 and 680-1.2 appear to be very uniform with only slight curvature. The 680-.6 fibers were cut with the microtome procedure, while the 680-1.2 fibers were cut with the razor blade cutter. The photomicrograph of the medium-diameter fiber, Sample 260-2.42, shows fibers of greater curvature, probably because of the longer lengths. The largest diameter fibers, represented by Sample P-1643-67-6, are quite cylindrical in shape. Some of the fibers do exhibit some nonuniformities along the length. The ends of the fibers do not appear to have been damaged by the cutting procedure.

The lower modulus samples and the glass fiber sample are shown in Fig. 28. Extreme curvature occurs in the fibers of Sample P-1643-67-2. Because these fibers were drawn especially for this work rather than for commercial use, it is believed that stresses set up in the drawing procedure caused the curvature. The fibers of the low-modulus sample, P-1643-67-3, do not exhibit such curvature and have shapes comparable to the higher modulus fibers (Sample 260-2.42), the average diameter of

Nylon Sample 680-.6 Magnification 40X
d=16.79 μ L=0.60 mm. L/d=35.7

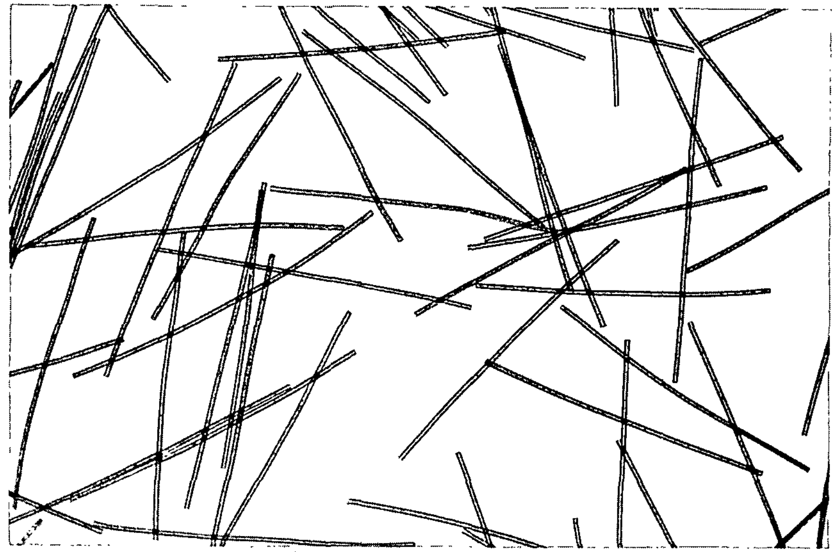

Nylon Sample 680-1.0 Magnification 42X
d=16.79 μ L=0.98 mm. L/d=58.4

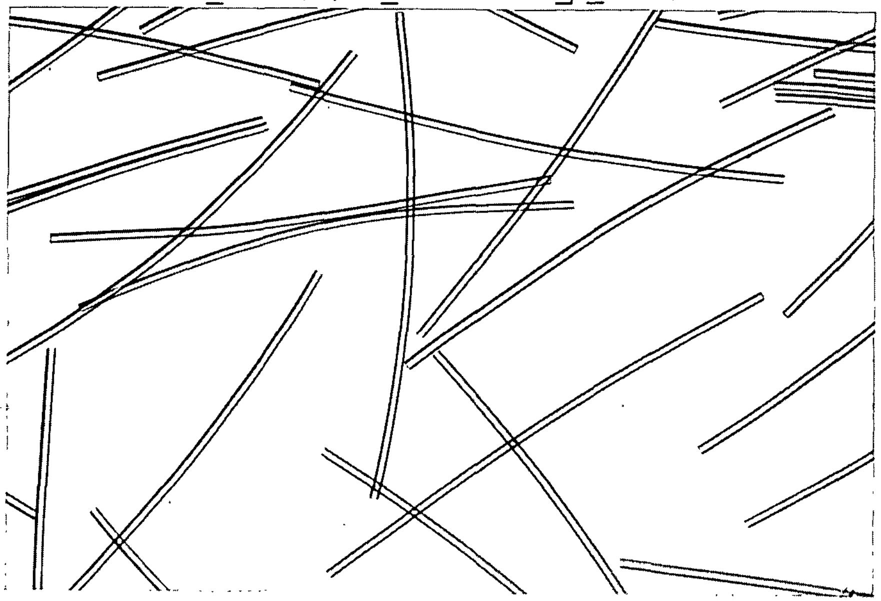

Nylon Sample 260-2.42 Magnification 26X
d=44.85 μ L=2.53 mm. L/d=56.4

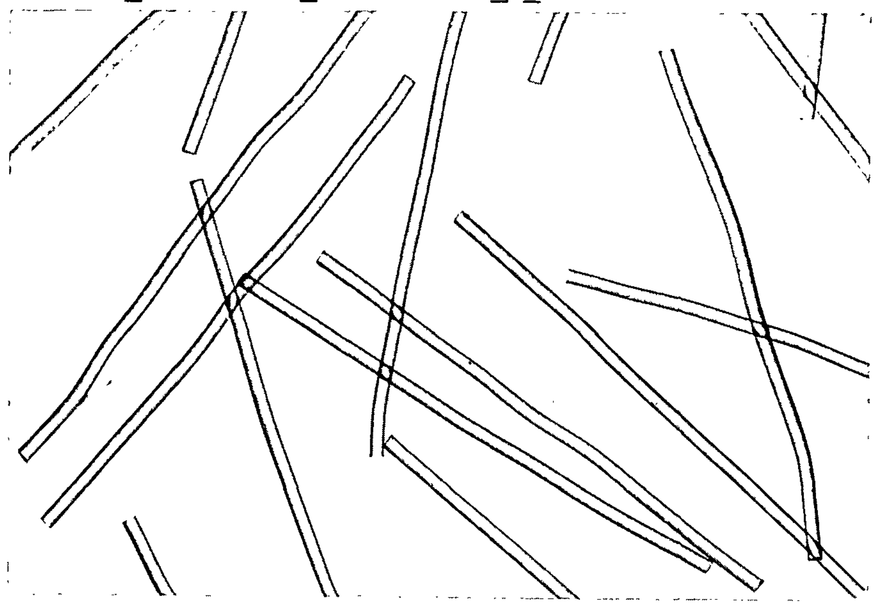

Nylon Sample (P-1643-6)-2.5 Magnification 27X
d=75.45 μ L=2.73 mm. L/d=36.2

Figure 27. Photomicrographs of Representative Samples of Fibers

Nylon Sample (P-1643-2)-1 Magnification 24X
$\underline{d}$ = 14.95 μ
$\overline{L}$ = 0.98 mm.
$\overline{L}/\underline{d}$ = 65.6

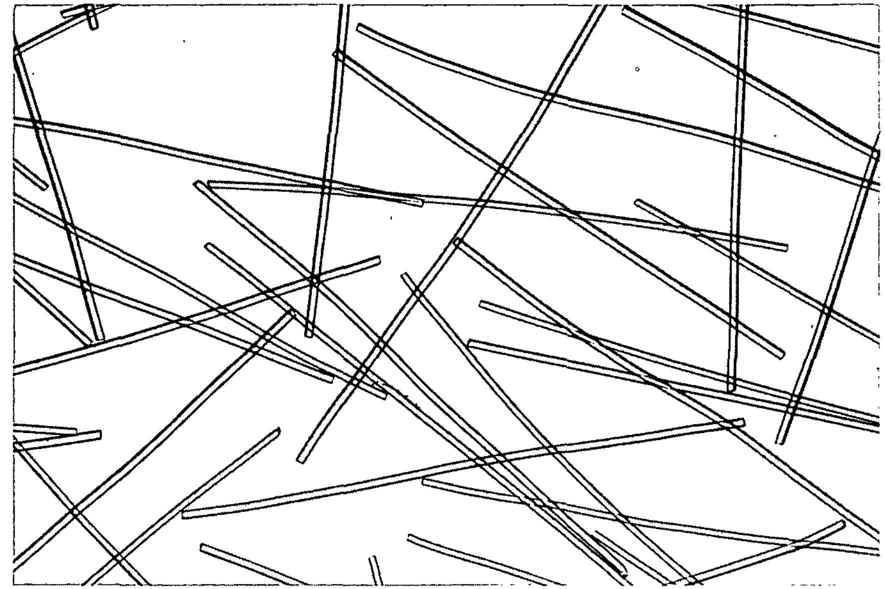

Nylon Sample (P-1643-3)-2.5 Magnification 27X
$\underline{d}$ = 43.86 μ
$\overline{L}$ = 2.73 mm.
$\overline{L}/\underline{d}$ = 62.2

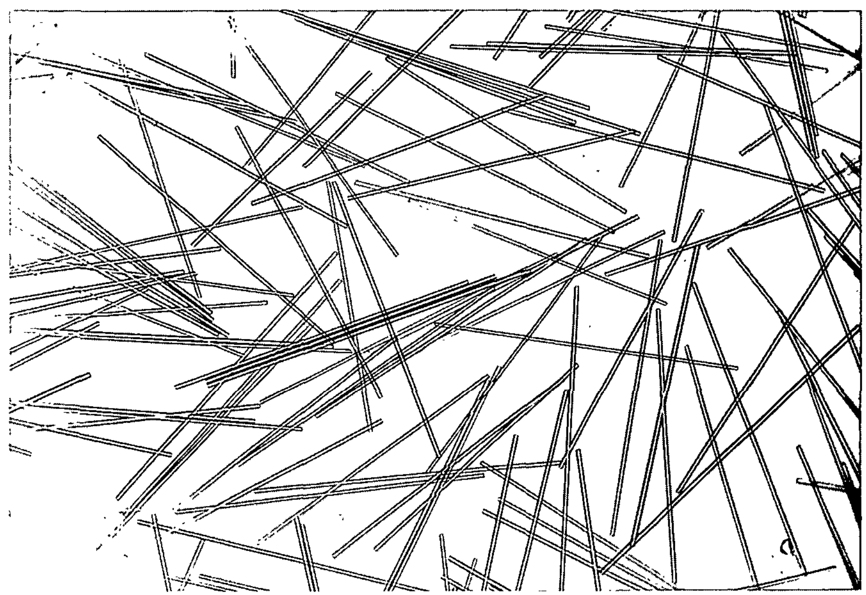

Glass Sample (O.C. 13,35) Magnification 42X
$\underline{d}$=12.86 μ $\underline{L}$ = 0.98 mm. $\underline{L}/\underline{d}$ = 76.2

Figure 28. Photomicrographs of Representative Samples of Fibers

which is also approximately 45 microns. The glass fibers (Sample O.C. 13.35) appear to be very straight and uniform in length.

CLASSIFICATION OF SUSPENSION SHEAR BEHAVIOR

In rheology, the flow behavior of complex fluid systems (i.e., fluids, fluid mixtures, or fluid-solid mixtures) may be classified according to the macroscopic phenomenology of the systems determined from viscometric studies. When a system is studied in a concentric cylinder viscometer, the behavior is usually characterized in terms of the applied torque, $\underline{T}$, and the bob angular velocity, $\omega_{\underline{b}}$, which are respectively proportional to the shear stress and shear rate ranges in the apparatus. Though this phenomenological approach to fluid system classification is convenient, it can be misleading in that the molecular characteristics of the fluid flow may not be properly represented. In this work, the macroscopic modes of suspension behavior are classified by means of the $\underline{T}$-$\omega_{\underline{b}}$ relationship. However, visual observations of the fiber phase behavior under conditions of shear are included, and a general theory for the flow behavior of the fluid phase is postulated in the next section.

Four different classifications of suspension behavior (see Fig. 29) were observed. For the first type (I) of behavior, the applied torque, $\underline{T}$, was directly proportional to the bob angular velocity, $\omega_{\underline{b}}$. The second type (II) of behavior showed a $\underline{T}$-$\omega_{\underline{b}}$ relationship which curved concave to the torque axis. Behavior Types III and IV also exhibited curved $\underline{T}$-$\omega_{\underline{b}}$ relationships, but the curves were concave to the bob angular velocity axis.

It was shown previously in the section entitled Stability of Flow in the Instrument that the fluids used in this work could be characterized by a Type I behavior, up to a certain bob angular velocity which depended on the fluid

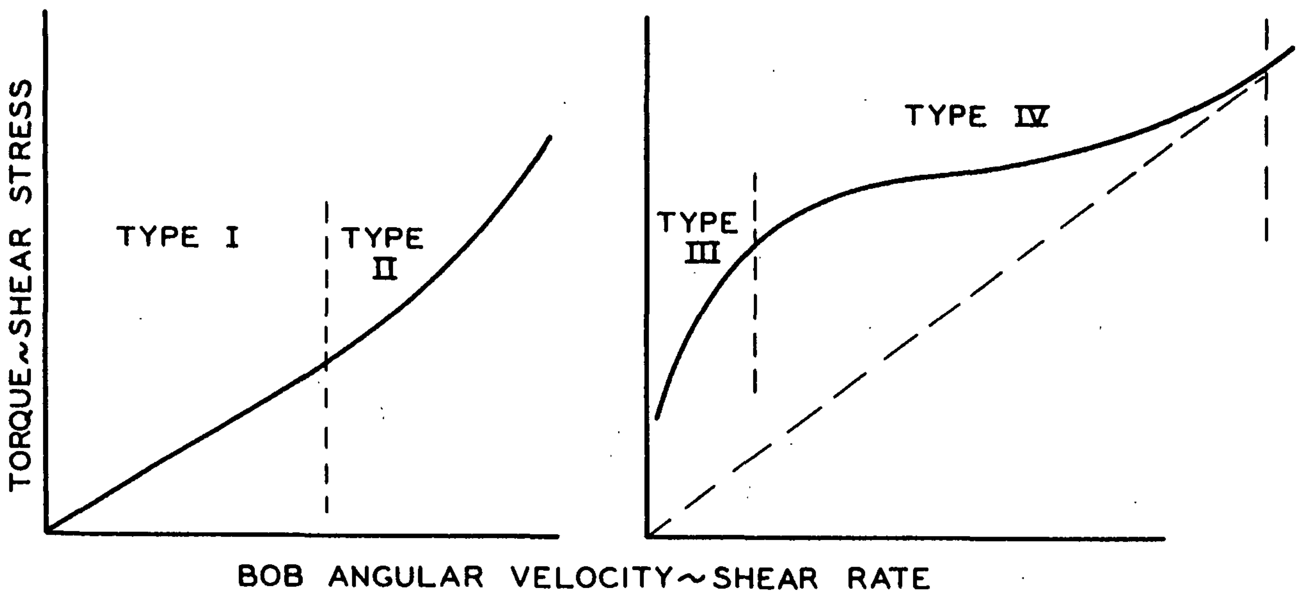

Figure 29. Types of Synthetic Fiber Suspension Behavior Observed in This Work

viscosity and density (see Table II). Below certain concentrations (see Table V) depending on the fiber shape and axis ratio, nylon fibers suspended in the high-viscosity (0.0702-poise) organic solution also exhibited Type I behavior up to a bob angular velocity of 0.794 sec.$^{-1}$ corresponding to a maximum shear rate of 2.2 sec.$^{-1}$. Glass fibers (sample O.C. 13.35) suspended in the relatively low-viscosity (0.0510 poise) organic solution showed a linear $\underline{T}$-$\underline{\omega_b}$ relationship for volume concentrations as high as 1% at bob angular velocities up to 0.25 sec.$^{-1}$ (shear rate = 0.7 sec.$^{-1}$). Typical $\underline{T}$-$\underline{\omega_b}$ data for this type of behavior are shown in Fig. 30 and 31 and are tabulated in Tables XV and XVI in Appendix IV.

No aggregates of fibers were detected in the suspensions of straight fibers [Samples 260- ; O.C. 13.35- ; 680- ; and (P-1643-6)-] at the low concentrations. Fiber collisions were observed, but the fibers did not remain in apparent contact with one another after such a collision. Viewed from above the annulus, the

TABLE V

APPROXIMATE FIBER CONCENTRATIONS AT WHICH NON-NEWTONIAN FLOW OCCURRED IN THE CONCENTRIC CYLINDER VISCOMETER OVER A SHEAR RATE RANGE OF 0.02 TO 2.2 SEC.$^{-1}$

Sample No.	Length-Diameter Ratio	Concentration, volume %
260-0.9	22.2	2.1[a]
260-1.5	37.5	2.8[a]
260-4	94.3	1.2
260-6	135.5	0.58
260-0.4	23.1	1.7[a]
680-0.6	35.5	1.8[a]
680-1.0	58.3	2.5
680-2.0	101.5	1.3
680-2.5	162.4	0.53
11925-2.5[b]	162.4	0.07
11925-2.0[b]	101.5	0.15
(P-1643-2)-1[b]	58.3	0.49

[a] Maximum concentration studied because of available supply of fibers, not necessarily the concentration where non-Newtonian flow begins.

[b] Curved fibers (see Fig. 28).

majority of the fibers appeared to be aligned in the direction of flow. This would be expected from a consideration of the equation for the rotary motion of a fiber around a vertical axis, i.e.,

$$\frac{d\phi}{dt} = G_o \cos^2\phi \qquad (10),$$

where ϕ is the complement of the angle between the projection of the fiber in a horizontal plane and the direction of flow. According to the above equation, fibers aligned in the flow direction, $\phi = 90°$, should have an angular velocity of zero. Actually, a zero angular velocity would not be expected because the diameters

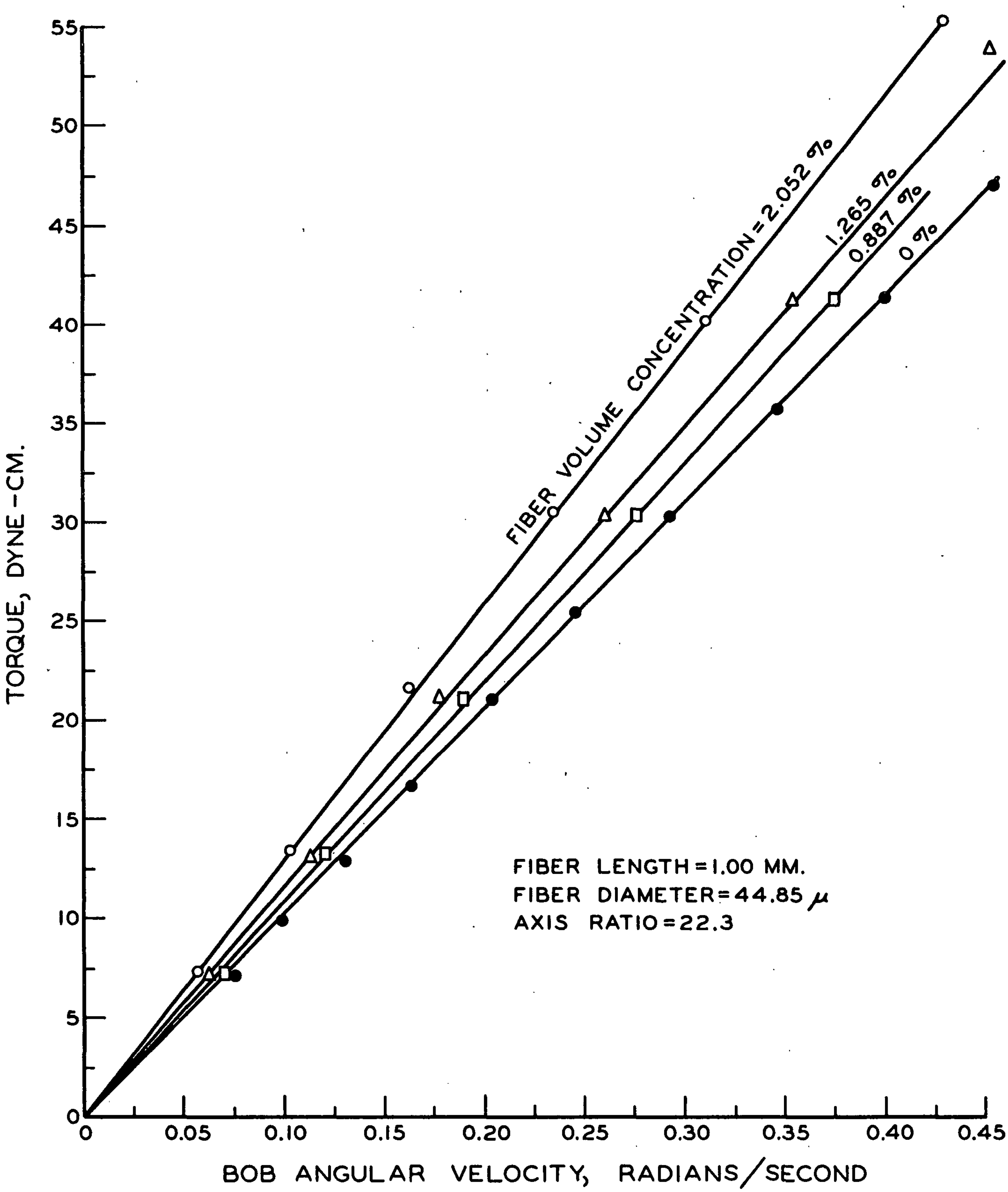

Figure 30. Torque-Angular Velocity Relationship for a Fiber Suspension

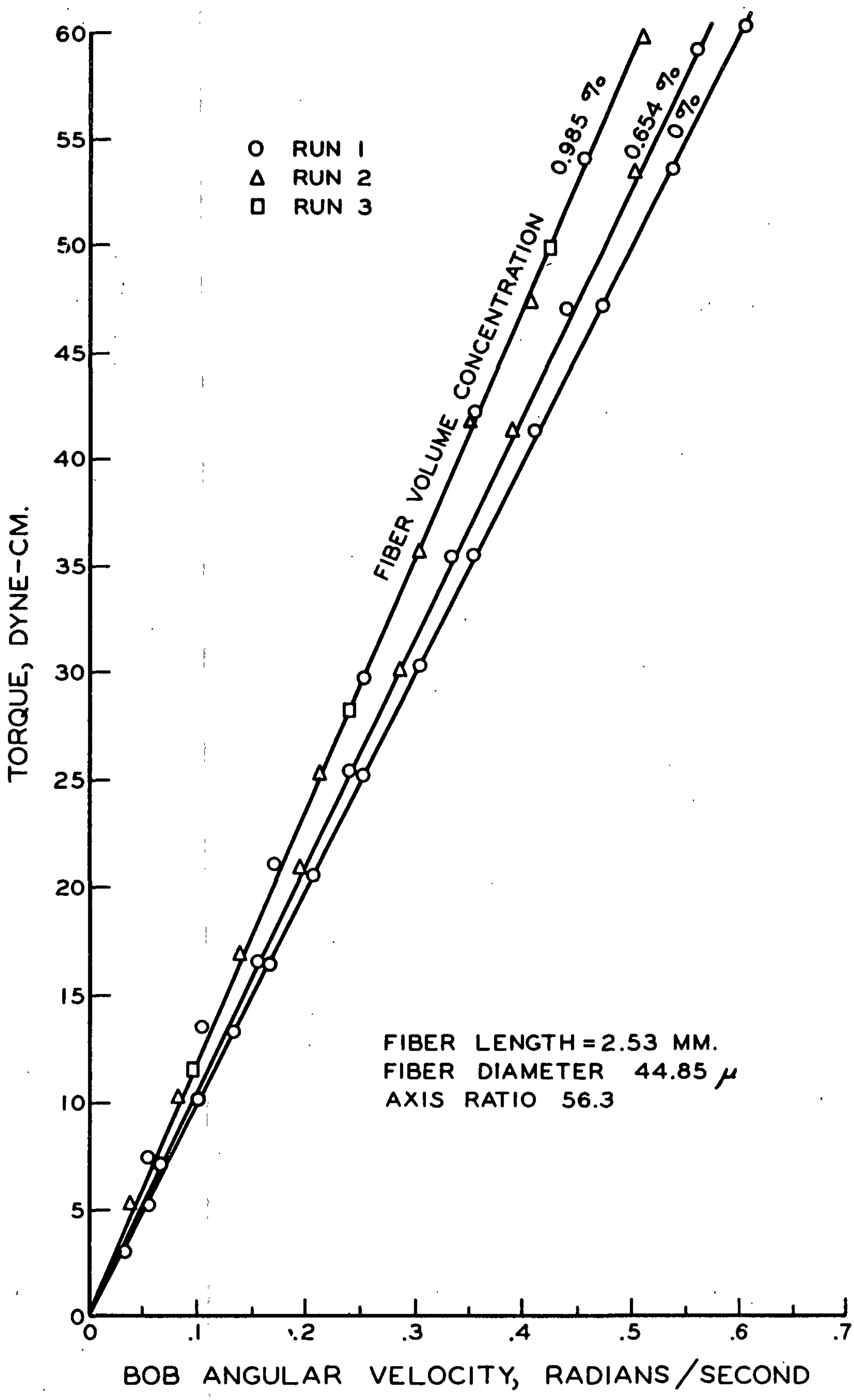

Figure 31. Representative Data Indicating the Reproducibility of the Viscosity Runs with Synthetic Fiber Slurries

of the fibers are finite and thus the relative velocities of the fluid layers on the surface of a fiber oriented parallel to the flow direction would exert a shearing motion on the fiber. When fibers were perpendicular to the flow direction, $\phi = 0$, Equation (10) predicts that the angular velocity should be a maximum. Thus, the fibers would be expected to spend more time in the flow direction than in other positions.

The curved fiber suspensions [Samples 11925- and (P-1643-2)-] contained many small (2-10 fibers) aggregates of fibers. The fibers not aggregated did not appear to have any preferred orientation such as that observed for the straight fibers. The aggregates became more numerous and larger as the axis ratio and/or concentration were increased. Table V shows that under the shear conditions employed in this study, fiber curvature greatly limited the concentration range over which the Type I flow behavior occurred.

Experimentally, it has been shown that the presence of fibers in a Newtonian fluid in laminar shear flow need not change the general flow behavior of the fluid. From a rigorous theoretical standpoint, the equations describing the motion, either translatory or rotatory, of a particle in a fluid should contain inertial terms which would change the $\underline{T}$-$\omega_{\underline{b}}$ relationship. Oseen's investigations (37) showed that the complete equation of motion [see Equation (1)] for a fluid may be replaced by Stokes' [see Equation (3)] or the linearized Oseen equation [see Equation (5)] for small Reynolds numbers. For the case of an infinite cylinder undergoing translation, Lamb (38) has shown that the Oseen equation which includes some inertial terms must be used in order to satisfy all flow conditions. Finn (39) experimentally verified Lamb's equation by measuring the drag force on a very long, thin wire ($\underline{L}/\underline{d}$ = 1500) in the absence of wall effects ($\underline{d}/\underline{D}$ = 1500).

For a small spherical particle in translation at low Reynolds numbers, Re, Lamb (38) showed that Stokes' and the Oseen equations yielded nearly identical results. This indicates that for small particles in slow motion the magnitude of inertial terms in the Oseen equation is negligible compared to that of the viscous terms. For such particles as disks (40) and spheres (41) in "creeping flow," it has been shown experimentally that inertial effects are negligible. For the slow translation of finite cylinders in a viscous fluid, White (42) found that they may attain a constant velocity in a purely viscous manner. At Re less than 0.25, the inertial effects were negligible and only at Re greater than unity did they become appreciable.

The Reynolds number used in describing the limits of the viscous flow associated with the motion of the above particles is defined as the ratio of the product of the particle diameter, d, and velocity, u, to the kinematic viscosity, γ, of the fluid ($Re = ud/\gamma$). It would be extremely difficult to determine an exact Reynolds number for a cylindrical fiber rotating in a shear field because a knowledge of the relative velocity between the fiber and the fluid would be required. However, if it is shown that the Reynolds number for the extreme case of a fiber held stationary in the shear field is less than unity, it should follow that the Reynolds number for a rotating fiber should be less than unity and the inertial forces should be negligible. The diameter of the largest fiber used in the study was 7.6×10^{-3} cm., while the kinematic viscosity of the suspending solution was 6.15×10^{-2} sq. cm. per sec. The maximum angular velocity attained by the bob in any run was 0.795 radians per sec., which is equivalent to a linear velocity of 2.02 cm. per sec. The Reynolds number for such a system was 0.25. Using any of the other fibers or a lower bob velocity would only decrease the Reynolds number.

Type II behavior exhibited by fiber suspensions subjected to shear stresses was defined by a plot of $\underline{T}$ versus $\omega_{\underline{b}}$ which curved concave to the torque axis. Such behavior occurred in the suspensions of glass fibers when a certain bob angular velocity (ca. 0.25 sec.$^{-1}$) was attained (see Fig. 32). As discussed in the section on the Stability of Flow in the Instrument, this type of $\underline{T}$-$\omega_{\underline{b}}$ behavior indicates that inertial forces are appreciable in the fluid system. These forces can result from two effects acting separately or in combination. They are: (1) instability of the rotational flow in the annulus resulting from the geometry of the apparatus, and/or (2) inertial forces due to the flow past the rotating fibers.

It is unlikely that the inertial effects due to the flow around the fibers were appreciable. The viscosity of the organic solution in which the fibers were suspended was 0.051 poise, while the density was 2.6 g./cc. The diameter of the glass fibers was 12.86 microns. For the maximum fluid velocity attained in the annulus, 2.02 cm./sec., the Reynolds number based on the fiber dimension was only 0.13. As shown previously, the inertial effects for the flow around a cylinder become appreciable only at $\underline{Re}$ >1.0.

Since inertial effects due to the flow around the fibers are unlikely, the curvature in the $\underline{T}$ vs. $\omega_{\underline{b}}$ plot must result from instability in the annulus due to the fluid itself. In Fig. 32, the start of the curved section of the plot lies between angular velocities of 0.225 and 0.275 sec.$^{-1}$. It was shown in Table II that instability in the pure solution occurred at a bob angular velocity of 0.262 sec.$^{-1}$. Furthermore, above a bob angular velocity of 0.300 sec.$^{-1}$, the suspensions showed the vortices described by Taylor (35) for solutions in unstable flow containing a dye. Thin layers of the suspension contained fibers which appeared to be oriented in a horizontal plane. These layers bounded cells of fibers which were

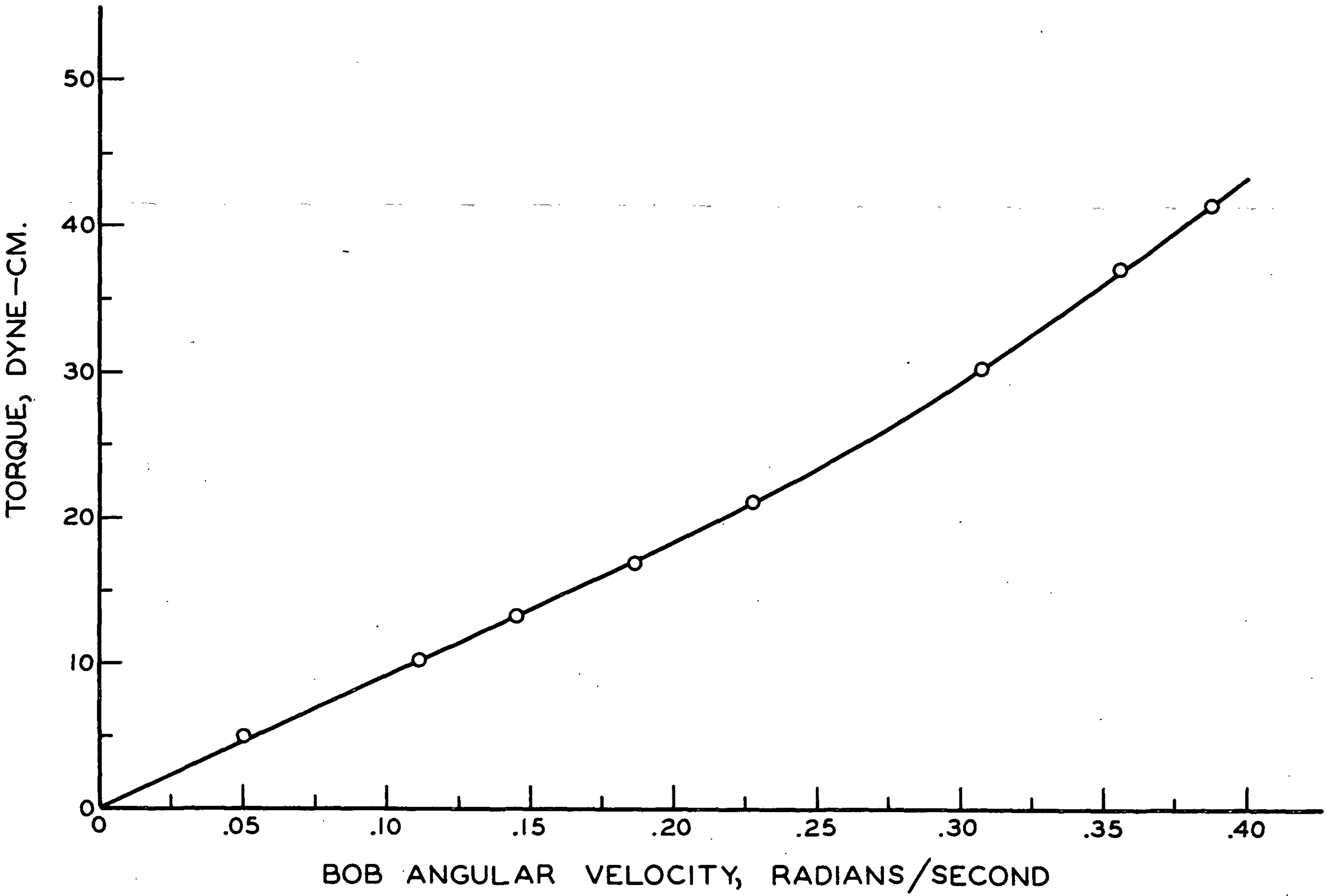

Figure 32. The Shear Behavior of a Suspension of Glass Fibers

randomly oriented. The width of a cell was about equal to the annulus width, which is in line with Taylor's observations.

At concentrations above those listed in Table V, suspension behavior designated as Type III was observed. A typical $\underline{T}$-$\omega_{\underline{b}}$ relationship for these suspensions is shown in Fig. 33. The curves are concave to the velocity axis, indicating that at high torques an increase in torque produced a larger change in bob angular velocity than a similar torque increase in a lower torque range. The curves also appear to indicate that a certain torque was required to set the bob in motion.

Visual observations of the fiber phase of the suspension during shear suggest an explanation for this behavior. Over the shear rate range studied (0.02-2.2 sec.$^{-1}$) a major portion of the fiber phase remained immobile. At the very low torques ($<$ 6 dyne-cm.), the fibers were in apparent contact with the surface of the bob. When a torque was reached where the bob began to turn, only a few fibers near the bob moved. At higher torques, a clear fluid annulus between the bob and the fiber phase was observed. No measurements were made, but it appeared that this fluid layer increased in width as the torque was increased.

If it is assumed that the major portion of flow occurred in this clear fluid annulus (it was not completely clear since a few fibers had become dislodged from the fiber phase and moved in this annulus), then the system resembles a narrow annulus viscometer. For such an apparatus it was shown that the $\underline{T}$-$\omega_{\underline{b}}$ relationship could be expressed by the following equation:

$$T = \frac{4\pi\mu_o h\omega_b}{1/r_1^2 - 1/r_2^2} \qquad (46)$$

The change in torque with respect to a differential angular velocity change is:

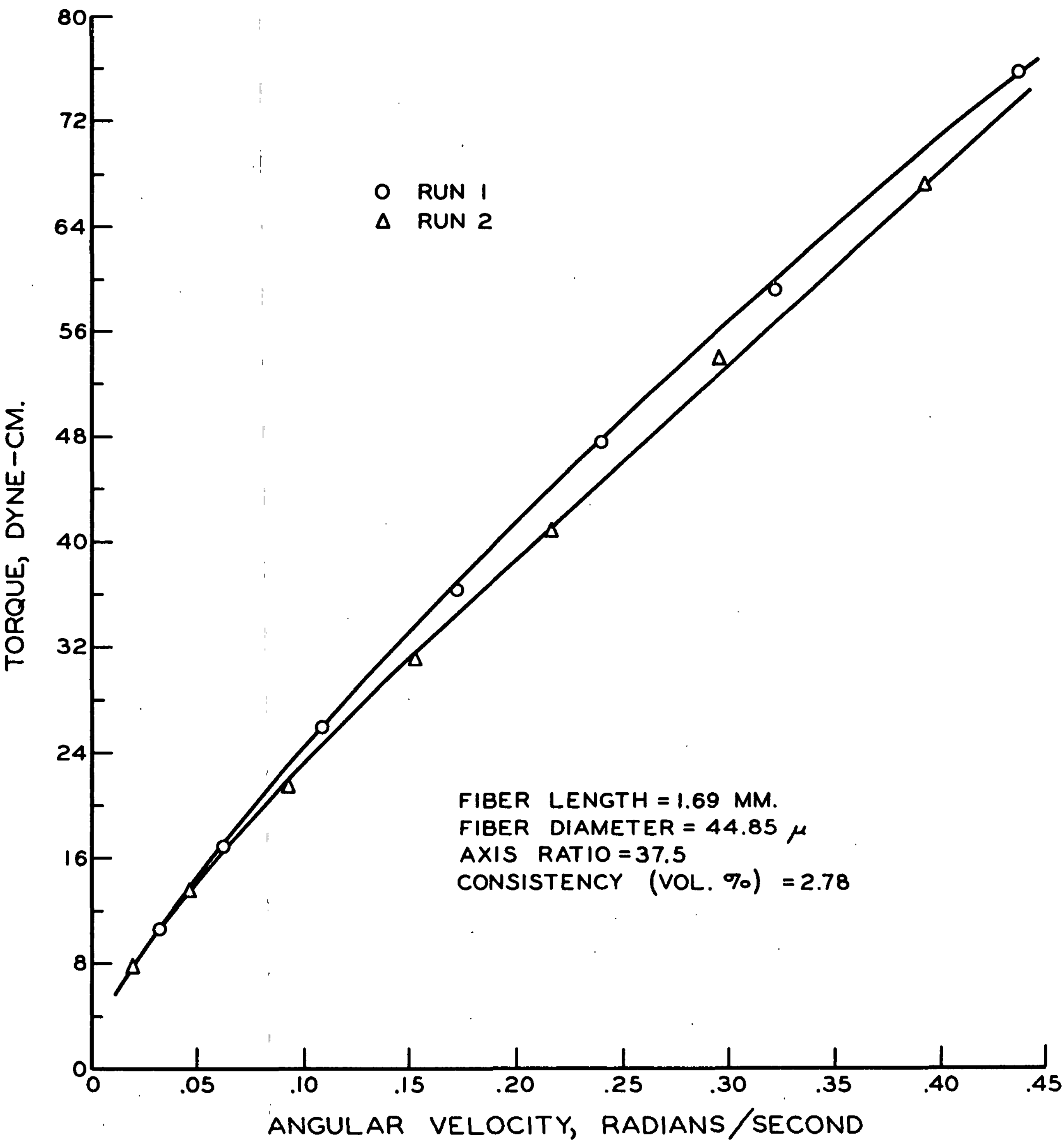

Figure 33. The Non-Newtonian Flow Behavior of Fiber Slurries

$$\frac{dT}{d\omega_b} = \frac{4\pi\mu_o h}{1/r_1^2 - 1/r_2^2} \tag{48}$$

For a suspension behavior such as Type I, the quantities on the right-hand side of Equation (48) are constant over all angular velocities, and a straight-line relationship is observed. However, if the radius r_2 of the clear fluid annulus increases with an increase in ω_b, the quantity $(1/r_1^2 - 1/r_2^2)$ would also increase and the slope $dT/d\omega_b$ would decrease. The experimental T-versus-ω_b data show a decrease in slope with increasing ω_b. Based on the visual observations and the theoretical considerations, a proposed mechanism for Type III suspension behavior is as follows: Initially, a rigid fiber network suspended in a fluid is present in the annulus. The fibers at the boundaries of the network contact the inside surfaces of the apparatus. These fibers exert static frictional forces on the bob and a certain torque must be attained before these forces are overcome. The motion of the fluid past the fibers near the bob surface causes them to deform, creating a clear fluid annulus. As the flow velocity is increased, a greater deformation occurs and the clear fluid annulus width increases. It is probable that if the forces on the network were increased to a certain point, the network of fibers would fail. However, for the fibers in the organic solution, such forces were not attained. This mechanism of suspension behavior is similar to that proposed by Richardson (6) for the flow of a sulfite wood pulp suspension in a concentric cylinder viscometer and Robertson, et al. (43) and Bugliarello and Daily (12) for the flow of pulp slurries in a pipe.

Over a given range of shear stresses depending upon the fiber concentration (only fiber sample 260-2.42 with a diameter of 44.85 μ and an axis ratio of 56.3 was studied), nylon fibers suspended in a sucrose solution exhibited a rheological behavior termed Type IV. In these suspensions, fiber flocculation and network formation occurred at much lower concentrations (0.08 to 0.6%) than observed for similar fibers in the organic solution. Flocculation is known to be a result of the mechanical and chemical characteristics of a system. It is thought that physicochemical factors in the sucrose solution-nylon fiber system played the most important part in producing or preventing flocculation. Such factors as the change in surface energy of the nylon in the solutions, the change in the charge distribution on the surface of a fiber, and/or weak hydrogen bonding between the fibers by a water "bridge" in the aqueous suspension might be possible. Some evidence of the effect of such factors was obtained in a study of the flocculation in a 0.5%-consistency suspension at different pH's. Large, dense flocs were observed at a pH of 2 while the amount of flocculation decreased to an apparent minimum at a pH of 8. The pH at which the study was performed was about 6.5. One explanation of this effect is through the presence of charges on the fibers. At high pH's, the electrostatic forces on the nylon constitute a potential barrier between fibers. When the isoelectric point [pH 2.6-3.1 (32)] of the nylon is reached, fibers can approach within the range of van der Waal's forces and aggregation would occur. The fact that flocculation doesn't occur in the organic solution indicates that the problem is more complicated than the above analysis shows. Because the fibers would not be expected to have charges in the particular organic solution used, some other explanation of the absence of flocculation must be found. The scope of this work was limited so that an explanation is not readily apparent from the data taken.

It is believed that mechanical factors such as fiber entanglement were not as important in causing flocculation as those mentioned above. A microscopic examination of the fibers indicated no significant fiber curvature in the solution. The low viscosities (3-6 cp.) and the low shear rates (2.2 sec.$^{-1}$, maximum) meant that fiber bending due to the fluid forces was not appreciable, even though the modulus of the fibers in a sucrose solution was about 25% of that in the organic solution (see Table III in the Physical Characteristics of the Fibers section).

The flow behavior of this system as defined by the $\underline{T}$-$\omega_{\underline{b}}$ curve is shown in Fig. 34. It is felt that there are three regions of flow represented in the figure. Though the bob rotated in the suspension at the initial torques (ca. 2 dyne-cm.), it is quite possible that at a much lower torque, static friction forces were exerted on the bob by the fibers, and like type III suspension-behavior, a torque would be required to move the bob. At the low torques and low bob angular velocities, the system of flocs and fibers did not appear to move. This behavior is similar to that of suspensions undergoing Type III behavior. At a given torque, a distinct line of shear was observed in the viscometer annulus. The fibers between the bob and this shear line were moving and showed a preferred orientation in the direction of flow. The fiber phase between this line and the inner wall of the cup did not move. As the torque was increased, the line of shear moved outward from the bob closer to the cup. Finally, some torque was reached where the fibers in the entire annulus were in flow. Type IV behavior was characterized by the $\underline{T}$-$\omega_{\underline{b}}$ data obtained as the shear line moved outward across the annulus. This behavior is represented by most of the curved portion of the $\underline{T}$-$\omega_{\underline{b}}$ plot in Fig. 34. At higher torques, the $\underline{T}$-$\omega_{\underline{b}}$ relationship became linear. It appears that this linear portion may be extrapolated through the origin indicative of Newtonian or Type I flow behavior.

Richardson (6) observed a flow behavior similar to Type IV for suspensions of pulp fibers. He attributed the line of shear in the fiber phase to a yielding of a fiber network. The shear stress at any radius in the annulus is $\underline{T}/2\pi\underline{r}^2\underline{h}$. If the network is homogeneous, then the yield stress at any radius should be constant. Therefore, higher torques would be required to cause a network to yield

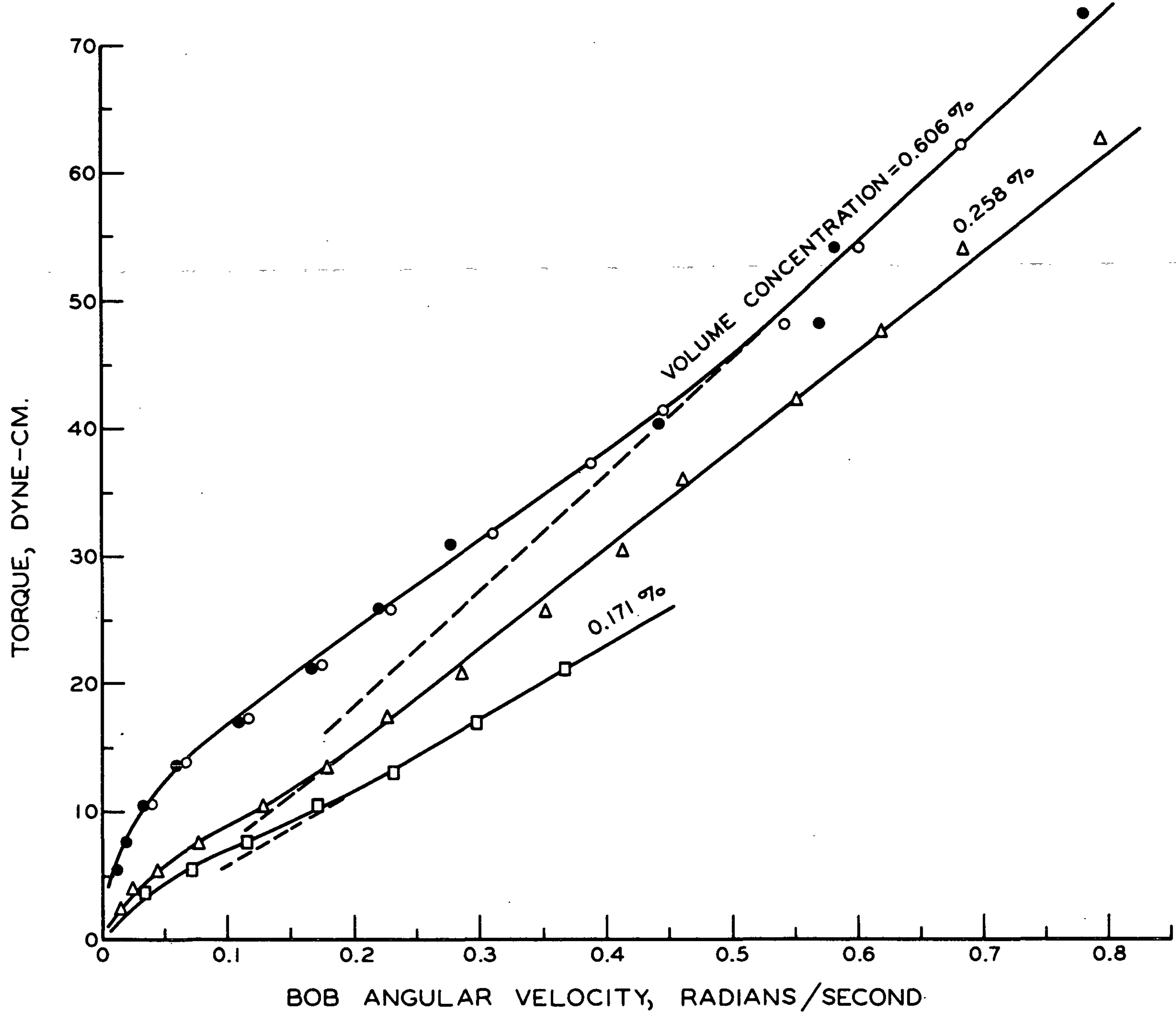

Figure 34. Shear Behavior of Nylon Fibers Suspended in a Sucrose Solution

near the surface of the cup than near the bob. No quantitative measurements were made of the yield stresses in these studies. Because of the importance of this quantity in relation to the flow of suspensions in which networks are present, this would be an area of interest for future studies.

The presence of fiber-wall and fiber-fiber attractive forces was assumed in the explanation of Types III and IV suspension behavior. Han (44) has questioned the importance of these forces in determining suspension behavior. He postulates that the fibers are surrounded by a very thin, stagnant fluid film which prevents the molecular forces between two fibers or a fiber and a solid surface from becoming appreciable. This hypothesis may be somewhat justified in that the assumption that there is no fluid slip at the wall of a pipe used in the theoretical derivation of the Poiseuille equation has been experimentally verified for various pipe materials.

If the Types III and IV suspension behavior are analyzed with regard to such a fluid film theory, a plausible explanation of the experimental results may still be obtained. For the case where the fibers appear to contact the apparatus walls, it will be assumed that a fluid film exists between the bob and the boundary of the fiber phase. In this case, the static friction forces between the bob and the fibers would be negligible and the bob should rotate upon application of the first increment of torque. Most of the flow would occur between the edge of the network and the bob and therefore the system would approximate a very narrow annulus viscometer. Since the fluid is Newtonian, Equation (46) can be employed to represent the fluid behavior. Because the distance between the fiber phase and bob surface is very small, the term $(1/r_1^2 - 1/r_2^2)$ will also be extremely small, and for low torques, ω_b necessarily would be small. It is quite conceivable that the angular velocity would be so small that bob movement would not be detected under the experimental conditions at low torques. Also, the initial slope of a $\underline{T}$ versus $\omega_{\underline{b}}$ plot would be very steep, which might be expected if the data in Fig. 33 were extrapolated to the origin.

For the nylon fibers suspended in the sucrose solution, surface charges on the fibers could still control the distance of approach between the fibers, but the frictional resistance to relative motion between the fibers would result from viscous flow rather than a distortion of molecular forces. Flocculation is a dynamic process whereby flocs are continuously formed and destroyed. If it is assumed that the geometry of the space between two fibers resembles two parallel flat plates, the fibers will separate (deflocculate) more rapidly under a given stress as the distance between them is increased. This conclusion is based on the equation for the movement of parallel flat plates separated by a viscous fluid, i.e., $\underline{F}/\underline{A}' = \mu_o \, \underline{u}/\underline{h}'$, where $\underline{F}/\underline{A}'$ is the shear stress, $\underline{u}$ is the relative velocity between the plates, $\underline{h}'$ is the distance between the plates, and μ_o is the fluid viscosity. Therefore, at the isoelectric point of nylon, the fibers would be very close together and the rate at which they could be separated by a given stress would be less than at high pH's where the fibers were further apart. This agrees with the observations discussed previously.

At this time, it is not possible to resolve the actual nature of the fiber-fiber and fiber-solid forces present in suspensions. It is felt that this problem could be clarified by a study such as that of Wollwage (45) who attained a limited amount of success in the determination of the magnitude of the forces between two fibers in a fluid.

FLOW THEORY

In the preceding section it was shown that under the given set of experimental conditions, synthetic fiber suspensions exhibited four types of rheological behavior based on viscometric data. However, without the visual observations of the fiber phase behavior, such a classification is almost meaningless. These observations in combination with the experimental data enable a general theory for the flow in fiber suspensions to be advanced. The basic premise of this theory is that if a fluid is Newtonian, the presence in the fluid of a fiber or fibers the dimensions of which are many times that of the fluid molecules does not alter the original Newtonian behavior of the fluid.

Each of the four types of suspension behavior previously discussed supports this theory. For Type I, the torque was directly proportional to the bob angular velocity indicative of Newtonian flow. It should be recalled that the fibers in suspensions exhibiting Type I behavior were present in different volume concentrations, axis ratios, shapes and degrees of aggregation. Because the entire system behaved in a Newtonian manner, it should follow that the fluid phase was also Newtonian. This observation supports the theoretical analyses of fiber suspension flow of Jeffery (16) and Burgers (17).

Type II behavior was shown to be a result of inertial effects occurring above a given shear rate in a fiber suspension which had exhibited Newtonian behavior at lower shear rates. The presence or absence of inertial effects in a fluid system is not a criterion of whether or not the system is Newtonian. This is emphasized by the fact that inertial effects became appreciable in the pure fluid at about the same shear rate as that observed for the suspension of fibers. Furthermore, the bob angular velocity at which instability occurred agreed very well with that (see Table II) predicted by the theory of Taylor (35). Therefore, it can be again concluded that the fluid phase of the particular suspensions (glass fibers) was Newtonian.

In the third type (III) of suspension behavior, the major portion of the fibers in the suspension were not moving under the shear forces and most of the flow occurred in a clear fluid annulus between the bob and a fiber network. The shape of the $\underline{T}$-$\omega_{\underline{b}}$ curve was explained on the basis of an increase in annulus width with an increase in bob angular velocity. Under the shear conditions the fluid phase in flow would be expected to be Newtonian. Were it possible to hold the distance between the bob and the network boundary constant, in all probabilities a linear $\underline{T}$-$\omega_{\underline{b}}$ curve would have been obtained.

The fourth type (IV) of suspension behavior also involved a continuous change in the experimental conditions under which the $\underline{T}$-$\omega_{\underline{b}}$ measurements were made. As the torque on the bob was increased, a greater portion of the suspension in which networks were present flowed. It has already been demonstrated that the flow of fibers (Type I behavior) suspended in a fluid should be Newtonian. The supposition of Newtonian flow is further strengthened by the fact that when a torque was reached where fibers in the entire annulus moved, the torque became directly proportional to the bob angular velocity.

The implications of this theory are felt to be quite important. In the viscous flow region the laws governing the behavior of a Newtonian fluid are well defined. If the fluid in a fiber suspension retains its Newtonian characteristics, then calculations involving the gross flow behavior of such a suspension will be simplified. Deviations from macroscopic Newtonian or Type I flow will not be due to changes in the fluid phase, but rather to changes in the experimental conditions. For instance, in plug flow in pipes the fluid velocity variation has been observed to be confined to a narrow annulus of clear fluid between the plug and the pipe wall (<u>12</u>). The annulus width increases with an increase in the total flow. Under conditions of actual Newtonian flow, the gross measurements might indicate a non-Newtonian fluid. This interpretation would be in error because the measurements would be taken under conditions of different flow geometry.

THE QUANTITATIVE ANALYSIS OF THE FLOW OF FIBER SUSPENSIONS

Introduction

Of the four types of fiber suspension behavior discussed, Type I is the least complex to analyze from an experimental standpoint. The considerations in the theoretical section have shown that the slopes of the shear stress-shear rate ($\underline{T}$-$\omega_{\underline{b}}$) plots are proportional to the viscosities of the fiber suspensions. Furthermore, these viscosities are related to the properties of the fibers in the suspensions. Therefore, when suspensions do undergo Newtonian flow, viscosity measurements should provide a useful tool in detecting differences in properties of fibers in such suspensions.

No satisfactory theory has been advanced for the flow of fiber suspensions (Type II) in which inertial effects are appreciable compared to the viscous effects. The work at M.I.T. (12) has presented a qualitative analysis of this type of flow for pulp fiber suspensions. They determined the transfer of momentum under turbulent pipe flow conditions for pure fluid and for fiber suspensions. The fibers tended to increase the efficiency of the momentum transfer. A continuation of this study was beyond the scope of this work.

The shape of the shear stress-shear rate curves for the Types III and IV suspensions present certain similarities to some of the more common rheological models for homogeneous fluid systems. For instance, one might compare the shapes of the curves in Fig. 29 with those for Bingham plastic and pseudoplastic materials shown in Fig. 35. The respective equations for the curves in the latter figure are:

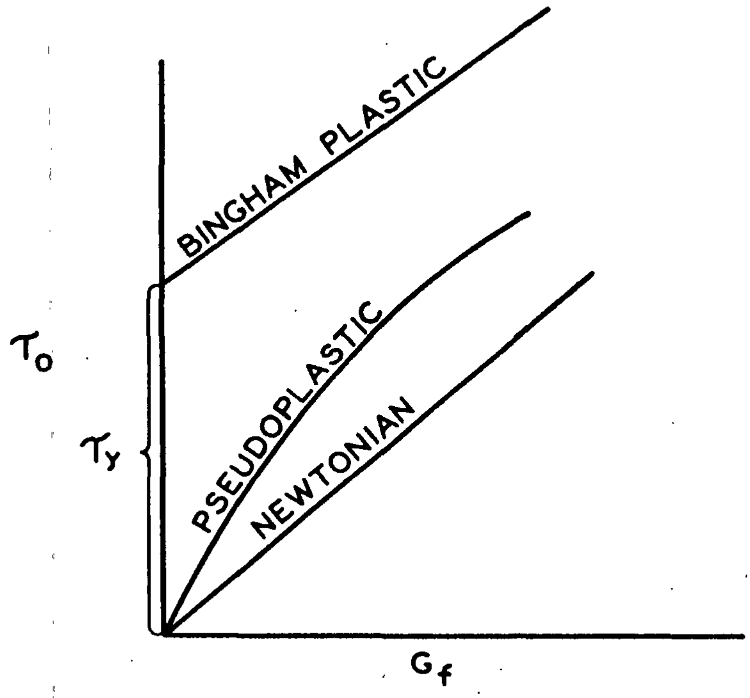

Figure 35. Rheological Behavior of Homogeneous Fluid Systems

$$\tau_o = \tau_y + \mu_f G_f \qquad (49)$$

and

$$\tau_o = K(G_f)^n \qquad (50)$$

where τ_o is the shear stress, τ_y is the yield stress, μ_f is the slope viscosity, G_f is the shear rate, and K is a proportionality constant. It is felt that such equations are useful in correlating the data. However, their use would also be dangerous in that the physical picture of the actual flow system would be misleading. For instance, Equation (49) indicates that a yield stress may be obtained from viscometry data. Though there appeared to be a positive torque intercept at zero bob angular velocity in Type III behavior, visual observations showed little evidence of any network yielding. Equation (50) shows that if K and n are known, then the shear stress at any point in the system may be calculated from a knowledge of the shear rate at that point. Consider the physical picture for fibers suspended in the sucrose solution. Part of the suspension may be flowing, while the rest is stationary. Equation (50) predicts that no shear stresses are present in the stationary portion because $\underline{G}_{\underline{f}} = 0$. However, because the torque is constant at every point in the suspension, the shear stress at any radius, $\underline{r}$ must be equal to $\underline{T}/2\pi\underline{r}^2\underline{h}$ and is therefore finite. For the present it is felt that it would be better to determine necessary quantitative data from such figures as 33 and 34, rather than fit the data with "standard" rheological equations. Also, if the flow theory presented applies, then it should be possible to rigorously describe the flow in Types III and IV suspensions if the geometry of the flow system is known.

Because of the limitations of the methods used to quantitatively analyze such suspension shear behavior as Types II, III, and IV, a greater emphasis was placed on the analysis of the Newtonian or Type I suspension flow behavior. Included in this study were the effects of the following variables on the suspension relative viscosity: 1) apparatus geometry (wall and end effects); 2) fiber axis ratio; 3) fiber shape; and 4) suspending solution properties.

<u>Viscometer End Effects for Fiber Suspensions</u>

The viscosity of a liquid in a concentric cylinder viscometer can be determined by Equation (46). Since the equation was developed on the assumption that the cylinders are of infinite length, then it is necessary to correct for end effects. If the end effect is proportional to the viscosity of a solution of suspension, then it will be eliminated when a relative viscosity is determined. Lindsey and Fisher (<u>10</u>) made a thorough study of the end effects associated with a concentric-cylinder apparatus and showed that at viscosities less than one poise, the end effect changed considerably with a change in viscosity. The solutions used in this work had viscosities in the low centipoise region, so it was necessary to determine just how the effect changed for fiber slurries at different consistencies.

The end effect is actually a combination of effects. There is a drag due to the stress on the bottom of the cylinder and the change in stress distribution on the cylindrical surface due to the existence of the ends. A formal solution for the magnitude of the end effect in terms of the apparatus dimensions has been obtained by Oka (46). However, because of the gross differences in the viscometer used in this study as compared to conventional concentric viscometers, it was desirable to experimentally determine the magnitude of the end effect under various conditions.

The technique used was similar in principle to that discussed by Oka and carried out by Lindsey and Fisher. The liquid level was varied in the viscometer and the apparent viscosity, T/ω_b, was determined. If it is assumed that the end effect is independent of the liquid level, a linear relationship between the apparent viscosity and the liquid level, h, will yield an end correction at zero height. The typical data plotted in Fig. 36 indicate that such a linear relationship does exist for both pure solutions and fiber slurries. The intercept on the ordinate axis was used as the correction for the apparent viscosity. The relationship between the end correction and the apparent viscosity of a system which completely fills the annulus of the viscometer is shown in Fig. 37. These data (Appendix IV, Table XIX) were used in correcting all apparent viscosities of solutions and fiber slurries before the relative viscosities were calculated.

The data indicated that only the apparent viscosity and not the actual consistency or the properties of the fibers in the slurry contributed to the end

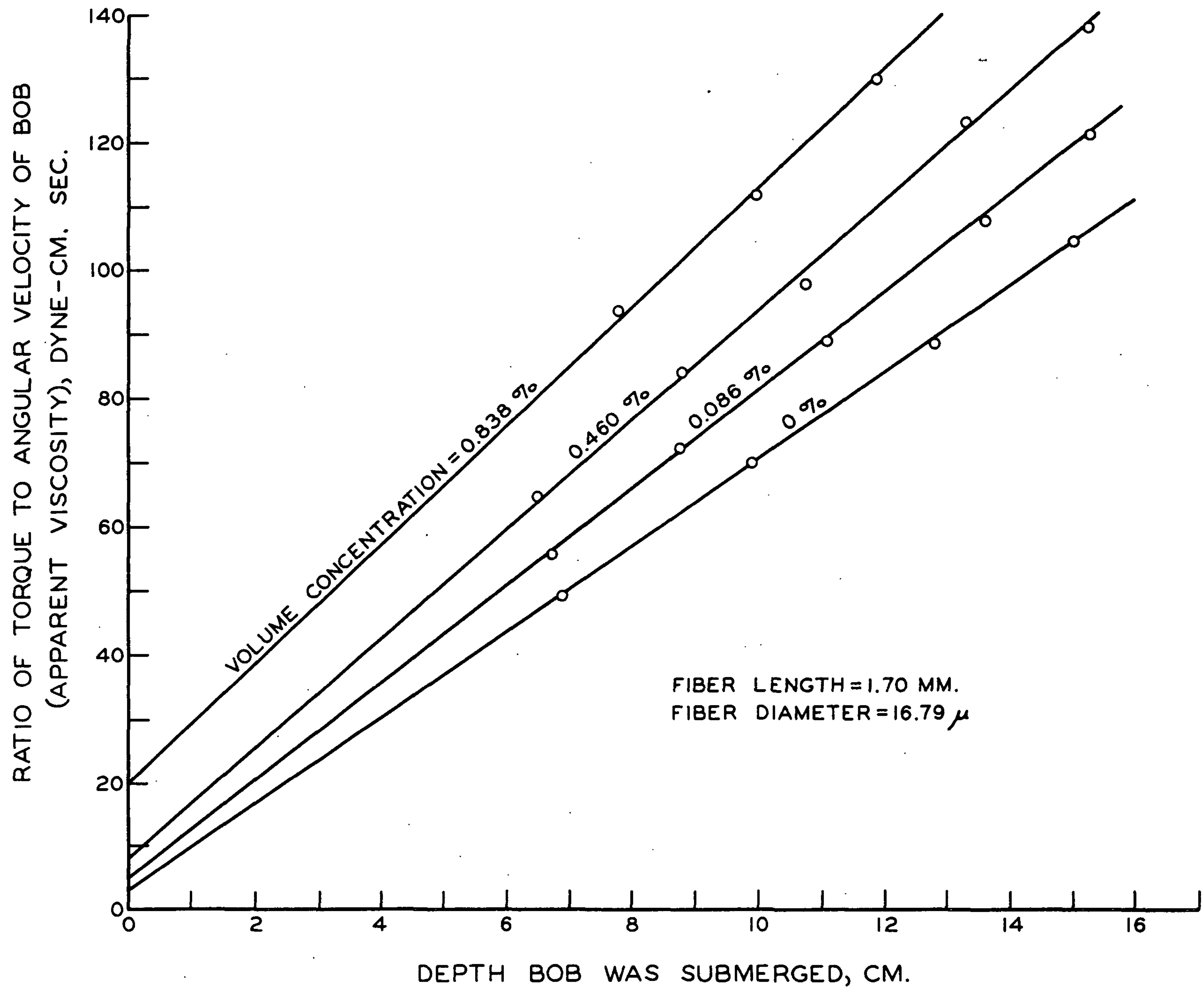

Figure 36. Determination of End Effects of Bob in Wide Annulus Viscometer

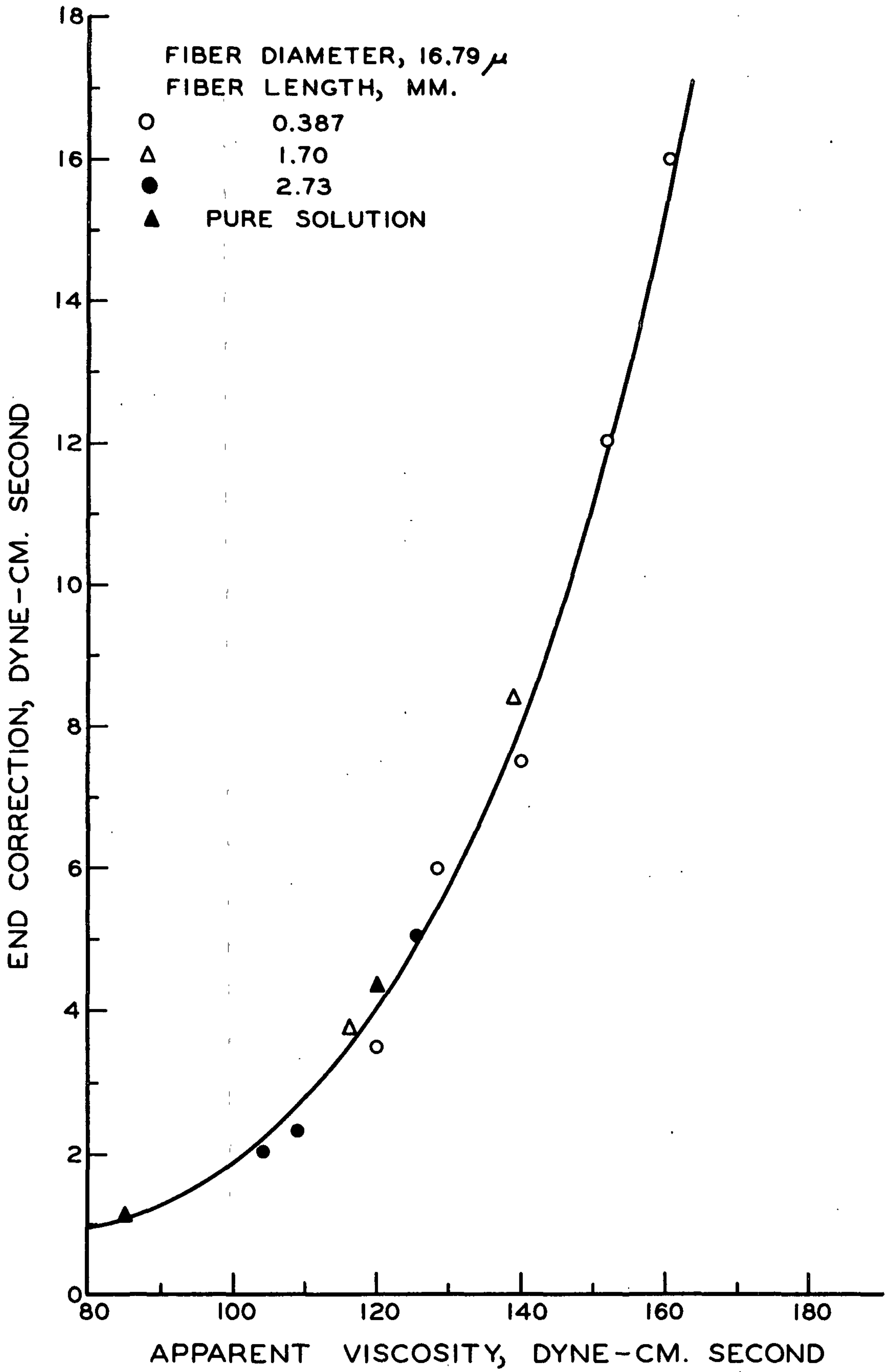

Figure 37. End Correction vs. Apparent Viscosity of Fluid

effect. The scatter in the data is felt to be a result of the high bearing air pressures needed to suspend the bob at low liquid levels. The use of the smoothed curve for making the actual corrections probably minimized the errors caused by this scatter.

The Dependence of the Relative Viscosity on the Concentration of a Synthetic Fiber Slurry

Three sets of viscosity runs were made with nylon fibers having different diameters (16.79, 44.85, and 75.5 μ), but axis ratios within the same range (20-170). The relative viscosity of a fiber slurry was defined as the ratio of the slope of the torque-angular velocity line for the slurry and that of the suspending solution. The slopes were corrected for viscometer and effects with the data shown in Fig. 37.

The data for the three sets of runs are shown in Fig. 38-40. The numerical values of the relative viscosity for given concentrations are tabulated in Table XX in Appendix IV. The reproducibility of the determination of the torque angular velocity relationship was better than 1%. However, because the relative viscosity was compared to a value of unity for the pure solution, the variation in this determination was as high as 10%. Because many concentrations were used in establishing the viscosity behavior of the slurries, it is felt that the variations were averaged and the curves as shown are quite representative.

The best data were obtained with the smallest diameter fibers. The experimental techniques were developed during the studies of the viscosities of the 44.85 μ diameter fiber slurries, so these data are more scattered than those taken with the smaller diameter (16.79 μ) fibers. A change in the experimental procedure in making the viscosity runs with the large diameter (75.45 μ) fibers increased the

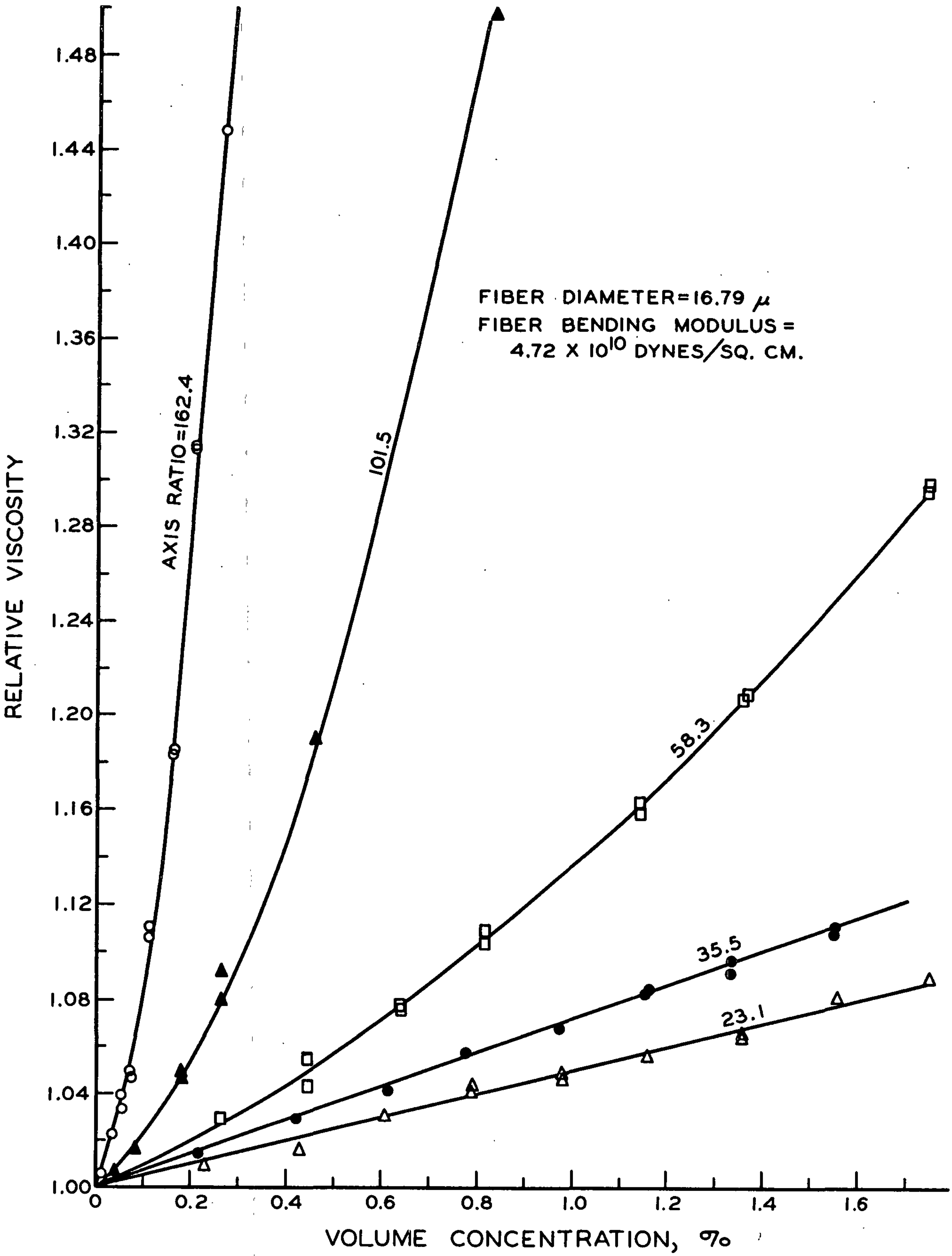

Figure 38. Relative Viscosity-Concentration Relationship of Fiber Slurries

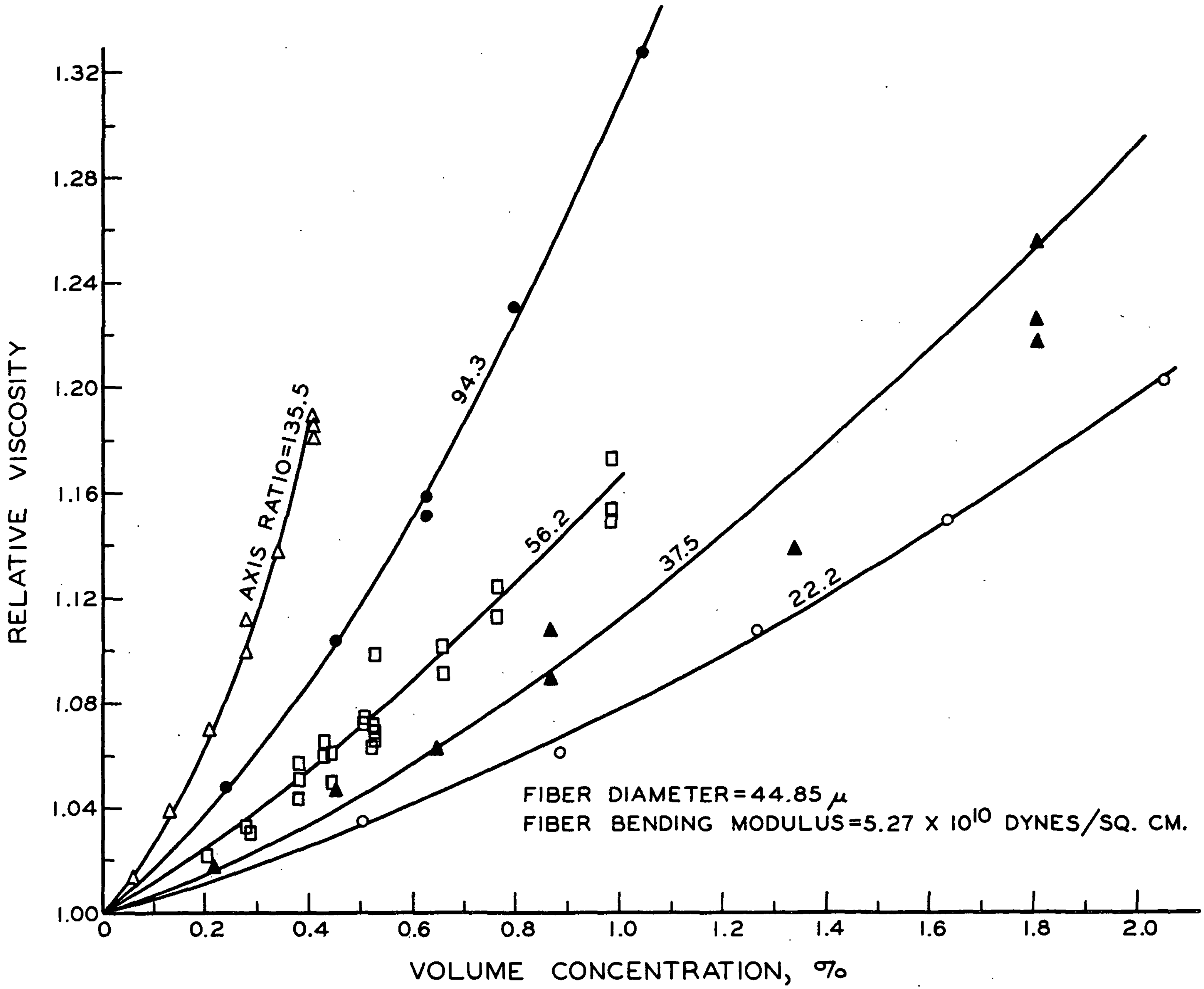

Figure 39. Relative Viscosity-Concentration Relationship of Nylon Fiber Slurries

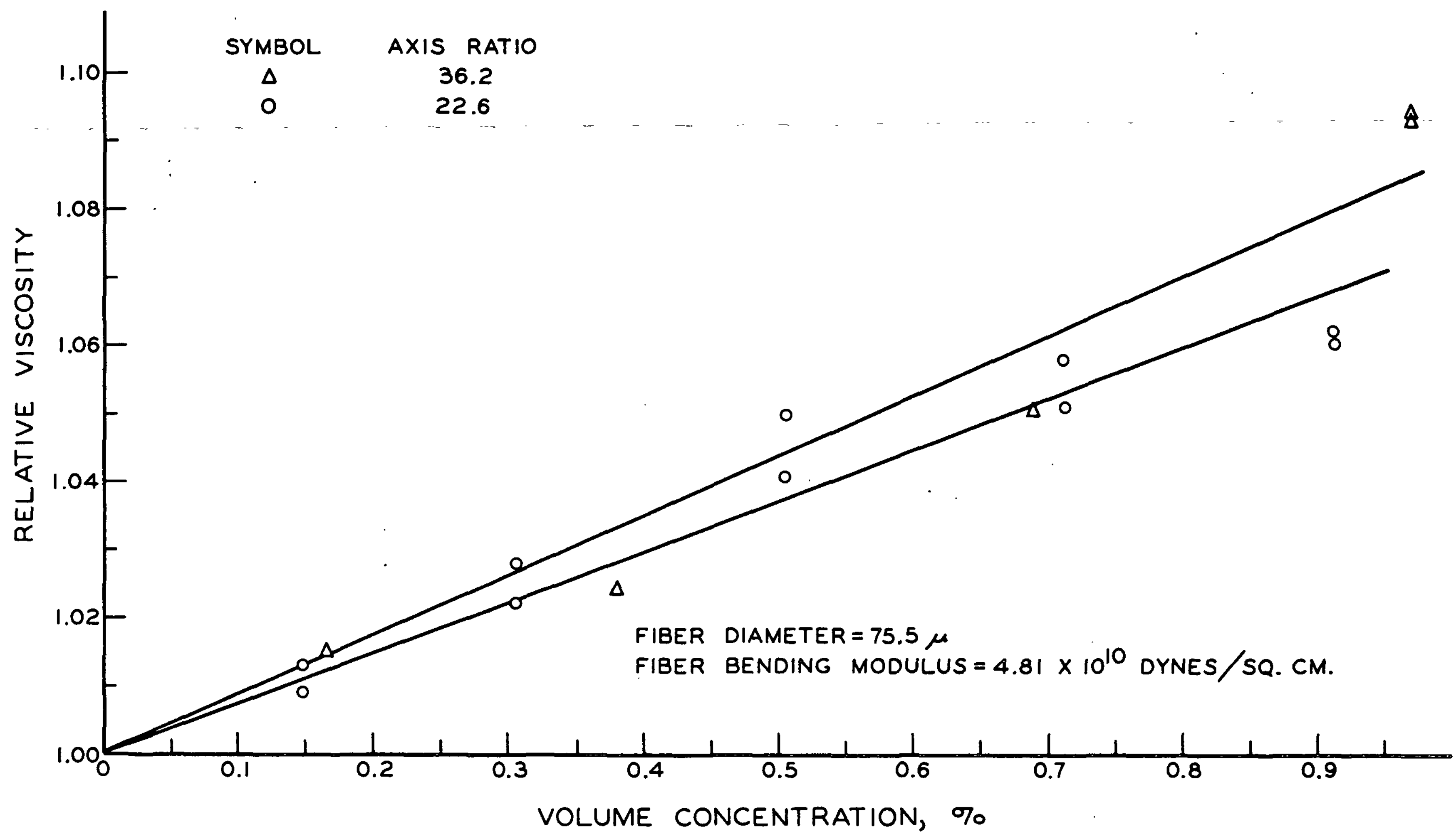

Figure 40. Relative Viscosity-Concentration Relationship of Nylon Fiber Slurries

scatter of the data. The procedure change was to increase the concentration by adding fibers to the slurry rather than to start with a high concentration of fibers and reduce the concentration by removing fibers. However, the data that were obtained were statistically significant and followed the general pattern observed with the other fibers, so the work was not repeated.

The data obtained for the smallest (Fig. 38) and largest (Fig. 40) diameter fibers show a linear viscosity-concentration relationship at axis ratios below 40. However, curvature was observed (see Fig. 39) in this axis ratio range for the slurries of the 44.85 μ diameter fibers. This curvature is slight for concentrations of 0 to 1%, so it is possible that the scatter in the large-diameter fiber data caused the effect to be masked.

It was shown in the theoretical section that the approximate analysis of Burgers (17) for the flow of fiber slurries resulted in the relation,

$$\mu_r = 1 + \alpha_o C, \tag{26}$$

where,

$$\alpha_o = \frac{(L/d)^2}{6(\ln \frac{2L}{d} - 1.8)} \sin^4\theta \sin^2 2\phi$$

The coefficient α_o is a function of the axis ratio and orientation of the fiber with respect to the shear field. This equation is only intended to be a "reasonable approximation" of the actual conditions. In view of this, it is interesting to note that the general form of Equation (26) may be obtained by dimensional analysis, as follows:

The motion, ω_b, of a bob in a slurry of fibers is felt to be governed by the applied torque per unit bob length, T', the viscosity of the suspending liquid, μ_o, the fiber length, L, the fiber diameter, d, the fiber concentration (number of fibers per unit volume), N, the bob radius, r_1, and the cup radius, r_2, i.e.,

$$\omega_b = \phi(L,\ d,\ T',\ N,\ \mu_o,\ r_1,\ r_2) = \alpha' L^a d^b T'^c \mu_o^f r_1^g r_2^i \tag{51}$$

Solving for the exponents and substituting yields an equation of the form:

$$\frac{T'}{\omega_b} = \alpha' \left(\frac{L}{r_1}\right)^{-a} \left(\frac{d}{r_1}\right)^{-b} (N r_1^3)^{-e} \left(\frac{r_2}{r_1}\right)^{-i} \mu_o \tag{52}$$

This equation may be further simplified if certain experimental and theoretical work is considered. First, the term, T'/ω_b should be proportional to the viscosity, μ_f, of the suspension. Next, Hersey (47) showed by dimensional analysis that the flow equation for a concentric cylinder viscometer should be: $T'/\omega_b \sim \mu_o r_1^3 (r_2/r_1)^{P_o}$. Also, Einstein (48) has shown that the viscosity of a very dilute suspension of spheres is directly proportional to the concentration of the spheres. This theory has been proved experimentally. These facts would seem to indicate that the exponent e equals -1, while the exponent $b = -a$. Substituting into Equation (52) and solving for the relative viscosity, one obtains the following:

$$\mu_r = \frac{\mu_f}{\mu_o} = 1 + \alpha' \left(\frac{L}{d}\right)^{-a} N r_1^3 \left(\frac{r_2}{r_1}\right)^{-i} \tag{53}$$

From this result, one might conclude that α_o is indeed a function of the axis ratio under the conditions assumed in the derivation.

The best line was drawn through the experimental points in the viscosity-concentration plot by making a regression analysis of the data. The solid lines in Fig. 38-40 represent the loci of the points on these lines. The μ_r-C data which exhibited a linear relationship were correlated with an equation similar in form to Equation (26). Where curvature occurred in the μ_r-C relationship, the empirical equation: $\mu_r = 1 + \alpha_o C + \alpha_1 C^2$ was used to correlate the data. This equation has the same form as that derived from theoretical considerations by Vand (49) for suspensions of spheres in which interaction occurs. The values of α_o and α_1 are included in Table VI along with the values obtained by Eirich, *et al.* (8) and Nawab and Mason (9).

The graphical relationship between α_o and the axis ratio is shown in Fig. 41. For purposes of comparison, the relationships between *L/d* and α_o as determined from Burgers' equations are also shown. Even though a logarithmic relationship for *L/d* is indicated by the form of the equations, over the narrow range of axis ratios studied (20-180), it may be approximated by a straight line (see Fig. 41). At axis ratios less than 10, the relationship deviates from linearity (see Fig. 42) and the concentration coefficient increases as the axis ratio decreases. According to Equation (26), when *L/d* is about three, α_o becomes infinite. However, Burgers did not intend for the equation to apply in this range, because he stated that *L/d* had to be much greater than unity. If the viscosity behavior of a cylinder with an axis ratio of 1 may be approximated by that of a sphere, then α_o at this axis ratio should be 2.5 from Einstein's (48) theory. The linear extrapolation of the nearly linear portion of Burgers α_o-*L/d* relationship for fibers in the *x-y* plane and the data for the fibers at a *d/D* of 0.00088 yields a value of α_o of about 2.4 at *L/d* = 1. It is believed that at least for *L/d*'s between 1 and 10, α_o decreases with decreasing *L/d*. The data of Eirich, *et al.* (8) appear to confirm this hypothesis (see Fig. 42).

The experimental data may also be represented by a linear relationship. However, for the fibers which yield the lowest viscosity increases (16.79 μ diameter fibers), the slope of the α_o-*L/d* relationship is about twice that of the "theoretical" line representing a fiber slurry which yields a maximum viscosity increase. Increasing the fiber diameter causes the deviation to be even greater. This effect

TABLE VI

CONCENTRATION COEFFICIENTS α_o AND α_1 AND SLOPES OF α_o VERSUS L/d PLOTS

Sample	Diameter, microns	L/d	α_o	α_1
680-.4[a]	16.79	23.1	4.91	--
680-.6		35.5	7.07	--
680-1.2		58.3	9.08	444.0
680-2.0		101.5	14.87	5779.0
680-2.5		162.4	22.24	53886.0
260-.9[a]	44.85	22.2	5.71	205.4
260-1.5		37.5	7.60	355.9
260-2.42		56.2	10.59	612.8
260-4.0		94.3	16.08	1475.0
260-6.0		135.5	19.85	6515.0
(P-1643-6)-1.5[a]	75.5	22.6	7.29	--
(P-1643-6)-2.5		36.2	9.05	--
O.C. 13.35[b]	12.86	78.0	12.61	--
Nawab and Mason (9)[c]	3.5	43.2	8.2	120
		75.0	15.2	260
		113.0	18.5	960
Eirich, *et al.* (8)[d]	40.0	5	5.1	
		10.5	5.5	
		17.0	6.4	

	Sample	Slope
Experimental	680	0.123
	260	0.128
	P-1643-6	0.131
Theoretical (17)	x-y	0.071
	min.	0.046

[a]Nylon fibers.

[b]Glass fibers.

[c]Rayon fibers.

[d]Silk fibers.

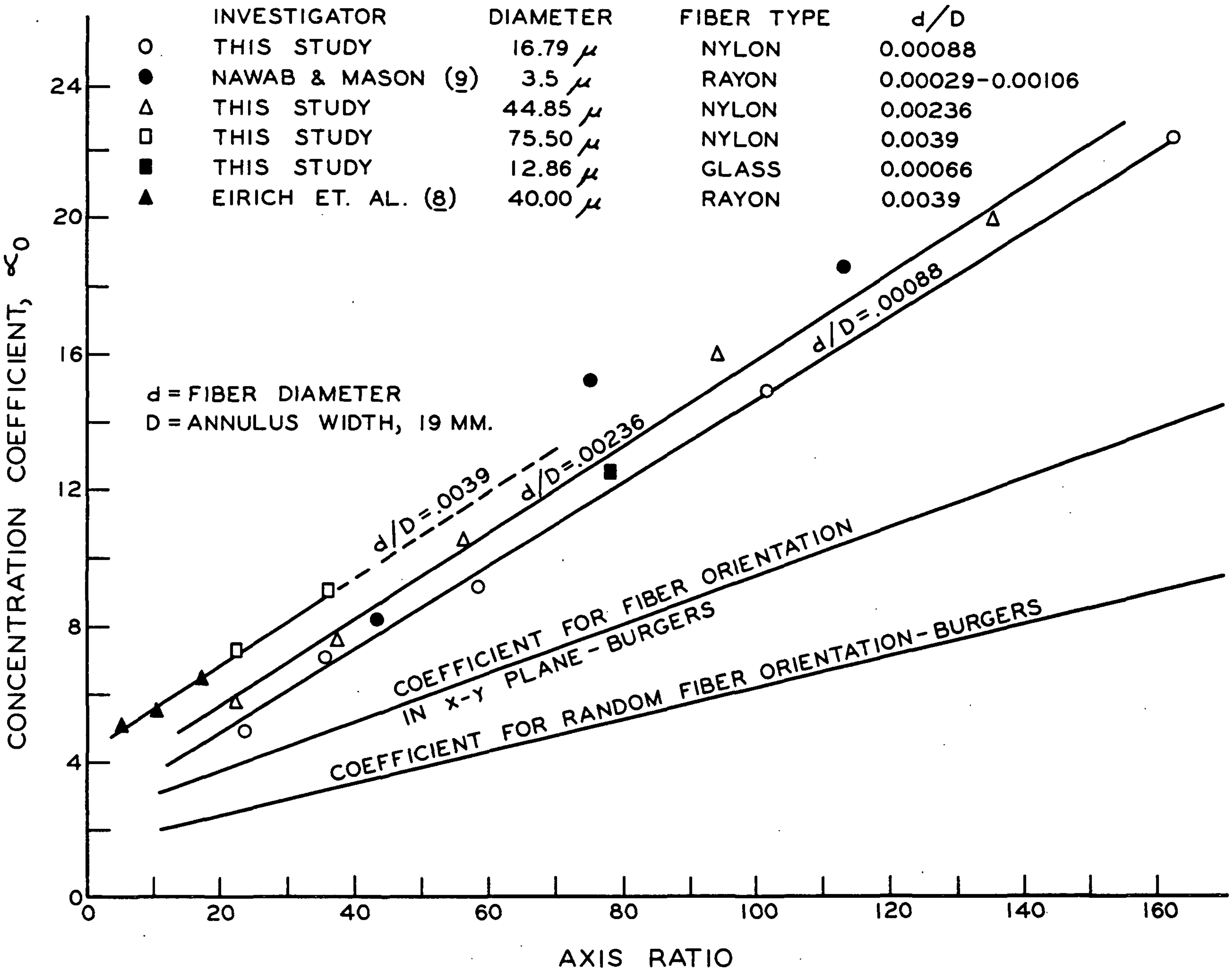

Figure 41. The Relationship Between the Concentration Coefficient α_o and the Fiber Axis Ratio

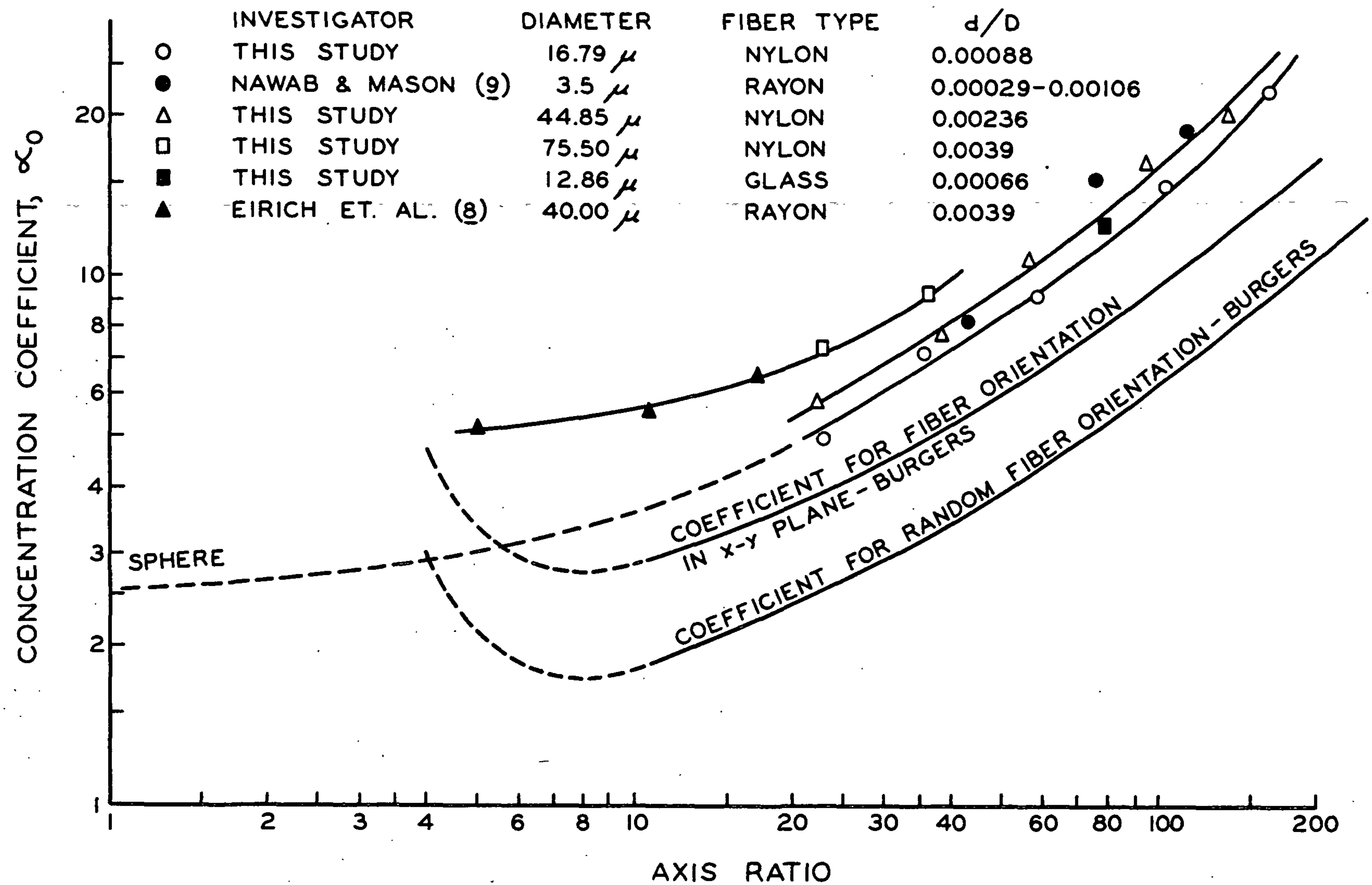

Figure 42. The Relationship Between the Concentration Coefficient, α_o and the Fiber Axis Ratio

is believed to be a result of fiber-wall interaction and it will be discussed later in a separate section.

Before any explanation is made of why the experimental data do not agree with the theoretical relationships, it is desirable to review how well the experimental work conforms to the conditions of fiber slurry flow stated earlier in the Theoretical section. It has been established that the maximum Reynolds number encountered in the flow past an individual fiber is less than the Reynolds number at which the inertial effects become appreciable. This satisfies the condition of viscous flow. The size of the fibers is much larger than the dimensions of the molecules in the suspending solution; thus, there should be no slip at the surface of a fiber.

Equation (26) was developed under the assumption that there was no interaction between the flow fields of the fibers. As previously stated, no theoretical work has been done relating the fiber properties to the flow behavior of a fiber suspension in which interaction occurs. Theoretical studies (49) of the effect of interactions on the flow of suspensions of spheres have shown that the coefficient, α_o, is unaffected by interactions. By analogy, the coefficient, α_o, for a fiber suspension would be expected to be independent of interactions. It will be assumed that this is the case in this study.

In the previous work (8, 9) with synthetic fiber suspensions, it was shown that the flow behavior was affected by the size of a fiber with respect to the apparatus dimensions, i.e., wall effects were present. If the concentration of a suspension in which wall effects occur is held constant and the length and diameter values of the fibers in the suspension are proportionally increased, so that L/d is constant, the viscosity will increase. This is a result of additional flow disturbances of the fibers near the wall which are greater than the contributions of the fibers near the center of the annulus.

For spheres (37) the magnitude of the effect is proportional to d/D where d is the fiber diameter and D is the annulus width. Han (44) has shown that for a fiber settling in a bounded fluid, the wall effect is a function of both fiber diameter and length. However, for flow of fiber suspensions in a concentric cylinder viscometer Nawab and Mason (9) did not observe any wall effects up to a d/D of 0.0016 and an L/D of 0.12. In the study of the 16.79 μ diameter fibers the maximum values of d/D and L/D were 0.00088 and 0.14, respectively. Therefore, it is believed that the wall effects were not appreciable for suspensions of these fibers. The effect of the wall on the viscosities of suspensions of fibers with larger dimensions will be discussed in a later section of the report.

The final condition to be satisfied is that of using rigid cylindrical fibers. With the exception of Sample P-1643-2 the fibers used (see Fig. 27 and 28) were cylindrical with only a very slight curvature occurring along the axes of some of the fibers.

There is also some question as to whether or not the forces on the fiber in a shear gradient are great enough to cause it to deform. From Burgers' equation (14) for the fluid forces on a cylindrical fiber rotating in a shear field, Forgacs and Mason (50) derived the following equation for the minimum product of the shear rate, G, and the fluid viscosity, μ_o, at which a rodlike particle with a bending modulus of E_b will buckle:

$$(G\mu_o)_{critical} = \frac{E_b(\ln \frac{2L}{d} - 1.75)}{2(\frac{L}{d})^4} \tag{54}$$

For the case of the fiber with the greatest axis ratio (162.4) and the lowest bending modulus (1.85×10^{10} dynes per sq. cm.), the critical shear rate at which bending would be expected to occur as calculated from the above equation was 7.18×10^2

$\sec.^{-1}$. The maximum rate of shear attained in this study was 2.2 $\sec.^{-1}$. The experimental shear rate for fiber bending as determined by Forgacs and Mason showed agreement with the value predicted by Equation (54) to within a factor of 4. Because of the order of magnitude difference in the predicted critical rate of shear and the maximum rate of shear used in this work, it is extremely doubtful if fiber bending due to the fluid forces affected the viscosity determinations.

As an experimental check on the problem of fiber bending, the concentration dependence of the viscosity of a slurry of glass fibers was determined. These fibers were not only uniformly cylindrical (see Fig. 28), but possessed a bending modulus approximately 25 times greater than that of the nylon fibers. The relative viscosity _versus_ concentration relationship is shown in Fig. 43, while the slope of the line or the concentration coefficient, α_o, is plotted in Fig. 41. Because this value falls on the same line as the data for the small-diameter nylon fibers, it is felt that this is further proof that there is no appreciable deviation in the results due to fiber bending.

It has been shown that each of the five conditions which Burgers specified as necessary for his derivation has been satisfied to a high degree in this study. However, there is still some question regarding the validity of the assumption that no interaction occurs between fibers. Even though these experimental conditions closely approximate those required for Burgers' derivation, the data do not agree with the theoretical behavior of a slurry of cylindrical fibers.

An empirical equation representing the experimental relationship between the axis ratio and the concentration coefficient for the 16.79 μ fibers is:

$$\alpha_o = 2.26 + .123(L/d) \qquad (55)$$

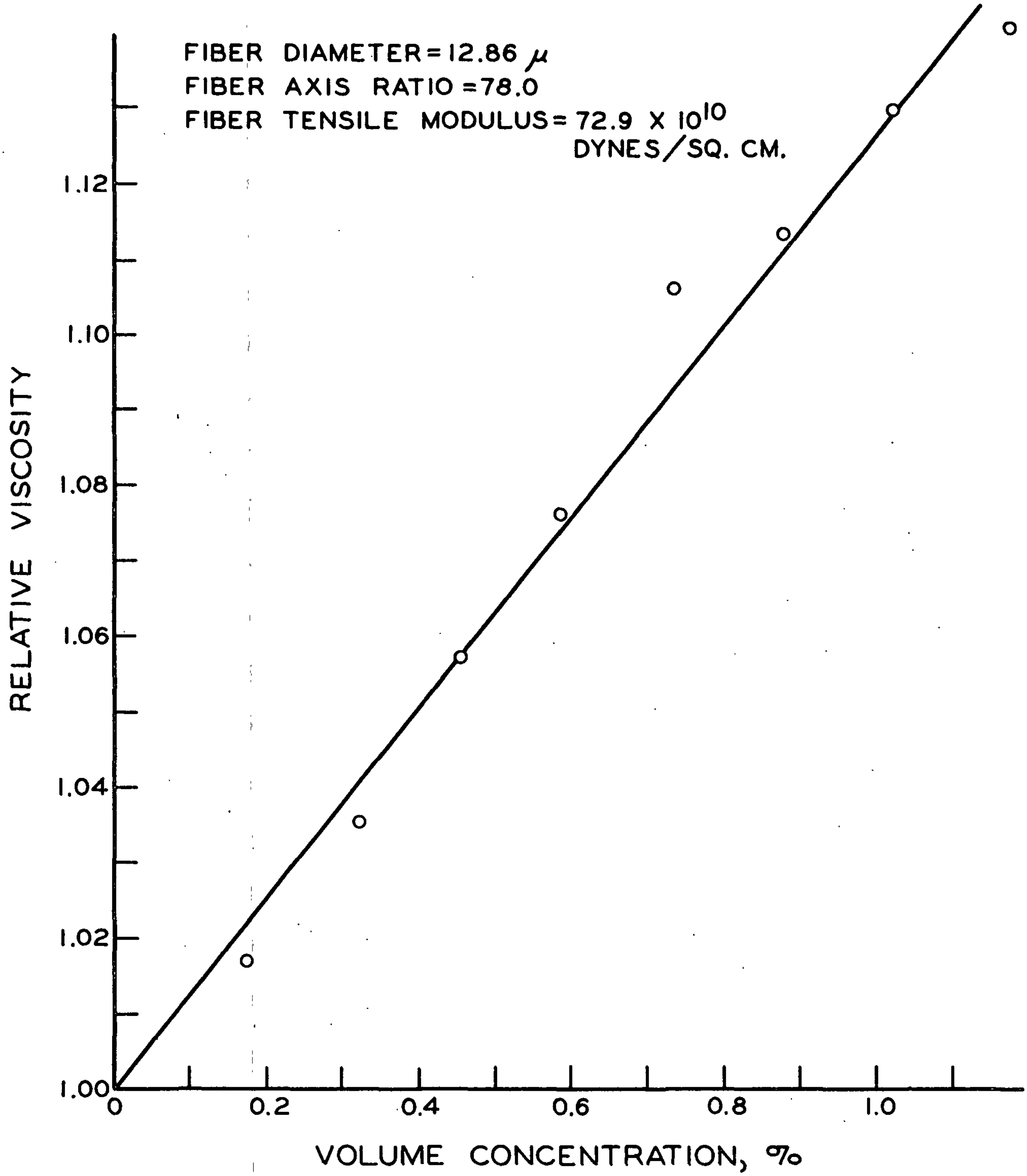

Figure 43. Relative Viscosity-Concentration Relationship of Glass Fiber Slurries

while Burgers' theoretical relationship for the coefficient for fibers aligned in the *x-y* plane may be represented by the following equation over the range of axis ratios from 0 to 160:

$$\alpha_o = 2.32 + .071(L/d) \tag{56}$$

Thus, it may be seen that the slope of the line representing the experimentally determined concentration coefficient-axis ratio relationship differs from the predicted relationship for fibers aligned in the *x-y* plane by somewhat less than a factor of two. Actually, the experimental relationship could possibly be different from the theoretical by more than a factor of two. Binder (51) indicated that above an axis ratio of 15, the fibers become preferentially oriented in a horizontal plane. Mason and Manley (52) actually measured the orbit distributions of very dilute concentrations ($< 62 \times 10^{-4}$ ml./ml.) of dacron fibers covering a range of axis ratios from 20 to 115. They found that the change in the orbit phase of these fibers reached an equilibrium state in which the average orbit was somewhere between that in a slurry of randomly oriented fibers and one in a slurry in which the fibers rotated parallel to the *z*-axis. However, Arlov, *et al*. (44), studying the interaction of pulp fibers in a laminar shear field, observed that the orbit of a fiber tended to approach the *x-y* plane after an apparent collision with another fiber. It was previously pointed out that interaction was surely present in the lowest concentration fiber slurries used in this work.

There are no data on the orientation of fibers in more concentrated slurries, but it is logical to assume that the fibers are not completely oriented in the plane of flow. Any fiber orientation other than in the *x-y* plane would mean that the experimental concentration coefficient would differ from the predicted coefficient by more than a factor of two.

One of the major reasons for the discrepancy between the theoretical and experimental values of α_o is that the equations are only intended to be good approximations of the flow behavior of cylindrical fiber suspensions. Quoting Burgers regarding his method of representing the effect of a fiber on the surrounding liquid: "... the field produced by ... forces (acting at points on the fiber axis) will be a tolerable approximation to the field which will exist outside the actual body and, consequently, the system of forces will give an approximate picture of the forces which are exerted by the body when immersed in a field." Burgers also represented the flow field around a cylinder in slow translation in a viscous fluid by the same technique used for a rotating cylinder. That is, a system of forces was visualized as being located on the cylinder axis producing fluid velocity components relative to the fiber which vanished at the fiber surface.

Experimentally, the study of the translation of cylindrical fibers is more straightforward than a study of suspension flow. All the variables in the theoretical equation [Equation (57)] specifying the slow movement of a fiber through a viscous liquid can be accurately determined. For this reason, it would be instructive to compare Burgers' equation for this motion with the experimental relationship.

Burgers' equation for the drag force on a cylinder in creeping translation is:

$$F_{\infty} = 4\pi\mu_o dU\phi(L/d) \tag{57}$$

where

$$\phi(L/d) = \frac{L/d}{\ln\frac{2L}{d} + \frac{1}{2}}$$

U is the fluid velocity perpendicular to the axis of the cylinder, and μ_o is the fluid viscosity.

The drag force on a cylinder in slow translation may be determined experimentally with the aid of the following equation:

$$F_\infty = \frac{\pi}{4} d^2 L(\rho_s - \rho)g = 4\pi\mu_o dU\phi'(L/d) \tag{58}$$

where ρ_s is the density of the fiber, ρ is the liquid density, and $\phi'(L/d)$ is the experimentally determined axis ratio function. If the physical characteristics of a cylinder in creeping motion are known as well as its equilibrium velocity, the axis ratio functions in the above equations may be determined. In 1945, White (42) measured the velocities attained by copper wires of known dimensions in glycerin solutions.

The functions $\phi(L/d)$ and $\phi'(L/d)$ calculated from White's data are listed in Table VII for wires of different axis ratios. The experimental data were corrected for wall effects by Han (44) using the method of Brenner (53). In this case, where it was possible to experimentally match very closely the assumptions used in deriving Equation (57), the experimental function, $\phi'(L/d)$, is greater than the "theoretical" function, $\phi(L/d)$, by a factor of about 4/3. Burgers does state that a more exact calculation would yield a drag force slightly higher than that predicted by the equation.

It is felt significant that the drag force for a cylinder in slow translation and the increase in viscosity of a fluid due to the presence of the cylindrical fibers are both underpredicted by Burgers' force method. Both equations, Equations (26) and (57), were developed on the assumption that the system of forces along the axis of a fiber followed a continuous relationship. The general form of this relationship may be represented by the force distribution equation for a rotating

TABLE VII

A COMPARISON OF BURGERS' SOLUTION FOR THE AXIS-RATIO DEPENDENCE OF THE DRAG FORCE ON A CYLINDER IN SLOW TRANSLATION WITH THAT DETERMINED EXPERIMENTALLY

L/d	Ø(L/d) Burgers (17) "Theoretical"	Ø'(L/d) White (42) Experimental	Ratio Ø'(L/d)/Ø(L/d)
4.9	1.76	2.35	1.33
11.0	3.07	4.12	1.33
15.9	4.02	5.36	1.33
19.6	4.70	6.25	1.33
23.2	5.35	7.15	1.33
28.1	6.22	8.25	1.32
36.7	7.65	10.20	1.32
50.1	9.80	13.20	1.35

cylinder:

$$f(\ell) = 8\pi\mu_o\, G_o[A_1(\ell/L) + A_2(\ell/L)^3]\sin^2\theta\sin\phi\cos\phi \qquad (14),$$

where the shear gradient, G_o is replaced by the fluid velocity U and (ℓ/L) is raised to different powers in the equation describing the force distribution on a cylinder in translation. In order to find the drag force on a fiber in translation, the forces must be summed over the entire length of the fiber. As shown in the theoretical section, the disturbance of a fluid caused by a rotating fiber is determined from the magnitude of the force doublet M on the fiber. This doublet is also calculated by the proper summation of $f(\ell)$ over the fiber length. If $f(\ell)$ is underestimated by Equation (14), then the drag force and viscosity due to the disturbance would also be lower than that determined experimentally.

It may be postulated that the force distribution does not precisely follow such an equation because of the discontinuities in the flow around the ends of the cylinders. This hypothesis could be tested if the flow behavior of cylinders with very large axis ratios could be studied. Then, if the flow around the ends does cause increased flow disturbances at low axis ratios (20-180), the effect would be expected to diminish at the higher $\underline{L}/\underline{d}$ ratios. It should be noted that this approach yields a viscosity equation for suspensions of spheres equivalent to that derived by the more rigorous method of Einstein (48). There would be no end effects for this case.

At the present time, there is no theoretical relationship for the viscosity of cylindrical fiber suspensions where interaction occurs. It has been shown that viscosity data for these suspensions may be correlated by an equation of the form: $\mu_{\underline{r}} = 1 + \alpha_o\underline{C} + \alpha_1\underline{C}^2$. A qualitative physical picture of an interaction effect was obtained by Mason and Manley (52) who showed that an apparent collision between two fibers greatly changed their rotation orbits. Such collisions do occur at very low concentrations. In an analysis of fiber behavior in a turbulent flow field where fiber orbits were approximated by spherical surfaces, Mason (54) showed that a fiber with an $\underline{L}/\underline{d}$ of 40 in a 0.01% concentration (by volume) suspension underwent about three collisions per second. In laminar flow the orbit of a fiber roughly corresponds to the surface of a double cone. This would decrease the number of collisions, but it is felt that there would still be enough physical interactions to invalidate the assumption of complete freedom of fiber motion. Because of the abrupt changes in a fiber orbit resulting from a collision, at certain times a fiber would not be able to follow any of the components of the fluid velocity in the shear field. It was assumed in the derivation of the viscosity equation that the fiber motion was such that a fiber followed all the fluid velocity components except that directed along the axis. Because this is not strictly true, an increase in the viscosity over that predicted by Equation (26) would occur.

The μ_r-C relationship for the smallest (16.79 μ) diameter fibers (see Fig. 33) is linear over a concentration range of 0 to 1.70% for L/d's of 35.5 and 23.1. In these cases the interaction effect is not appreciable. For the next size diameter (44.85 μ) fibers (see Fig. 34) a slight curvature is observed over this L/d range and is felt to be a result of wall effects. The data for the largest diameter (75.5 μ) fibers (see Fig. 35) were correlated with straight lines, but the data scatter was such that any curvature due to wall effects would have been masked. Where curvature of the μ_r-C relationship for the 16.79 μ and the 44.85 μ diameter fibers occurred, the values of the coefficient α_1 were determined and reported in Table VI. Vand (49) has shown that α_1 is a function of α_o for suspensions of spheres. It appears that this also holds true for fiber suspensions as evidenced from the data in Fig. 44. It is interesting to note that Mason and Nawab's (9) data follow the same general trend.

At this time, complete experimental verification of the theoretical work concerning the interaction of spheres in suspension has not been accomplished. A theoretical analysis of the interaction effect for fibers would be even more complex to perform. Therefore, any attempts to explain the observed relationship between α_o and α_1 would necessarily be quite empirical and perhaps misleading. It does appear that both coefficients are functions of the axis ratio of fibers and the data recorded may be of more value when a suitable interaction theory has been advanced.

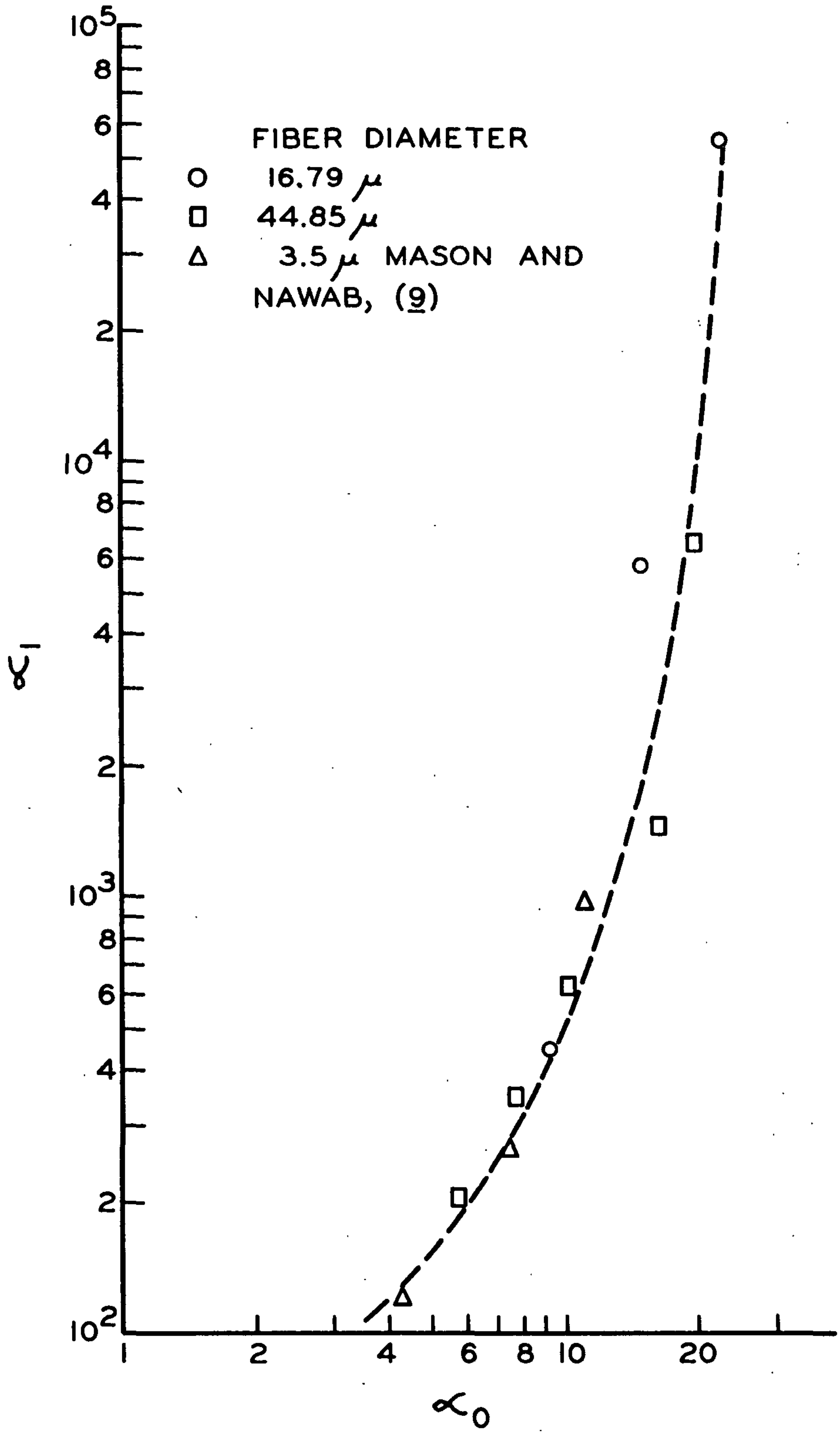

Figure 44. The Relationship Between the First Order Concentration Coefficient, α_o and the Second Order Coefficient, α_1

MODIFICATIONS OF BURGERS' EQUATIONS

The analysis of the experimental data has shown that Burgers' equations describe the general behavior of the viscosity of cylindrical fiber slurries with respect to the axis ratio of the fibers. Certain "simplifications" in the development of the equations as well as the failure of the experimental conditions to exactly match some of the assumptions used in deriving the equations are felt to be the cause of the discrepancy between the "theoretical" constants in the equations and those determined experimentally.

Nawab and Mason (9) proposed to use an "equivalent" axis ratio in the equation [Equation (28)] for the goniometric factor. This "equivalent" axis ratio r_e was determined experimentally with the aid of the following equation, the form of which was obtained from Jeffery's (16) equations for the motion of an ellipsoid in a shear field:

$$tG = 2\pi(r_e + \frac{1}{r_e}) \tag{59}$$

where t is the measured period of rotation of the fiber and G is the known velocity gradient of a flow field defined by the velocity components $u = Gy$; v, $w = 0$. The value of their experimental concentration coefficient, α_o, was between the values of the coefficient for random orientation and that for alignment in the x-y plane as determined from Burgers' equations modified to include the equivalent axis ratio, r_e.

Though this approach shows promise in representing empirically the flow behavior of a slurry, it is felt that it is an oversimplification which possibly masks the true physical picture. Mason and Nawab show that a single cylindrical fiber in a shear field executes a complete revolution in less time than Jeffery's equation would predict for an ellipsoidal particle of the same axis ratio. It is felt that this difference is due to the different flow pattern around the cylinder caused by the straight mantle and the finite end sections.

Burgers' drag force equation for the slow translation of a cylindrical fiber perpendicular to its axis is equivalent to Jeffery's equation for an ellipsoid of the same axis ratio for $L/d \gg 1$. However, as previously shown, the equation underestimates the experimentally measured drag force by a nearly constant factor. This supports Burgers' statement that the equation is only an approximation. It also raises doubt as to whether one can correct the goniometric factor in Equation (26) without also changing the rest of the equation which was derived from a consideration of the forces on the fiber.

For the present, it is felt that it would be better to use Burgers' equation for the viscosity of fiber suspensions only as a guide to the behavior with the realization of its limitations. The next logical step would be to attempt to perform a more exact analysis of fiber slurry behavior, keeping in mind the physical picture of the system which has grown out of this and past studies (8, 9).

Wall Effect

It was previously stated that the viscosity studies with the 16.79 μ diameter fibers were felt to be relatively free of wall effects. This supposition was based on the fact that the dimensions L and d of the fibers relative to the annulus width were within the range which Nawab and Mason (9) showed to be independent of wall effects.

A linear relationship was obtained when α_o's for the larger diameter fibers (44.85 μ and 75.5 μ) were plotted versus L/d keeping d/D constant. The data obtained by Eirich, _et al._ (_8_) also may be correlated in this manner. Nawab and Mason's coefficient for suspensions of fibers of $\underline{L}/\underline{d} = 43.2$ agrees with this work, but α_o at the higher $\underline{L}/\underline{d}$'s (75 and 113) appears high. They state that a large fraction of the larger $\underline{L}/\underline{d}$ fibers were curved which would account for the discrepancy (see section on Fiber Shape Effect). The trend of the data indicates that the increase in suspension viscosity due to the wall effect is not a simple relationship involving only the $\underline{d}/\underline{D}$ ratio. As would be expected from the work of Han (_44_) who showed that fiber length entered into a calculation of the wall effects for a fiber in creeping motion, the length also must be considered in determining the wall effects for fiber suspension flow. The lines representing the α_o-$\underline{L}/\underline{d}$ relationship are statistically parallel, even though the data do show a slight increase in slope (see Table VI) for an increased fiber diameter-annulus width ratio. Therefore, the percentagewise contribution of the walls to the viscosity increase decreases as the axis ratio increases.

If it is assumed that the experimentally determined lines in Fig. 41 are parallel and furthermore that the viscosity data for a 16.79 μ diameter fiber is unaffected by the walls, the data can be correlated by the following empirical equation:

$$\alpha_o(d/D) = \alpha_o(d'/D)[1 + \frac{k}{(L/d)^n}(d/D - d'/D)] \tag{60}$$

where $\underline{d}'/\underline{D}$ is the ratio at which the wall effect becomes appreciable. From the experimental data, the term $\underline{d}'/\underline{D}$ may be shown to be 0.0012, while the exponent $\underline{n}$ is approximately unity.

The form of Equation (60) leads to a possible explanation of both the wall effect and the behavior of the fiber slurries. Mason (_54_), using Jeffery's (_16_) equations, demonstrated that the theoretical orientation of the fibers changes with the axis ratio. Mason's results, shown in Table VIII indicate that as the axis ratio is increased, the fibers spend more time oriented in the direction of flow. If the major portion of the flow disturbance is directed along a fiber axis, as was assumed in Burgers' (17) derivation, then more interference would be expected when a fiber is oriented perpendicular to the direction of flow than when it is parallel to the flow direction. Since fibers with greater axis ratios are more preferentially oriented in the flow direction, it might be expected that the percentagewise contribution of the wall effect to the viscosity increase would be diminished.

TABLE VIII

ORIENTATION OF FIBERS IN FIELD OF FLOW (54)

	Fiber Fraction	
Axis Ratio	Oriented Within 0-5° of Direction of Flow	Oriented Within 0-10° of Direction of Flow
20	0.664	0.824
40	0.822	0.910
60	0.880	0.939

In order to verify the above hypothesis, more experiments must be performed. These experiments should seek first to determine at what d/D ratio the wall effect becomes appreciable. Further data are needed to verify the parallel nature of lines representing the concentration coefficient-axis ratio relationship at different d/D ratios. The average orientation of the fibers at the concentrations at which the viscosities were determined should also be measured. The scope of these experiments would necessarily be great, as well as the experimental difficulty. It is felt that such a study would be of value only when the behavior of a fiber slurry in which the wall effect is negligible is theoretically and experimentally defined.

Fiber Shape Effect

It was hoped that by using fibers of sufficiently low bending moduli the effect of this variable on the viscosity of fiber slurries could be determined. However, the calculation (see section on Suspension Viscosity) of the shear rate necessary to cause bending of the lowest modulus fiber available indicated that the order of magnitude of the shear rate required was unobtainable with the apparatus. During the characterization of the low modulus fibers, it became apparent that Samples 11925-2.5, 11925-2.0, and (P-1643-2)-1 exhibited extreme curvature even when cut to very short lengths. A photomicrograph of Sample (P-1643-2)-1 is shown in Fig. 28. Because high shear rates in a flow field would possibly cause a similar effect, it was decided to determine the flow behavior of these fibers. The general flow behavior was discussed previously in the section labelled Classification of Suspension Shear Behavior. It was shown that if the concentrations were low enough (see Table V) Newtonian flow behavior could be obtained. In this region it is useful to characterize the suspension behavior by the change in relative viscosity with change in the fiber phase volume fraction.

The $\underline{\mu_r}$-$\underline{C}$ relationships are shown in Fig. 45 while the data are recorded in Table XX, Appendix IV. These data were calculated in a manner similar to that used for suspensions of straight fibers. The values of α_0 and α_1 listed in the figure, as well as the shape of the curves show that the curved fibers in these suspensions cause a much greater increase in viscosity than straight fibers of the same axis ratio in suspensions of the same concentration. Tchen (55) used Burgers' approach to determine the drag force on a curved fiber in "creeping"

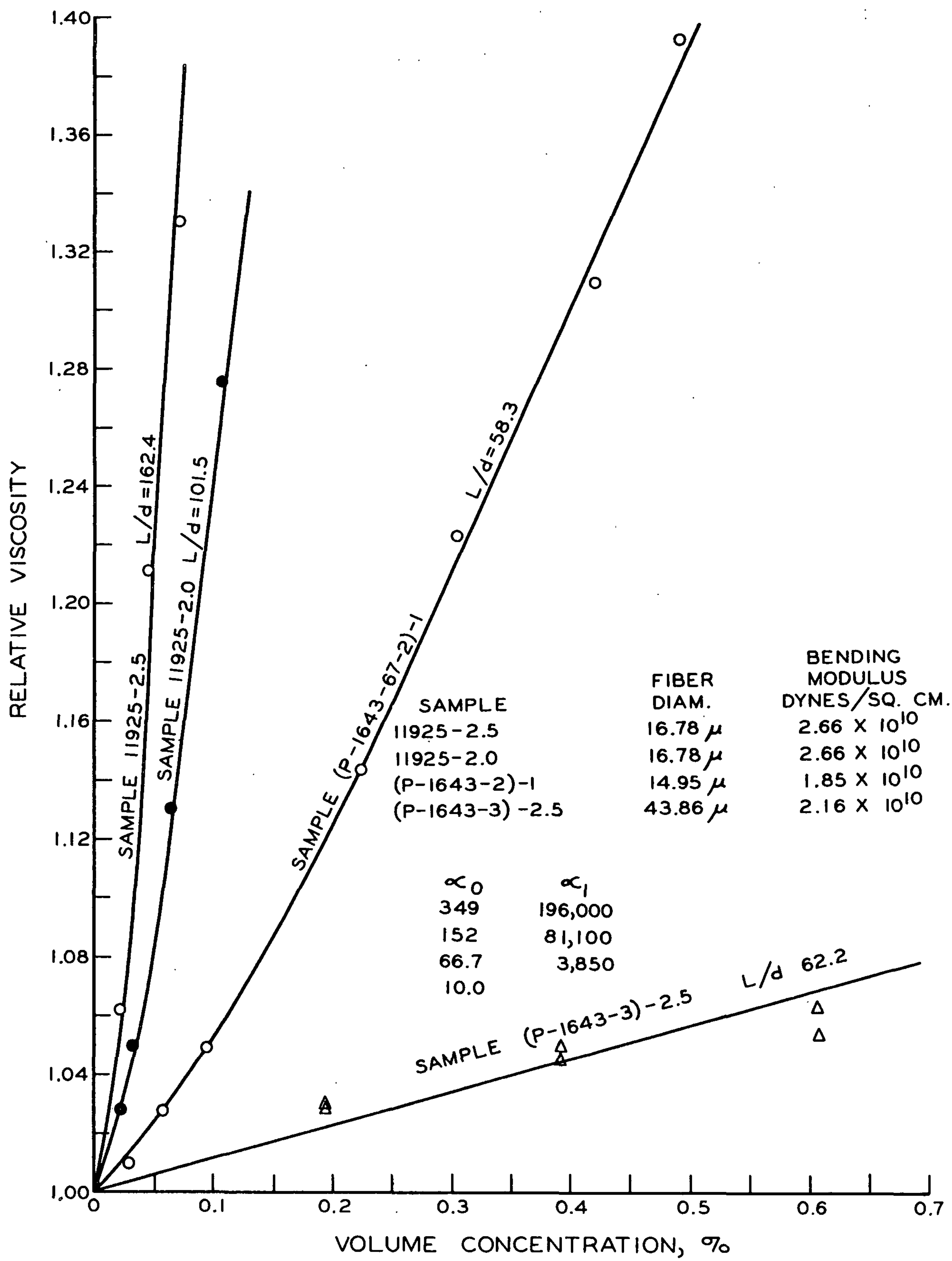

Figure 45. Relative Viscosity-Concentration Relationship of Nylon Fiber Slurries

translation in a viscous fluid. He demonstrated that the force on a curved fiber should be less than on a straight fiber with the same axis ratio. It was previously shown that the forces on a straight fiber rotating in a shear field may be calculated by a technique similar to that used to determine the forces on a fiber in slow translation. Furthermore, the viscosity increase of a fluid due to the presence of fibers is related to such forces. Therefore, it might be postulated that the viscosity increase due to curved fibers of a given $\underline{L}/\underline{d}$ should be less than if straight fibers of the same axis ratio were present in the fluid. It should be emphasized that the above argument was based on assumptions and analogies and can only be substantiated by actually determining the viscosity increase as a function of a characteristic curved fiber $\underline{L}/\underline{d}$ using an approach similar to that of Tchen.

Visual observations showed that small flocs were present in the suspensions even at the lowest concentrations. Fluid could become immobilized within these flocs and the effective fiber concentration would be increased. The flocs would also be less likely to follow the motion of the fluid, than a single fiber. Both fluid immobilization and fluid disturbances caused by the inability of such flocs to follow the undisturbed fluid motion would cause the viscosity of a curved fiber suspension to be greater than that of a straight fiber slurry ($\underline{L}/\underline{d}$ = constant) at the same volume fraction.

A suspension of low modulus fibers (P-1643-3)-2.5 of larger diameter (43.86 μ) was also studied. These fibers were much straighter than the other low modulus samples (see Fig. 28) and as a result the $\mu_{\underline{r}}$-$\underline{C}$ behavior was similar to that of the higher moduli fibers. In fact the value of α_o for this sample is in excellent agreement with that predicted from the α_o-$\underline{L}/\underline{d}$ relationship for the 44.85 μ diameter high modulus fibers shown in Fig. 41. The μ_r-C data for this sample are shown in Fig. 45 and recorded in Appendix IV, Table XX.

Effect of Suspending Fibers in an Aqueous Solution

It was previously shown (Fig. 34) that nylon fibers suspended in a sucrose solution exhibited nonlinear shear stress-shear rate behavior at concentrations where similar fibers suspended in the organic solution showed Newtonian behavior (see Fig. 31). This behavior of the fibers in the sucrose solution was attributed to the formation of fiber networks which could be broken down by increasing the shear rates. It was also shown that at a certain rate of shear depending upon the fiber concentration, the T-ω_b relationship became linear and the torque was directly proportional to the angular velocity. Viscosities of the suspensions were determined from the slopes of the linear portion of the T-ω_b curves. The μ_r-C relationship for the suspensions is shown in Fig. 46, while the data are tabulated in Table XXI, Appendix IV. Also shown in Fig. 46 is the viscosity curve for similar fibers (44.85 μ diameter and 56.2 axis ratio) suspended in an organic solution. This curve is the same as that for the 56.2 L/d fibers shown in Fig. 39.

The large difference between the two curves is again attributed to the formation of flocs (visible) in the sucrose solution as opposed to the lack of such flocs in the organic solution. The μ_r-C data for the fibers in the sucrose solution are not precise enough to determine the exact shape of the curve. Such scatter could be a result of the flocs and/or the anomalous behavior of the solution. The fluid behavior is further discussed in Appendix III. Because of the similarities of this system to a pulp fiber suspension, further viscometry studies of aqueous suspensions of synthetic fibers are suggested.

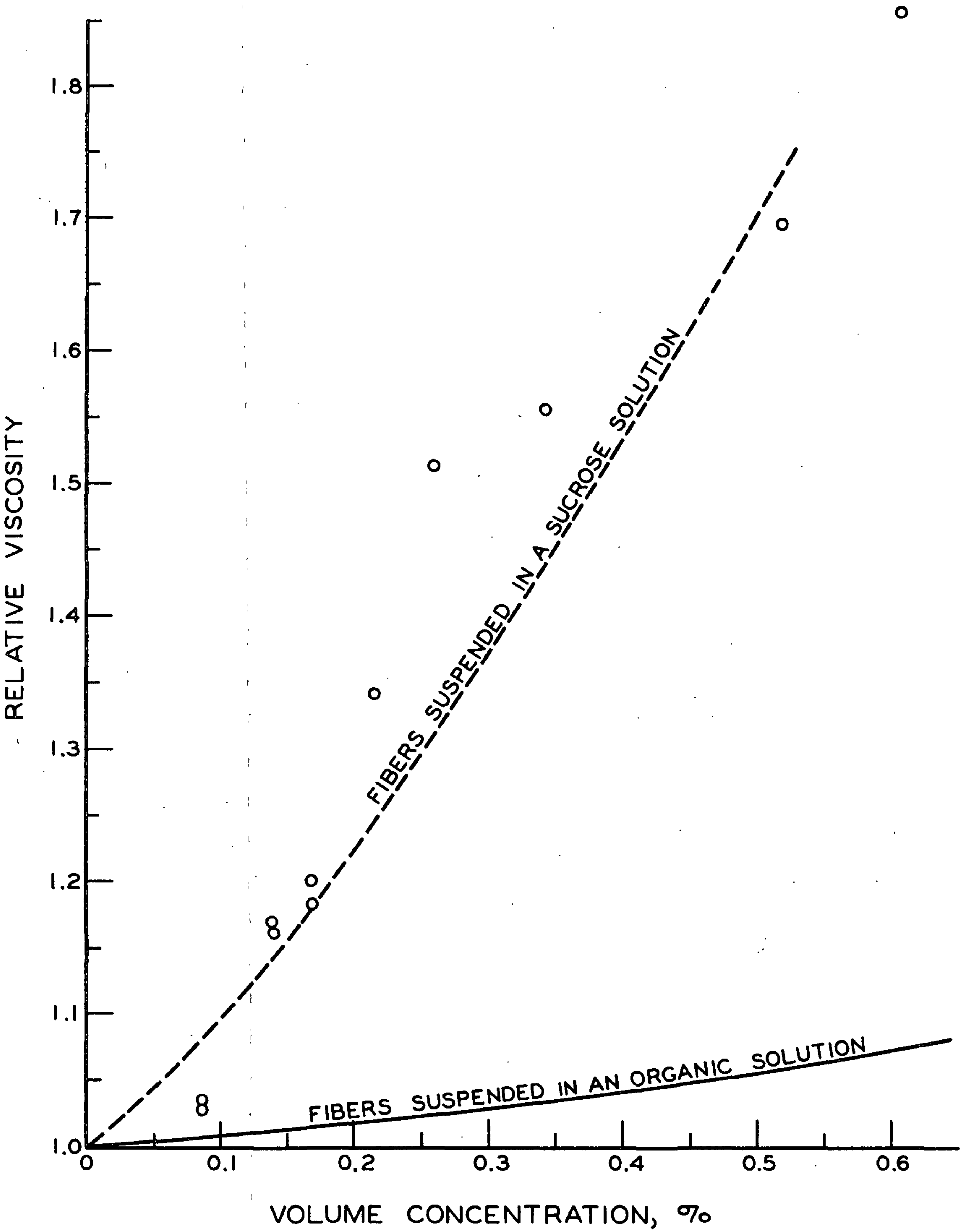

Figure 46. Relative Viscosity-Concentration Relationship of Nylon Fiber Slurries

THE STUDY OF THE STRESS-STRAIN BEHAVIOR OF FIBER SUSPENSIONS

Experimental difficulties involved in the measurement of the angular deflection of a fiber slurry subjected to a shear stress did not allow data of quantitative value to be taken during this phase of the study. The major sources of difficulty were:

1. Flocculation in slurries with fiber volume concentrations greater than 0.6% or fiber lengths greater than 2.42 mm. prevented the formation of reproducible networks. It was initially believed that even though flocculation occurred, the statistical nature of the size and distribution of the flocs would enable reproducible slurries to be obtained. This was not the case for the conditions stated above. In some cases for a given suspension a floc or series of flocs would bridge the annulus width causing the shear resistance of the slurry to be so great that no deflection of the bob could be observed even at the highest torques attained with the apparatus. In other runs, the network structure would be such that the bob would break loose from the suspension and rotate freely. This behavior could also be attributed to (2) below.

2. The geometry of the nylon loop material lining the bob and cup surface did not completely eliminate slip at the suspension boundaries.

3. Though attractive forces between individual fibers were present in the suspension, the nature of the forces was such that many fibers slipped past one another rather than undergo bending.

4. The apparent shear moduli of networks formed with fibers longer than 2.42 mm. or at consistencies greater than 0.6% were very large, resulting in small angular deflections at the stresses produced in the apparatus. The measurements

of these deflections with the long optical lever (see Fig. 16) were so sensitive that vibrations in the environment interfered with the measurements. However, during some of the stress-strain runs, the above factors appeared to have a minimum amount of influence on the data. An analysis of the data obtained in these runs yields an insight into fiber suspension shear behavior.

Figures 47 and 48 show the torque-strain behavior for slurries of 2.42 mm. long, 44.85 μ diameter fibers at volume concentrations of 0.534 and 0.766%, respectively. At the low concentration, the networks were more reproducible because less flocculation was present than at the higher concentrations. One of the assumptions made in deriving Equation (43), i.e.,

$$\Omega_r = K \frac{d^4 T}{hEIC^4} \left(\frac{1}{r^2} - \frac{1}{r_2^2}\right) \qquad (43),$$

was that the material was Hookean. The linear portion of the strain recovery data shown in Fig. 47 indicates that under certain shear conditions, this is true. The curvature of the torque-strain curves for both slurries is attributed to slippage within the network. When the slippage occurred initially at low torques, the curves are concave to the torque axis such as the two shown in Fig. 48. A decrease in the amount of slip at higher torques was noted for these suspensions and was probably a result of the fact that better contact was made between the bob and the suspension after the bob had rotated by a certain amount. The curves convex to the torque axis showed slippage at all torques. The irreversibility of this slippage is shown by the hysteresis loop in Fig. 47. The large increase in strain for a small increase in torque shown in the lower curve in Fig. 48 indicates a yield point in the suspension.

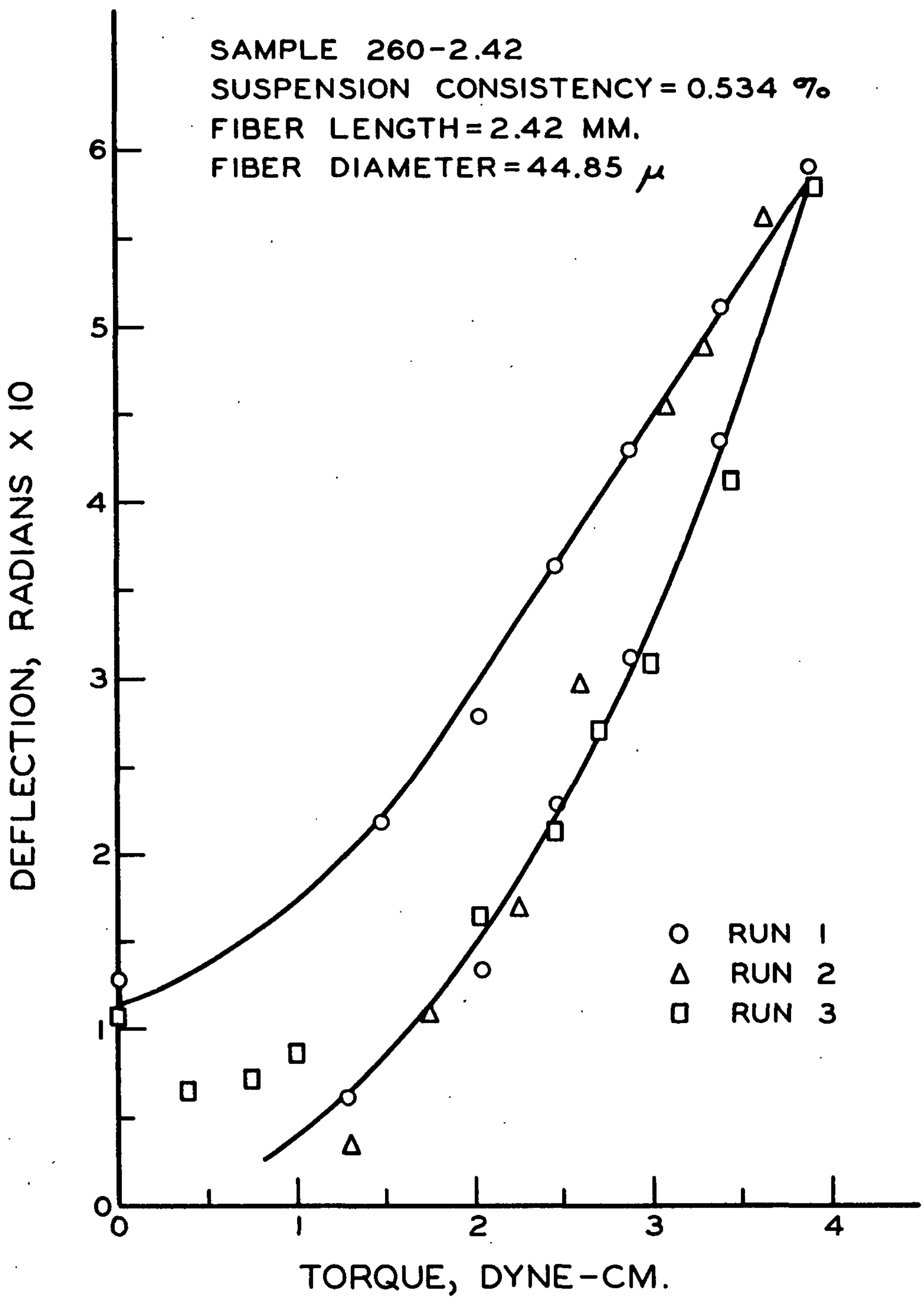

Figure 47. Torque-Shear-Strain Behavior of a Nylon Fiber Slurry

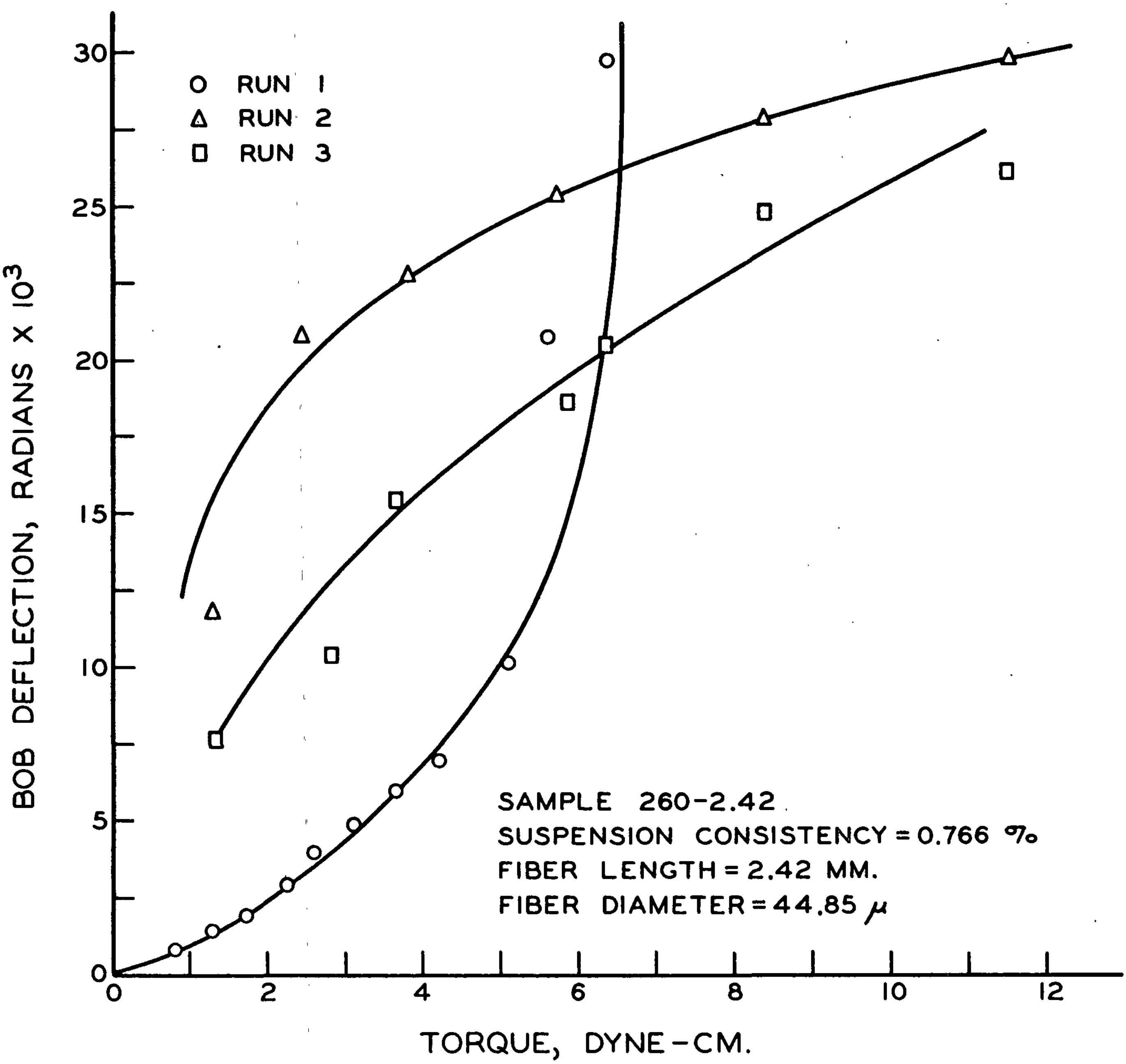

Figure 48. Torque-Shear-Strain Behavior of a Nylon Fiber Slurry

The experimental data show that an increase in the consistency of a nylon fiber slurry caused a much greater decrease in the strain in the network at a given stress than would be predicted by the analysis of a slurry in which the fibers were randomly oriented. Equation (43) predicts that the ratio of the slopes of the elastic portions of the stress-strain curves for the 0.534 and 0.766% slurries should be about 4.5, while experimentally the ratio is estimated to be 90. This result is felt to be due to the simplifications made is describing the geometry and stress reaction of a slurry in order to obtain Equation (43). For instance, it was assumed that only the bending forces in the network caused deformation. It is quite possible that many fibers undergo a longitudinal compression which would mean that much greater forces would be necessary to cause them either to slide out of position or to buckle. Also, the direction of the forces imposed on a fiber suspension could cause a fiber which slips to become realigned so as to resist the recovery forces exerted by other bent fibers. A possible exaggerated sequence of events in a fiber slurry is shown schematically in Fig. 49.

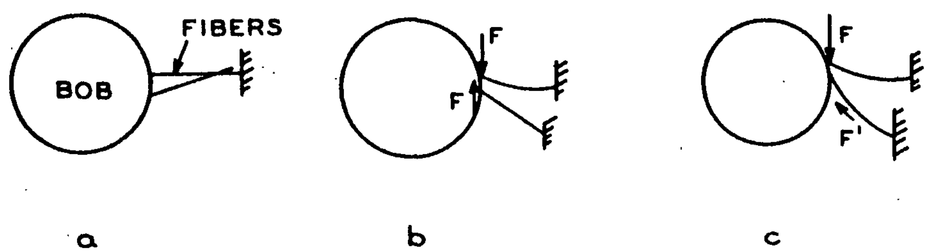

Figure 49. Possible Mechanism of Strain and Strain Recovery in a Nylon Fiber Slurry

Part "a" of Fig. 49 shows two fibers in the unstressed slurry. One is "pinned" by contacts with other fibers while the other is free to slip. When a force is imposed on the slurry (Fig. 49, part "b"), the "pinned" fiber bends while the other fiber slips and also becomes "pinned." Upon removing the external force (Fig. 49, part "c"), the bent fiber will attempt to reach an unstressed position while the other fiber will resist any recovery.

This "pinning" effect would be much more likely to occur in a more concentrated slurry or a slurry of longer fibers. The torque-deflection curves for a suspension of 10.8 mm. long, 44.85 μ fibers is shown in Fig. 50. Even though the consistency (0.222%) of these fibers was much lower than the consistencies used for the shorter length fibers, the angular deflection of the bob in the slurry was an order of magnitude less than the deflection of the other slurries at comparable torques. Equation (43) predicts that only concentration and fiber diameter should govern the shear behavior of a slurry in which the fibers are randomly oriented. Because the fibers were so long, it was impossible to achieve such a random orientation. Furthermore, stable flocs were present in the suspension. The size of these flocs was appreciable compared to the annulus width. Therefore, these results are indicative of how flocculation can greatly increase the shear resistance of a fiber slurry.

In Fig. 51 the change in the apparent strain distribution across the network observed during a successful stress-strain run with the 0.534%-consistency slurry is shown. The measurement was made by photographing the top surface of the slurry at two different shear stresses (torques). Dyed fibers in the slurry were used as guides in following the strain.

The equation used for predicting the strain change across the annulus with a change in torque was obtained from Equation (43). The strain, $\Omega_{\underline{rT}_1}$, at a given radius, $\underline{r}$, at a low torque, $\underline{T}_1$, was subtracted from the strain, $\Omega_{\underline{rT}_2}$, predicted for a higher torque at the same radius. The equation is:

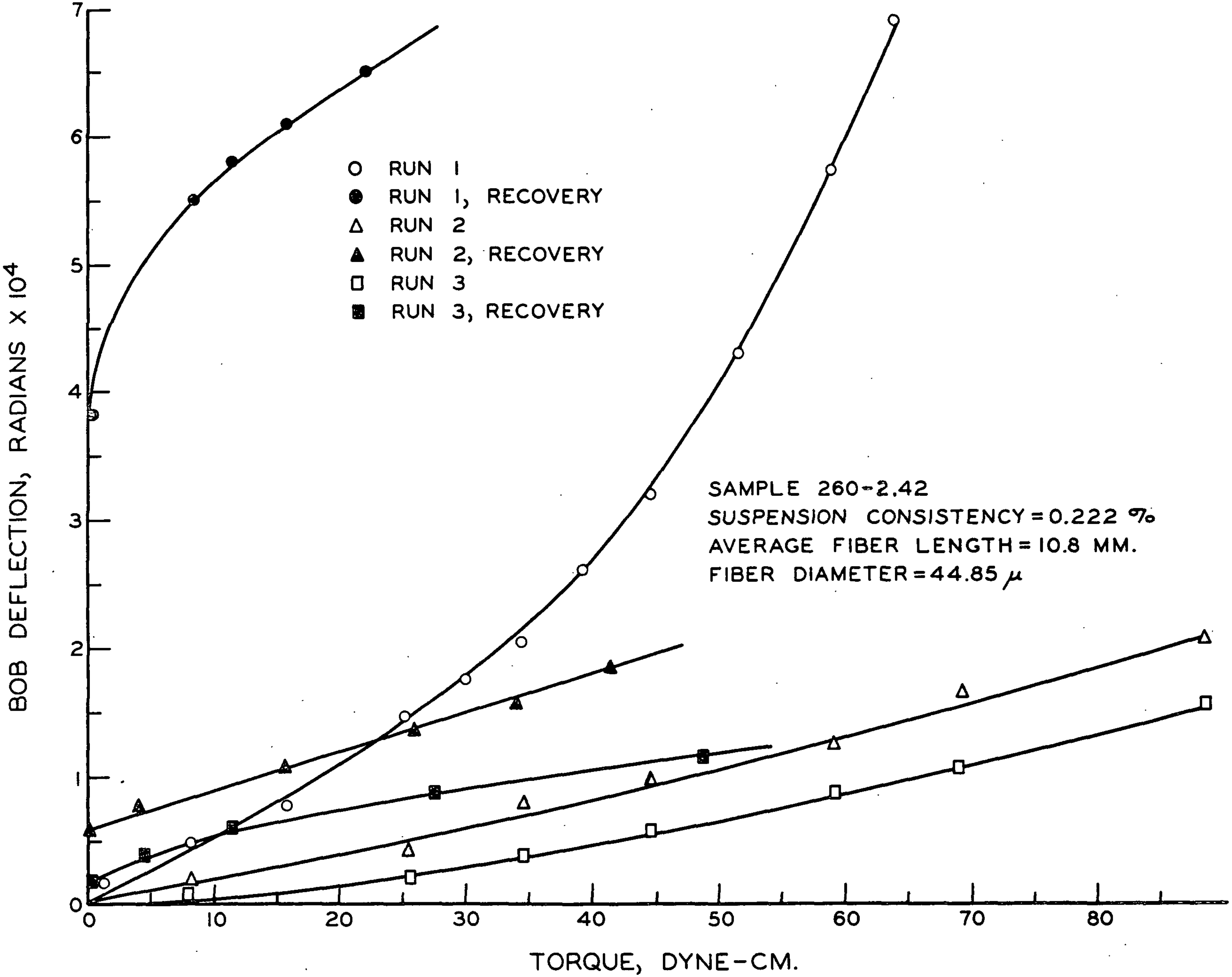

Figure 50. Torque-Shear-Strain Behavior of a Nylon Fiber Slurry

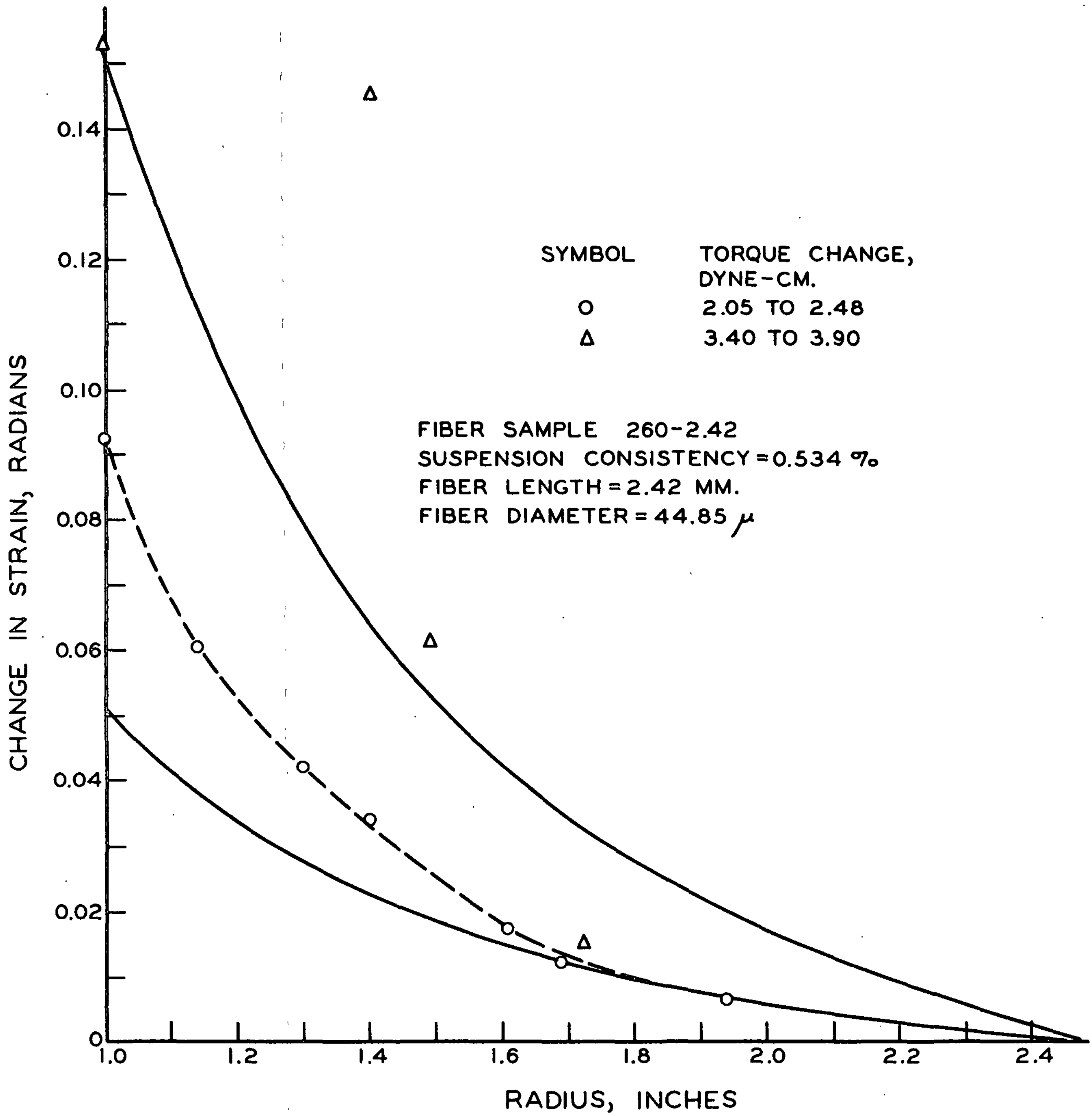

Figure 51. Change in Strain Across the Annulus
Caused by an Increased Torque

$$\Omega_{rT_2} - \Omega_{rT_1} = K'(T_2 - T_1)\left(\frac{1}{r^2} - \frac{1}{r_2^{\,2}}\right) \tag{61}$$

where K' is a constant depending on the suspension concentration, the fiber flexibility, EI, the fiber diameter, the suspension height, and the coefficient, K, which includes numerical factors and terms related to the geometry of the network. Because of the uncertainty in the value of K', it was evaluated from the experimentally determined angular deflection change observed for a change in torque. Knowing K', $(T_2 - T_1)$, and the value of $(r^{-2} - r_2^{-2})$ at any radius, the change in strain across the annulus could be calculated.

Since it was felt that the greatest slippage in the system occurred at the surface of the bob and in the slurry near the bob, K' was calculated from the experimental data on the strain change near the center of the annulus for the lowest torque change (0.43 dyne-cm.). Because of the small amount of data taken at the highest torque change (0.50 dyne-cm.), it was necessary to calculate K' from the deflection of the bob. The solid lines in Fig. 51 represent the predicted variation in strain change across the annulus, based on the assumption that K' may be calculated from the experimental data.

The low torque change data do not follow the relationship predicted with the aid of Equation (61) and the experimentally determined K' at radii near that of the bob. This is felt to be a result of fiber slippage at the surface of the bob and in the slurry at the higher shear stresses near the bob. There is some indication that at radii near the cup surface the relationship might hold. This might be expected because the shear stresses in this region are much lower than those near the bob. The strain data taken for the larger torque change are quite scattered. However, it does appear that much greater movement occurred in the slurry near the bob than would be expected from a consideration of the slurry behavior at the lower torque change. This could be a result of actual yielding of the entire network. Because a portion of the strain recovery data is linear and thus more nearly conforms with the assumption of a Hookean material under which Equation (61) was developed, it would be better to determine the strain change in a network during recovery.

It was postulated in the Theoretical section that the shear stress required to cause a fiber network to yield was a function of the force acting over a small increment of area c^2 of the network in which the bending of an individual fiber element, b, occurred. The relationship for the force f on the small increment was:

$$f = Fc^2/A' \qquad (33),$$

where F is the total force acting over the area A'. It is also shown in Appendix I that $c = b/2$ and in Appendix II that the average distance between points of contact, $b = 0.54\ d/C$, where C is the suspension volume concentration and d is the fiber diameter. It is assumed that a critical force f_c is required in order that one fiber slip past another fiber. As the concentration of a slurry is increased, there would be more points of contact between fibers so that a greater applied stress will be required to attain the critical force per point of contact. If τ_y is the yield stress of a suspension, then Equation (33) may be written as:

$$\tau_y = K''C^2 \qquad (62),$$

where K" includes d^{-2}, f_c, and numerical terms.

In a survey of the literature, values of the yield stress for different pulp slurries (6, 12, 43, 56-64) and a nylon slurry (14) were obtained. All the data except that of Richardson (16) and the nylon data in this study were calculated from suspension flow in a round pipe. The yield stress was considered to be equal to the wall stress on the surface of the pipe at which the fiber plug began to disintegrate. This corresponded to the first transition point on a friction factor-velocity curve. The data for each study plotted in Fig. 52 were nearly linear on a log-log graph with the slopes of the lines ranging from 1.4 to 2.5. The solid line in the figure represents the average slope of all the lines which is 2.2. The yield stresses of the 2.42 mm. long fiber slurries determined in this study fall on a line with a slope of 1.96. Considering the fact that these measurements were made in different flow systems with different fiber suspensions, the data show a remarkably similar trend. It would be presumptive to say that these data confirm the concentration squared term in the above equation, but it is believed that it shows that the method of approach has some promise.

The performance of the viscometer in measuring the torque-strain behavior of a pulp slurry was determined. A long fiber (average fiber length ca. 3.3 mm.) spruce sulfite pulp slurry at a consistency of about 0.15% was subjected to a range of torques in the apparatus. The data are tabulated in Appendix IV, Table XXIII and are shown in Fig. 53. This slurry exhibited much greater rigidity at the low consistency than the suspensions of nylon fibers of comparable length (2.42 mm.) at the higher consistencies. The linear portion of the recovery curve indicates that part of the slurry behavior is elastic. The preliminary nature of the data prevents any further detailed conclusions from being made on this system.

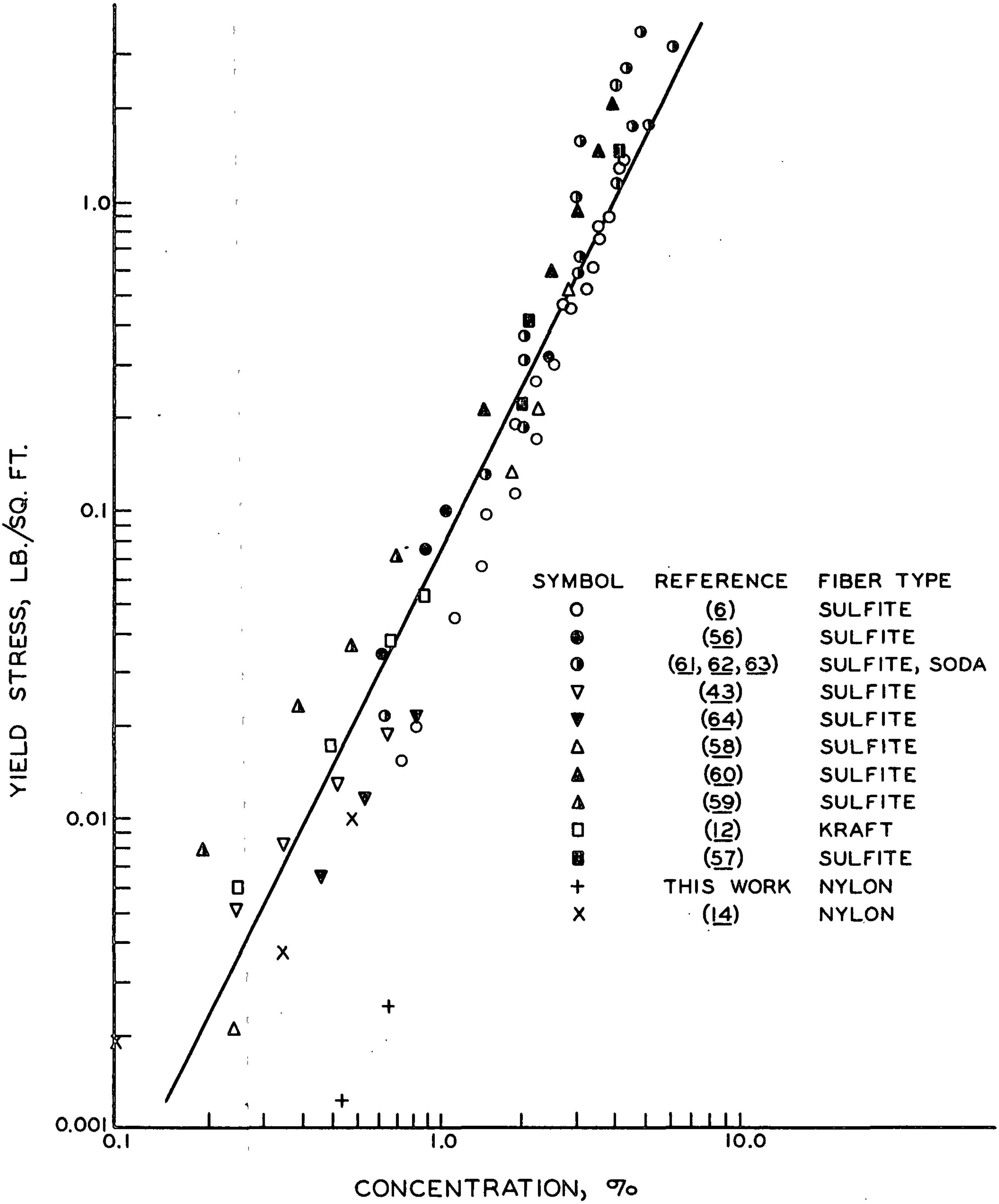

Figure 52. Relationship Between Yield Stress and Concentration of Fiber Slurries

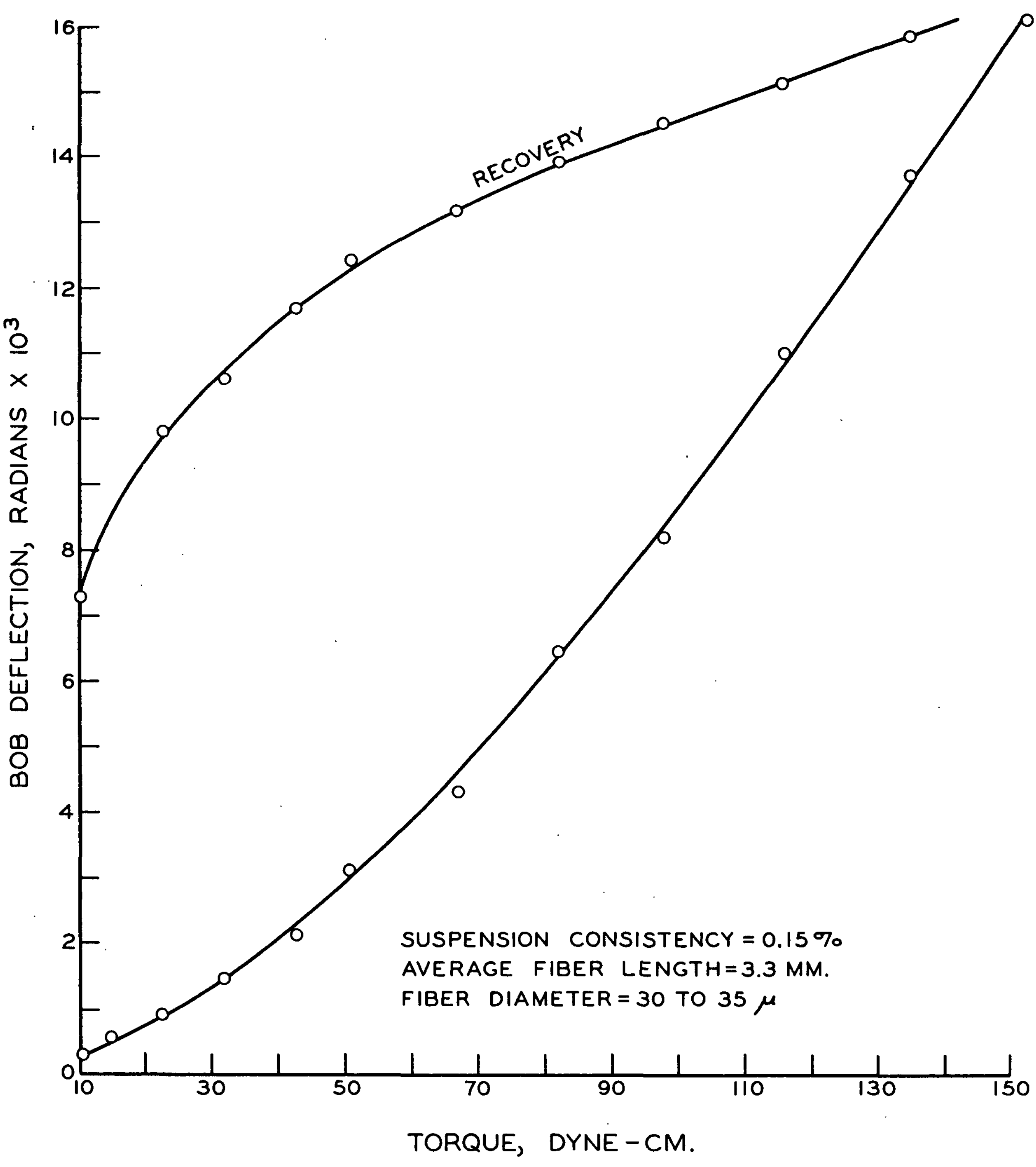

Figure 53. The Torque-Shear-Strain Behavior of a Spruce Pulp Suspension

FUTURE STUDIES IN LIGHT OF THE SIGNIFICANCE OF THIS WORK

In future studies of the gross flow behavior of fiber suspensions, an attempt should be made to determine the boundary conditions of the actual flow system. For instance, for plug flow in a pipe, a technique should be devised to measure the clear fluid annulus width. Assuming that the major portion of the flow occurs in this annulus under the boundary conditions of no slip at the pipe wall ($\underline{u} = 0$) and a fluid velocity at the boundary of the plug equal to the plug velocity, the rigorous equations of fluid flow could be solved to determine the forces necessary to transport a given suspension through the pipe. If it is shown that the forces determined by such calculations agree with the experimentally determined forces, the supposition that the presence of fibers in a fluid does not alter the original Newtonian behavior of the fluid will be strengthened. Such a finding would be of immense help in designing future studies of suspension flow. The fiber properties would not affect the basic flow mechanisms, but would only change the boundary conditions of the system in which the flow was occurring. Again using plug flow of a fiber suspension in a pipe as an illustration, stiffer fibers in a plug at a given consistency would prevent the plug from deforming as much as if it were composed of fibers of the same dimensions but of greater flexibility. The clear fluid annulus for the plug of flexible fibers would be greater than that for the plug with the stiff fibers and, therefore, the more flexible plug would be expected to move at a higher velocity than the plug of stiff fibers under the same forces. If the compression modulus of the plug were known in terms of the fiber properties, then one might predict the deformation of the plug or fiber network caused by the hydrodynamic forces. Because the mechanical properties of a network of fibers would govern the boundary conditions under which fluid flow occurs, future studies which determine the network stress-strain properties in terms of the individual fiber properties are necessary.

The present study of the mechanical properties of synthetic fiber networks has indicated to some degree the complex problems which will be encountered in further experimental and theoretical studies of more or less randomly oriented fiber structures. The important role which fiber structures play in the paper-making operations makes it highly desirable to continue this work, even though it might entail a lengthy and difficult statistical study. It is felt that the semitheoretical equations advanced in this work provide a basis for designing such a study.

The study of the flow of nylon fibers suspended in an aqueous solution indicated the possibility of using the apparatus for determining the yield stresses of networks formed in such a suspension. Because of the ease in measuring the apparent yield stress, this work could be extended to determine the effect of various fiber properties on the yield stress of a given network. There was also an indication that forces between fibers could be varied by changing the pH of the solution. Because the yield stress is felt to be related to flocculation, a contribution to the understanding of flocculation might be made if the effect of pH on the yield stress was determined.

In this work, data have been obtained for the flow of a suspension of fibers in which a continuous network is absent. This data strengthens the contention of previous investigators (8, 9) that the present theory for the flow of dilute fiber suspensions is inadequate. The approximate nature of the equations as well as the lack of an analysis of the effects of fiber interactions are probably the main reasons for the discrepancy between theory and experiment. The experimental data obtained up to this time are felt to be sufficient for a quantitative analysis of fiber slurry flow. The extension of the work should be of a theoretical nature, starting first with an analysis of the interaction of two fibers in a well-defined flow field and proceeding to the more complex system of many fibers. When such a theory has been developed and the results have been compared with the present experimental data, it is highly probable that further experimental work will be justified.

The apparatus was shown to be useful in the study of the shear behavior of fiber slurries. Such an apparatus should prove equally useful in any work extending the results of this study. The unique design of the bob suspension and drive system makes it particularly applicable to studies of other fluid systems which exhibit viscoelastic properties.

SUMMARY AND CONCLUSIONS

A knowledge of the behavior of suspensions of particles undergoing shear is of particular importance to the understanding of such industrial operations as the preparation of coatings, printing, and the formation of fibrous sheets of paper. At the present time a void exists in the understanding of the rheological behavior of fiber suspensions. Only a limited amount of data has been obtained for the Newtonian region of fiber slurry flow. Even less data exist for the region of suspension flow where structural or network effects are present. The purpose of this study was to design an experimental program to investigate the flow of synthetic fiber suspensions and to interpret the experimental results by phenomenological and theoretical analyses. Snythetic fiber suspensions were chosen as the systems to be studied because of the ability to assign definite values to such fiber properties as length, diameter, density, and flexibility.

Theories were presented in order to determine which fiber and slurry properties governed the particular type of slurry behavior. The theory for the flow of a Newtonian fiber suspension was developed chiefly by Jeffery (16) and Burgers (17). They showed that the inability of a fiber rotating in a laminar flow field to conform exactly to the movement of the fluid caused a disturbance to be superimposed on the original motion of the fluid. This disturbance increased the energy loss of the suspension over that of the fluid, thus causing the suspension viscosity to be greater than the fluid viscosity. Assuming laminar flow, large, rigid particles, no wall effects, and no fiber interactions, Burgers showed that the relative viscosity of a fiber suspension is given by the following equation:

$$\mu_r = 1 + \alpha_o C \tag{23}$$

where $\alpha_o = [(\underline{L}/\underline{d})^2/6(\ln \frac{2L}{\underline{d}} - 1.8)] \sin^4\theta \sin^2 2\phi$. Burgers' technique involved the substitution of a system of forces for the action of the fibers on the liquid so that the Navier-Stokes equations as simplified by Oseen (18) could be used. Average values of the goniometric factor, $\sin^4\theta \sin^2 2\phi$, were calculated for fibers randomly oriented and for fibers distributed in the plane of flow.

The theory for the stress-strain deformation of a slurry in which fiber networks existed was derived by assuming that the slurry was composed of randomly oriented units which bend according to a simple beam equation when stressed. Though it was realized that such an equation was an oversimplification in light of the true geometry of an actual fiber network, it was hoped that an indication of the important variables governing the stress-strain behavior of a slurry could be obtained. The final result showed that the deflection of such a network was directly proportional to the applied stress and inversely proportional to the product of the concentration to a power and the fiber flexibility.

A sensitive concentric cylinder viscometer was designed and constructed for the purpose of studying the shear behavior of fiber suspensions. The inner bob was suspended from a nearly frictionless air bearing. Rather than apply a torque to the bob through a direct mechanical coupling, an eddy current clutch-type drive was employed to cover a torque range of 1 to 300 dyne-cm. This arrangement allowed the strain-strain recovery curves of fiber networks to be determined. Extremely low shear stresses could be applied to the synthetic fiber slurries so that the yield stresses of fiber networks were not exceeded. These low shear stresses also enabled shear rates to be obtained in the fiber slurry flow studies where inertial forces were not appreciable. At these low shear rates, fiber bending due to fluid forces was shown to be improbable. Studies of the viscosity behavior of pure fluids using a narrow annulus viscometer showed that the apparatus was capable of measuring the absolute viscosities of pure fluids with an accuracy of less than 1%. This is an indication that the apparatus was properly designed and precisely constructed.

The synthetic fibers were characterized with respect to their diameter, density, and tensile and bending modulus of elasticity. The fiber length distribution at any one axis ratio was carefully controlled by cutting skeins of the fibers with a parallel array of evenly spaced razor blades. For very short lengths (<1 mm.), the fibers were cut with a microtome. Fibers ranging in diameter from 12 to 75 microns and in length from 0.4 to 6 mm. were used. During the major portion of the flow studies, the fibers were suspended in a solution of mineral oil and tetrachloroethane of the same specific gravity as the fibers. A solution of sucrose having the same density as the fibers was used in the shear stress-strain measurements.

The general shear behavior of a fiber suspension was classified by the shape of the curve representing the relationship between the torque and the resulting bob angular velocity. On this basis, four types of suspension shear behavior were defined. Below a given concentration depending upon the fiber axis ratio and shape, nylon and glass fibers suspended in an organic solution exhibited a linear torque, $\underline{T}$ - bob angular velocity, $\omega_{\underline{b}}$ relationship over a certain range of bob angular velocities. This is the type (I) of behavior for which Jeffery (4) and Burgers (5) developed their suspension flow theories. Above a given angular velocity the $\underline{T}$-$\omega_{\underline{b}}$ relationship curved concave to the torque axis. The occurrence of this type (II) of behavior was shown to be highly dependent on the fluid viscosity and density, indicating that inertial flow forces had become appreciable compared to the viscous forces.

Type III suspension shear behavior was described by a $\underline{T}$-$\omega_{\underline{b}}$ curve concave to the bob angular velocity axis. This behavior was typical of nylon fibers suspended in an organic fluid at concentrations higher than the critical concentrations below which Type I behavior occurred. A strong continuous network was observed throughout the suspension and the major portion of the fluid flow appeared to take place in a narrow annulus between the bob and the network. Nylon fibers suspended in a sucrose solution also yielded a $\underline{T}$-$\omega_{\underline{b}}$ curve concave to the $\omega_{\underline{b}}$ axis. Visual observations indicated that the behavior of these suspensions was different from the Type III behavior, so it was designated as Type IV. Fiber networks present in the suspension were continuously broken down as the shear stress on the suspension was increased. When a given shear stress ($\sim \underline{T}$) was reached, continuous networks in the network had been broken down by the shearing action and the suspension showed Type I behavior, i.e., the torque became directly proportional to the bob angular velocity.

Based on the visual observations of the motion of the fiber phase of the suspensions during shear, it was postulated that the flow in each type of suspension shear behavior was Newtonian. Using this flow concept, it was possible to explain the shape of the $\underline{T}$-$\omega_{\underline{b}}$ curves. It was indicated that if the postulation of Newtonian flow can be proved by further studies, the analysis of the flow behavior of fiber suspensions will be greatly simplified in that one would need only to know the boundary conditions of the flow system in order to rigorously describe the flow.

A greater emphasis was placed on the analysis of the Type I suspension shear behavior, because of the relatively simple experimental set-up required to specify the flow boundary conditions. According to the theories (48, 16, 17) of the shear behavior of dilute suspensions, the presence of particles in a Newtonian fluid should increase the energy dissipation or the viscosity of the fluid. The increase in energy dissipation due to the particles should thus be proportional to the relative viscosity of the suspension which in turn should depend on the particle shape, size, volume concentration, and deformability. Therefore, the effects of these variables on the relative viscosities of fiber suspensions were determined. The major conclusions of this part of the study are:

1. The extent to which slurries of rigid, cylindrical fibers behave as Newtonian suspensions depends upon the fiber axis ratio and the slurry concentration.

2. Under the experimental conditions employed in this study, the fibers make a greater contribution to the viscosity of a suspension than predicted by Burgers' equations.

3. Possible reasons for this discrepancy are:

    a. The approximate nature of Burgers' equations.

    b. The lack of an adequate theory to account for fiber interactions.

    c. The influence of curvature of the fibers.

4. Wall effects appear to be a complex function of the fiber axis ratio and the ratio of the fiber diameter to the annulus width.

5. Curvature of the fibers greatly increases their contribution to the viscosity of a suspension, probably due to increased fiber interaction.

6. The viscosity of aqueous suspensions of fibers is increased over that of the fibers at the same concentration in an organic solution. It is felt that fiber flocculation is also the cause of this phenomenon.

Very little quantitative data was obtained in the study of the stress-strain behavior of fiber slurries. However, certain qualitative data were obtained which indicated some promise for the theoretical approach of representing a fiber network employed in this work. The slurries suspended in the sucrose solution were subjected to shear stresses in the annulus of the apparatus and the deflection of the network was observed at each stress. A fibrous surface on the bob and on the inner wall of the outer cylinder minimized slippage at the extremities of the network. The study indicated that:

1. Fiber slurries may undergo elastic deformation, the magnitude of which depends on the slurry and fiber properties.

2. The elastic recovery of a fiber slurry is probably linear over a portion of the total recovery.

3. A hysteresis loop observed in the strain-strain recovery cycle of a network is probably due to irreversible fiber slippage and realignment.

4. The strain across a fiber network in an annular ring appears to be a function of the reciprocal second power of the radius, when fiber slippage is absent.

5. Pulp fiber networks exhibit much greater strength than synthetic fiber networks, probably because of greater forces of attraction at apparent contact points.

6. The yield stress of fiber networks appears to be related to the force on an apparent point of contact within the network and the square of the concentration of the suspension.

The initial phase of any extension of the work on the flow of dilute fiber slurries should be theoretical. A better theory for the flow of suspensions of cylindrical fibers is required in order to fully explain the observed experimental behavior. Extreme experimental difficulty is expected in further studies of the stress-strain behavior of fiber networks. Such a study would appear to be worth the effort in view of the important role which the networks play in the papermaking process. The concentric cylinder viscometer designed and constructed for use in this work should be applied to other fluid systems where low shear rates and stresses are required or where viscoelastic properties are observed.

NOMENCLATURE

$\underline{A}$	=	total area of annulus between the bob and outer cylinder, sq. cm.
$\underline{A}'$	=	area of a cube on which force is applied in shear, sq. cm.
$\underline{A}_1$, $\underline{A}_2$	=	adjustable coefficients in Burgers' equation for the force, $\underline{f}(\underline{\ell})$, at a point on a fiber axis
$\underline{b}$	=	average length of beam between supports, cm.
$\underline{c}$	=	thickness of the smallest layer of fibers in an annular space in which deflection occurs, cm.
$\underline{C}$	=	volume fraction of fibers in a suspension
$\underline{C}'$	=	constant of integration which describes the orbit of a fiber in a laminar shear field
$\underline{d}$	=	fiber diameter, cm.
$\underline{D}$	=	width of concentric cylinder viscometer annulus, cm.
$\underline{e}$	=	distance between two points of force application along a line
$\underline{E}$	=	modulus of elasticity of beam material, dynes/sq. cm.
$\underline{f}$	=	average force applied at a fiber-fiber contact point, dynes
$\underline{f}_c$	=	critical force on a fiber point of contact causing a fiber network to yield, dynes
$\underline{f}(\underline{\ell})$	=	force exerted on a fiber by the fluid in laminar shear at some point on the axis, dynes
$\underline{F}$	=	force on a plane in a fiber network, dynes
$\underline{g}(\underline{L},\underline{d},\underline{\ell})$	=	function describing geometry of a point on a fiber axis with respect to a co-ordinate system
$\underline{G}$	=	modulus of elasticity in shear, dynes/sq. cm.
$\underline{G}_o$	=	shear gradient of a fluid, sec.$^{-1}$
$\underline{G}_f$	=	shear gradient of a fiber suspension, sec.$^{-1}$
$\underline{h}$	=	height of slurry in a concentric cylinder apparatus, cm.
$\underline{h}'$	=	height of a cube on which force is applied in shear, cm.
$\underline{I}$	=	moment of inertia of beam cross section with respect to a centroidal axis, cm.^{4}

$\underline{k}$ = statistical constant used in beam bending equation

$\underline{k}_o$ = coefficient describing the shear gradient, sec.$^{-1}$

$\underline{K}$ = proportionality constant

$\underline{\ell}$ = distance from center of fiber to any point on the fiber axis, cm.

$\underline{\ell}_o$ = total length of fibers in a suspension, cm.

$\underline{\ell}_p$ = average projected length of the fibers onto a circular plane, cm.

$\underline{\ell}_t$ = length of fibers within a cylindrical surface passed vertically through a fiber slurry in the annulus of a concentric cylinder apparatus, cm.

$\underline{L}$ = fiber length, cm.

$\underline{M}$ = fluid force doublet acting axially on a fiber, dyne-cm.

$\underline{N}$ = number of fibers per unit volume, cm.$^{-3}$

$\underline{O}$ = origin of a co-ordinate system

$\underline{P}$ = $\underline{x}\cos\alpha + \underline{y}\cos\beta + \underline{z}\cos\gamma$

$\underline{r}$ = radius of a cylindrical surface between the inner and outer cylinders of a concentric cylinder viscometer, cm.

$\underline{r}'$ = $\sqrt{\underline{x}^2 + \underline{y}^2 + \underline{z}^2}$

$\underline{r}_1$ = radius of bob, cm.

$\underline{r}_2$ = inner radius of outer cylinder, cm.

$\underline{Re}$ = Reynolds number for flow past a particle

$\underline{S}$ = shear strain, cm./cm.

$\underline{t}$ = time fiber has rotated in a laminar shear field, sec.

$\underline{T}$ = torque applied to a concentric cylinder viscometer system, dyne-cm.

$\underline{u}$ = component of velocity in the $\underline{x}$-direction, cm./sec.

$\underline{u}'$ = component of velocity disturbance in the $\underline{x}$-direction, cm./sec.

$\underline{u}_s'$ = component of velocity disturbance in the $\underline{x}$-direction at the surface of a fiber, cm./sec.

$\underline{u}_\theta$ = fluid velocity component in the meridian plane described above, perpendicular to the fiber axis, cm./sec.

u_ϕ = fluid velocity component perpendicular to the meridian plane formed by a fiber and the z-axis of a co-ordinate system the center of which coincides with the fiber center, cm./sec.

$u_{\parallel}$ = fluid velocity component directed along the axis of a fiber, cm./sec.

U = fluid velocity perpendicular to a fiber axis

v = component of velocity in the y-direction, cm./sec.

v' = component of velocity disturbance in the y-direction, cm./sec.

V = total volume of a slurry in a concentric cylinder viscometer

$\vec{V}$ = fluid velocity vector, cm./sec.

w = component of velocity in the z-direction, cm./sec.

w' = component of velocity disturbance in the z-direction, cm./sec.

W = total weight of fibers in a slurry, g.

x, y, z = rectangular co-ordinates, cm.

y' = distance from beam neutral axis to the most remote element of the beam, cm.

α_o = first-order concentration coefficient in viscosity equation, dyne-sec./sq. cm.

α_1 = second-order concentration coefficient in viscosity equation, dyne-sec./sq. cm.

α, β, γ = respective angles between a fiber and the x-, y-, and z-axes of a co-ordinate system the center of which coincides with the fiber axis center

Δ = change in velocity of a fluid due to the presence of fibers in the fluid, $sec.^{-1}$

θ = angle formed by fiber and z-axis of a co-ordinate system the center of which coincides with the fiber center

μ_o = fluid viscosity, dyne-sec./sq. cm.

μ_f = absolute viscosity of a fiber suspension, dyne-sec./sq. cm.

μ_r = relative viscosity of a fiber suspension

τ_o = shear stress on a fluid or suspension, dynes/sq. cm.

τ_y = yield stress of a material, dynes/sq. cm.

ϕ = angle formed by the meridian plane through the fiber axis (see $\underline{u}_{\phi}$) and the plane formed by the $\underline{z}$- and $\underline{y}$-axes

$\Omega_{\underline{r}}$ = total deflection at a radius, $\underline{r}$, of a fiber network in an annulus between two concentric cylinders, radians

$\omega_{\underline{b}}$ = angular velocity of bob in a concentric cylinder apparatus, $sec.^{-1}$

γ = kinematic viscosity of a fluid, sq. cm./sec.

ACKNOWLEDGMENTS

The author sincerely appreciates the guidance and encouragement contributed by the thesis advisory committee during the course of this study. Members of the committee were Dr. S. F. Kurath, chairman, Dr. R. W. Nelson, and Dr. H. D. Wilder.

Suggestions of Dr. J. A. Van den Akker were very helpful during the initial design of the viscometer. The experience and skill of Mr. H. Marx of the Institute Machine Shop were invaluable in the construction of the mechanical sections of the apparatus, while the aid of Mr. K. W. Hardacker in setting up the electrical components of the apparatus is gratefully acknowledged.

Special mention should be made of the kind consideration of Mr. J. Donald Howell of the E. I. du Pont de Nemours & Co., Inc., in making available to the author various samples of nylon fibers. The assistance of Mr. R. L. Jones and Mr. J. R. Peckham in obtaining the respective glass and pulp fiber samples and their physical property determinations is also appreciated.

The suggestions and criticisms of Mr. S. T. Han and Dr. W. L. Ingmanson of the Institute Chemical Engineering Department contributed measurably to the author's understanding and analysis of the flow of fiber suspensions.

The work of Mrs. Elizabeth Cary in preparing and editing the original manuscript is also gratefully acknowledged.

Other members of the Institute staff made lesser but valuable contributions to the success of this work and their help is sincerely appreciated.

LITERATURE CITED

1. Fischer, E. R., J. Colloid Sci. 3:73(1948).

2. Conway, B. E., J. Polymer Sci. 18:257(1955).

3. Maron, S. H., and Krieger, I. M. In Eirich's Rheology. Vol. 3, p. 121. New York, Academic Press, 1960.

4. Zettlemoyer, A. C., and Myers, R. R. In Eirich's Rheology. Vol. 3, p. 145. New York, Academic Press, 1960.

5. Forgacs, O. L., Robertson, A. A., and Mason, S. G. In Bolam's Transactions symposium of papermaking fibers. p. 447. Surrey, England, British Paper and Board Makers' Association, 1958.

6. Richardson, R. J. The flow of wood pulp slurries. Doctor's Dissertation. Cambridge, Mass., Massachusetts Institute of Technology, 1954. 353 p.

7. Head, V. P., Tappi 35:260(1952).

8. Eirich, F., Bunzl, M., and Margaretha, H., Kolloid-Z. 75:20(1936).

9. Nawab, M. A., and Mason, S. G., J. Phys. Chem. 62:1248(1958).

10. Lindsey, C. H., and Fischer, E. K., J. Appl. Phys. 18:989(1947).

11. Mason, S. G. Personal communication, 1961.

12. Bugliarello, G., and Daily, J. W., Tappi 44:881(1961).

13. Wilder, H. D. Personal communication, 1961.

14. Daily, J. W., and Tsuchiya, A. Technical Report No. 4, TAPPI Project 147. New York, Technical Association of the Pulp and Paper Industry, 1959.

15. Ferry, J. D., and Park, G. S., Physics 6:356(1935).

16. Jeffery, G. B., Proc. Roy. Soc. London A102:161(1923).

17. Burgers, J. M. In Second report on viscosity and plasticity. Chap. 3. New York, Nordemann, 1938.

18. Oseen, C. W. In Burgers' chapter in Second report of viscosity and plasticity. p. 115. New York, Nordemann, 1938.

19. Van Wyk, J., J. Textile Inst. 37:T285(1946).

20. Jones, R. L. Unpublished work, 1960.

21. Bulletin No. X-82. Wilmington, Del., E. I. du Pont de Nemours & Co., Inc., May, 1958.

22. Wakelin, J. H., Voong, E. S. L., Montgomery, D. J., and Dusenburry, J. H., J. Appl. Phys. 26, no. 7:786(1952).

23. Lochner, J. P. A., J. Textile Inst. 40:T220(1949).

24. Nethercut, P. E. A fundamental study of the softening mechanism of paper plasticizers. Doctor's Dissertation. Appleton, Wis., The Institute of Paper Chemistry, 1949.

25. Kärrholm, E. M., and Schröder, B., Textile Research J. 23:207(1953).

26. Jones, R. L. The effect of fiber structural properties on the compression response of fibrous beds. Doctor's Dissertation, Appleton, Wis., The Institute of Paper Chemistry, 1962. 150 p.

27. Van den Akker, J. A., and Hardacker, K. W., Tappi 41, no. 8:224A(1958).

28. Estridge, R. The initial retention of fibers by wire grids. Doctor's Dissertation. Appleton, Wis., The Institute of Paper Chemistry, 1961.

29. Ilvessalo-Pfäffli, M-S., and Alfthan, G., Pulp and Timber 39:509(1957).

30. Barr, G. A monograph of viscometry. p. 236. London, Oxford University Press, 1931.

31. Eisenberg, H., J. Polymer Sci. 14:417(1954).

32. Stanley, J. S., J. Phys. Chem. 58:533(1954).

33. Reiner, M. Deformation and flow. p. 28. London, H. K. Lewis & Co., Ltd., 1949.

34. Hodgman, C. D., ed. Handbook of chemistry and physics. 39th ed. p. 1729. Cleveland, O., Chemical Rubber Publishing Co., 1957.

35. Taylor, G. I., Phil. Trans. Roy. Soc. London 223A:289(1922).

36. Lewis, Proc. Roy. Soc. London 117A:388(1927); in Barr's A monograph of viscometry. p. 224. London, Oxford University Press, 1931.

37. Frisch, H. L., and Simha, R., In Eirich's Rheology. Vol. 1, Chap. 14. p. 531. New York, Academic Press, 1956.

38. Lamb, H. Hydrodynamics. London, Cambridge University Press, 1932.

39. Finn, R. K., J. Appl. Phys. 24:771(1953).

40. Squires, L., and Squires, W. J., Trans. Am. Inst. Chem. Engrs. 33:1(1937).

41. Fayon, A. M., and Happel, J., A.I.Ch.E. Journal 6, no. 1:55(1960).

42. White, C. M., Proc. Roy. Soc. London 186A:472(1946).

43. Robertson, A. A., and Mason, S. G., Tappi 40:326(1957).

44. Han, S. T. Personal communication, 1962.

45. Wollwage, J. C. The flocculation of papermaking fibers. Doctor's Dissertation. Appleton, Wis., The Institute of Paper Chemistry, 1938. 177 p.

46. Oka, S. In Eirich's Rheology. Vol. 3, p. 37. New York, Academic Press, 1960.

47. Hersey, J., Wash. Acad. Sci. 6:525(1916); in Barr's A monograph of viscometry. p. 224. London, Oxford University Press, 1931.

48. Einstein, A. In Frisch and Simha's chapter in Eirich's Rheology. Vol. 1. p. 534. New York, Academic Press, 1956.

49. Vand, V., J. Phys. & Colloid Chem. 53:277(1948).

50. Forgacs, O. L., and Mason, S. G., J. Colloid Sci. 14:473(1959).

51. Binder, R. C., J. Appl. Phys. 10:711(1939).

52. Mason, S. G., and Manley, R. St. J., Proc. Roy. Soc. London A238:117(1956).

53. Brenner, H. Effect of finite boundaries on the Stokes resistance of an arbitrary particle. To be published in J. Fluid Mech.

54. Mason, S. G., Pulp Paper Mag. Can. 53:277(1948).

55. Tchen, C. M., J. Appl. Phys. 25:463(1954).

56. Nilson, B. M., Svensk Papperstidn. 47:357(1954).

57. Forrest, F., and Grierson, G. A. H., Paper Trade J. 92, no. 22:39(1931).

58. Guenter, T. E., and Ceaglske, N. J., Tappi 34:140(1951).

59. Mason, S. G., Tappi 33:440(1950).

60. Brecht, W., and Heller, H., Wochbl. Papierfabrik. 66:Tech Teil 264, 342, 380, 439, 474, 529, 587, 641, 714, 747(1935).

61. Durst, R. H., and Jenness, L. C., Tappi 37:417(1954).

62. Durst, R. H., and Jenness, L. C., Tappi 38:193(1955).

63. Durst, R. H., and Jenness, L. C., Tappi 39:277(1956).

64. Baines, W. D. The mechanics of flow of a dilute fibre suspension. National Research Council of Canada, Symposium of Flow of Suspensions, Ottawa, The Council, 1956.

APPENDIX I

DETERMINATION OF AVERAGE LENGTH OF A FIBER PROJECTED ON A GIVEN LINE

If a fiber is suspended in a fluid, the number of positions its ends may occupy is represented by the surface of a sphere (see Fig. 54). The length, L_p, of the fiber projected onto a plane through the center of the sphere is seen to be:

$$L_p = L \cos\theta \qquad (63).$$

The average projected length, $\bar{L}_p$, is given by:

$$\bar{L}_p = L\,\overline{\cos\theta} \qquad (64)$$

where $\overline{\cos\theta}$ is the average cosine of the angle between the fiber and the plane.

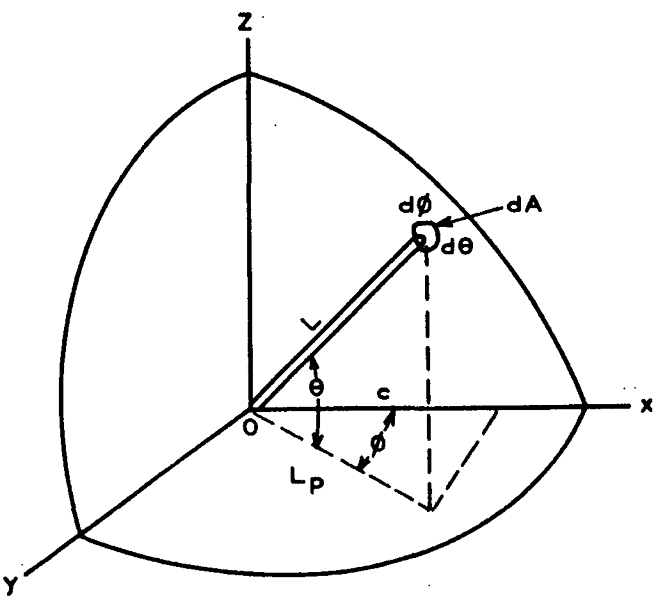

Figure 54. Diagram for Determining the Projected Length of a Fiber on Line Ox

Considering the increment, dA, the average value of the cosine of angle θ may be expressed by the following equation:

$$\overline{\cos\theta} = \int_0^A \frac{\cos\theta \; dA}{\text{Area Sphere}} \tag{65}$$

If the area increment is represented by polar co-ordinates, the average cosine equation becomes:

$$\overline{\cos\theta} = 2 \frac{\int_0^{\pi/2}\int_0^{2\pi} \cos^2\theta \; d\theta d\phi}{4\pi L^2} L^2 \tag{66}$$

$$= \pi/4.$$

Therefore, the average projected length of the fiber is:

$$L_p = \pi L/4 \tag{67}$$

In order to find the average projected length, c, of the fiber on the line Ox, the average cosine of the angle ϕ must be determined, i.e.,

$$c = L_p \, \overline{\cos\phi} \tag{68}$$

By a method similar to that used above to determine $\overline{\cos\theta}$, the value of $\overline{\cos\phi}$ may be shown to be:

$$\overline{\cos\phi} = \frac{4\int_0^{\pi/2} L_p \cos\phi \; d\phi}{2\; L_p} \tag{69}$$

$$= 2/\pi$$

Substituting for $\overline{\cos\phi}$ in Equation (68), the length of the fiber projected on the line Ox, is:

$$c = L/2 \tag{70}.$$

APPENDIX II

DETERMINATION OF THE AVERAGE DISTANCE BETWEEN POINTS OF CONTACT IN A FIBER SUSPENSION

Van Wyk (19) used a unique method to calculate the element length, b, for a system of randomly oriented fibers. He assumed that b was equal to the mean distance between the fibers. Realizing that some error could be introduced in using a given average value for this distance, he employed two techniques to determine the average. Both techniques yielded nearly identical results, so he concluded that the value of b resulting from his calculations was representative of the true average. Only one of his techniques will be employed here because the results are nearly the same for the two methods.

If an imaginary cylindrical surface of diameter $2d$ (d is the fiber diameter) is passed vertically through the slurry in the annulus, the length of fibers, ℓ_t, within this surface is the product of the total length, ℓ_o, of fibers in the annulus and the ratio of the area of the cylinder and the annulus area, A, i.e.,

$$\ell_t = \frac{\pi d^2}{A} \ell_o \qquad (71).$$

A spherical particle of diameter d dropped vertically along the axis of the tube would strike all the fibers extending through the imaginary surface. The number of times such a particle encountered a fiber would be equal to the number of particles in the tube. This number may be obtained by dividing the total length of fiber in the tube by the mean length of the interesected fiber. A method equivalent to determining the total and average length would be to calculate an average length of fiber passing through the tube horizontally and divide this value by the average length of a chord of a circle of diameter $2d$. The projected length of the fibers in the tube on a horizontal plane is equal to the product of the total length of fibers and an average cosine of the angle between the fibers and the horizontal. The average cosine of the angle is $\pi/4$ (see Appendix I), so the average projected length, ℓ_p, would be:

$$\ell_p = \frac{\pi^2 d^2 \ell_o}{4A} \tag{72}$$

The length of a chord at a distance x from the center of a circle of diameter $2d$ is $2\sqrt{d^2 - x^2}$. The relative frequency of occurrence of a given chord is given by the ratio of the area enclosed by two parallel chords at a distance x and $x - dx$ from the circle center and the circle area:

$$\text{frequency} = \frac{2\sqrt{d^2 - x^2}\,dx}{\pi\, d^2} \tag{73}.$$

The total length of the chords equals the sum of products of the frequencies and lengths or

$$\text{total length of chords} = \frac{\Sigma 4(d^2 - x^2)dx}{\pi\, d^2} \tag{74}.$$

The mean length of all possible chords in the circle is the ratio of the total length and the frequency of the chords, i.e.,

$$\text{mean chord length} = \frac{\int_{-d}^{+d} 4(d^2 - x^2)dx}{\int_{-d}^{+d} 2\sqrt{d^2 - x^2}\,dx} = \frac{16d}{3\pi} \tag{75}.$$

Dividing the total projected length [Equation (74)] by the average length [Equation (75)] of a chord in the $2d$-diameter circle, an equation for the number of fiber segments or number of contacts results:

$$\text{no. of segments} = \frac{3\pi^3 d\ell_o}{64A} \tag{76}.$$

If the height of the slurry in the annulus is h, then the sphere dropping along the axis of the imaginary cylinder would travel an average distance,

$$b = 0.69\,\frac{V}{d\ell_o} \qquad (77)$$

between contacts with the fibers, where V is the total volume of slurry. The total length of fibers in the suspension may be expressed in terms of the volume fraction, C, of fibers in the following manner:

$$\ell_o = \frac{4CV}{\pi d^2} \qquad (78).$$

Substituting for ℓ_o in Equation (77) yields:

$$b = \frac{0.54\,d}{C} \qquad (79).$$

APPENDIX III

VISCOSITY BEHAVIOR OF AQUEOUS SOLUTIONS

It was difficult to obtain reproducible viscosity values with aqueous solutions (ca. 1.14 sp. gr.) of either sucrose or glycerin. The data for the apparent viscosities of these solutions in terms of the applied torque and the bob angular velocity are reported in Table IX. The lowest viscosities were observed just after the solutions were placed in the apparatus. Upon allowing the solutions to remain in the apparatus for a given length of time, the viscosities increased. The viscosities could be caused to decrease by vigorously stirring the solutions. Care was taken to allow any eddy currents to subside prior to the determinations.

TABLE IX

VISCOSITY DATA FOR AQUEOUS SOLUTIONS

Solution	Condition	Apparent Viscosity, torque/ang. vel., dyne-cm./sec.
Sucrose	After addition to viscometer	71
	After two hours in viscometer	85
	After stirring	78
Glycerol	After addition to viscometer	162
	After two hours in viscometer	193
	After twelve hours in viscometer	224
	After stirring	181 181 183

It cannot be stated positively that the unusual behavior was due entirely to the fact that the solutions were sheared at low shear rates (< 0.88 sec.$^{-1}$) in the large annulus apparatus (bob diameter = 2.0 in.; cup diameter = 3.75 in.).

However, certain qualitative observations do support the possibility. It was initially believed that the effect was due to an interaction between the solution and a lucite bob, i.e., absorption of the material on the bob surface. However, the effect was still present when a copper bob was used. The specific gravity of the solutions were measured frequently and no changes were observed. The sucrose solution contained 50 p.p.m. of phenyl mercuric acetate, so it was doubtful if any changes in the solution viscosity behavior were a result of biological activity. Finally, organic solutions such as a tetrachloroethane-mineral oil solution (sp. gr. 1.14) showed no change in viscosity under the same conditions.

Viscosity data obtained in an Ostwald viscometer (no. 100) showed no such anomalous behavior. The viscosities could be reproduced to within 1%. This presents some conflict with the concentric cylinder apparatus observations, because the shear rate range in this viscometer was also below 1.0 $sec.^{-1}$. However, the method of placing the solution in the viscometer resulted in agitation of the fluid. As shown previously (Table IX), stirring of the glycerol solution in the concentric cylinder apparatus also enabled reproducible results to be obtained.

The results of this study indicate the possibility of anomalous flow behavior in aqueous solutions of glycerin and sucrose at low shear rates. Enough data were taken to show certain anomalies, but not enough were taken to clarify their exact nature. For this reason the study should be extended with particular emphasis on apparatus and concentration effects.

APPENDIX IV

EXPERIMENTAL DATA

TABLE X

PRESSURE NECESSARY TO SUSPEND A GIVEN WEIGHT FROM THE AIR BEARING (See Fig. 18)

Supported Weight, g.	Air Pressure, cm. tetra-bromoethane	Supported Weight, g.	Air Pressure, cm. tetra-bromoethane
75.6	6.80	451.7	33.65
115.5	9.85	476.9	35.00
146.1	11.90	485.3	35.60
195.8	15.35	495.4	36.65
241.6	18.60	511.9	37.80
272.2	20.40	530.0	39.00
352.1	26.40	546.3	40.15
378.0	28.50	563.0	41.30
395.6	30.10	570.0	41.75
440.0	32.80		

TABLE XI

CALIBRATION DATA FOR EDDY CURRENT DRIVE (See Fig. 19)

Rotor Speed, 900 r.p.m.		Rotor Speed, 2100 r.p.m.	
Current, amp.	Torque, dyne-cm.	Current, amp.	Torque, dyne-cm.
	Static Technique		
.360	2.87	.240	2.87
.460	4.94	.310	4.94
.590	7.80	.405	9.87
.650	9.87	.465	12.74
.730	12.74	.530	20.54
.845	17.67	.610	23.88
.915	20.54	.665	26.74
.965	23.88	.695	31.54
1.020	26.74	.765	39.35
1.110	31.54	.815	44.28
1.160	34.41	.845	47.62
1.235	39.35	.885	52.55
1.325	44.28	.925	57.50
1.355	47.62	.995	65.35
1.405	50.48	1.040	75.15
1.430	52.55	1.110	84.40
1.490	57.50	1.190	96.90
1.625	65.35	1.250	106.80
1.690	75.15	1.275	112.90
1.780	84.40	1.390	133.80
1.925	96.90	1.535	165.00
		1.675	200.00
		1.795	231.50
	Dynamic Technique		
0.40	3.43	0.40	9.66
0.50	5.66	0.50	15.80
0.60	8.45	0.60	23.38
0.70	11.93	0.70	31.9
0.80	15.80	0.80	42.5
0.91	20.50	0.90	54.6
1.00	25.30	1.00	62.8
1.105	30.9	1.11	83.2
1.225	37.9	1.22	100.1
1.325	44.5	1.30	114.7
1.40	49.8	1.41	133.5
1.52	58.3	1.50	turbulence
1.625	66.4	1.60	turbulence
1.685	72.3	1.72	turbulence

TABLE XII

DATA FOR DISTILLED WATER IN THE SMALL ANNULUS VISCOMETER
(See Fig. 20)

Torque, dyne-cm.	Bob Angular Velocity, radians/sec.	Torque, dyne-cm.	Bob Angular Velocity, radians/sec.
Run 1		Run 3	
0.609	0.0084	0.70	0.0097
1.56	0.0215	1.62	0.0229
2.84	0.0390	3.00	0.0412
4.66	0.0640	4.67	0.0642
6.80	0.0934	6.85	0.0941
9.51	0.131	9.55	0.131
12.60	0.173	12.66	0.174
16.35	0.225	16.25	0.223
19.92	0.274	19.63	0.270
Run 2		Run 4	
1.09	0.0152	2.98	0.0397
2.15	0.0295	3.62	0.0497
3.74	0.0514	5.58	0.0766
5.75	0.0789	7.95	0.109
8.07	0.111	10.75	0.148
11.15	0.153	14.11	0.194
14.50	0.199	17.53	0.241
18.18	0.250	19.71	0.271

Torque, dyne-cm.	Bob Angular Velocity radians/sec.
Run 5	
4.41	0.0605
6.50	0.0906
9.35	0.128
12.33	0.169
15.40	0.212
18.70	0.257

TABLE XIII

DATA FOR SUCROSE SOLUTIONS IN THE SMALL ANNULUS VISCOMETER
(See Fig. 21)

Torque, dyne-cm.	Bob Angular Velocity, radians/sec.	Torque, dyne-cm.	Bob Angular Velocity, radians/sec.
	Low Concentration		
Run 1		Run 2	
6.88	0.0237	3.60	0.0116
9.47	0.0319	5.71	0.0184
12.60	0.0414	8.14	0.0264
16.00	0.0528	11.00	0.0359
19.24	0.0652	14.13	0.0460
		17.94	0.0589
		19.32	0.0641
	High Concentration		
Run 1		Run 2	
2.83	0.00597	3.77	0.00847
4.63	0.0113	5.66	0.0136
6.91	0.0176	8.24	0.0208
9.62	0.0253	11.09	0.0287
12.83	0.0340	14.48	0.0382
16.50	0.0439	18.10	0.0488
Run 3			
4.50	0.0111		
6.85	0.0188		
9.56	0.0245		
12.68	0.0333		
16.27	0.0431		

TABLE XIV

DATA FOR LOW-VISCOSITY LIQUIDS IN LARGE ANNULUS VISCOMETER
(See Fig. 22)

Distilled Water

Torque, dyne-cm.	Bob Angular Velocity, radians/sec.	Torque, dyne-cm.	Bob Angular Velocity, radians/sec.
Run 1		Run 3	
0.93	0.0359	0.72	0.0200
1.09	0.0461	0.84	0.0296
1.18	0.0512	1.02	0.0436
1.24	0.0560	1.26	0.0589
1.32	0.0619	1.54	0.0744
1.84	0.0913	1.87	0.0973
		2.72	0.142
Run 2		3.22	0.156
		3.73	0.169
0.85	0.0271	4.26	0.186
0.99	0.0387	4.78	0.203
1.11	0.0470	5.35	0.222
1.25	0.0574	6.04	0.243
1.38	0.0673	6.97	0.266
1.54	0.0757		
1.75	0.0871	Run 4	
1.98	0.101		
2.24	0.114	0.97	0.0399
2.54	0.133	1.35	0.0653
2.83	0.139	1.86	0.0960
		3.04	0.146
		3.36	0.158
		4.26	0.184
		5.25	0.216

TABLE XIV (Continued)

Tetrachloroethane

Torque, dyne-cm.	Bob Angular Velocity, radians/sec.
Run 1	
0.91	0.0322
1.10	0.0408
1.25	0.0461
1.47	0.0541
1.77	0.0658
2.12	0.0776
2.52	0.0912
3.00	0.108
3.53	0.125
4.22	0.147
4.81	0.167
5.57	0.182
6.32	0.196
7.43	0.213
8.88	0.238
10.33	0.267
11.91	0.294
13.51	0.319
Run 2	
0.96	0.0340
1.34	0.0503
1.86	0.0715
2.43	0.0924
3.32	0.123
4.26	0.154
5.14	0.181
6.23	0.196

Torque, dyne-cm.	Bob Angular Velocity, radians/sec.
Run 3	
0.96	0.0306
1.90	0.0683
3.25	0.116
5.18	0.173
6.33	0.197
Run 4	
0.98	0.0333
1.66	0.0610
2.12	0.0733
2.42	0.0883
2.88	0.102
3.32	0.118
3.88	0.136
4.41	0.151
5.14	0.170

TABLE XIV (Continued)

Tetrachloroethane, Tetrabromoethane, and Mineral Oil Solution
(ca. 2.60 sp. gr.) (See Fig. 23)

Torque, dyne-cm.	Bob Angular Velocity, radians/sec.	Torque, dyne-cm.	Bob Angular Velocity, radians/sec.
Run 1		Run 2	
1.85	0.0201	3.29	0.0307
5.16	0.0527	7.51	0.0722
10.42	0.104	13.88	0.136
16.90	0.170	21.77	0.212
25.73	0.259	31.03	0.304
35.93	0.361	42.25	0.409
47.54	0.459	53.59	0.485
61.96	0.523	67.89	0.555
74.49	0.598	81.57	0.636

TABLE XV

DATA FOR HIGH-VISCOSITY LIQUIDS IN LARGE ANNULUS VISCOMETER
(See Fig. 24)

Sucrose

Torque, dyne-cm.	Bob Angular Velocity, radians/sec.	Torque, dyne-cm.	Bob Angular Velocity, radians/sec.
Run 1		Run 2	
5.10	0.0614	4.04	0.0499
6.11	0.0748	5.16	0.0644
7.51	0.0932	7.48	0.0960
8.72	0.109	10.16	0.135
10.36	0.133	13.54	0.182
11.63	0.152		
13.37	0.175	Run 3	
15.10	0.199		
16.82	0.223	5.16	0.0619
18.88	0.252	7.48	0.0935
21.07	0.280	10.31	0.133
		13.34	0.175
		16.74	0.222
		20.90	0.279

TABLE XV (Continued)

Tetrachloroethane-Mineral Oil Solution
(ca. 1.14 sp. gr.) (See Fig. 25)

Torque, dyne-cm.	Bob Angular Velocity, radians/sec.	Torque, dyne-cm.	Bob Angular Velocity, radians/sec.
Run 1		Run 3	
2.99	0.0366	1.74	0.0213
3.73	0.0459	2.46	0.0304
4.72	0.0579	3.54	0.0438
5.71	0.0704	4.34	0.0546
6.81	0.0849	4.83	0.0609
8.14	0.102	6.07	0.0757
9.64	0.121	7.77	0.0984
10.88	0.137	9.15	0.115
12.46	0.157	11.49	0.146
16.29	0.205	14.19	0.181
19.67	0.249	17.77	0.225
Run 2			
1.93	0.0236		
2.60	0.0318		
3.23	0.0399		
4.09	0.0508		
5.19	0.0645		
6.35	0.0795		
7.34	0.0924		
8.62	0.109		
10.47	0.132		
11.84	0.150		
13.47	0.169		
14.92	0.188		
16.55	0.208		
18.97	0.242		

TABLE XVI

TORQUE-ANGULAR VELOCITY DATA FOR FIBER SUSPENSIONS
(See Fig. 30)

Sample 260-1-17-Z-300: Fiber Length 1.00 mm.; Fiber Diameter 44.85 μ.

Torque, dyne-cm.	Bob Angular Velocity, radians/sec.	Torque, dyne-cm.	Bob Angular Velocity, radians/sec.
Consistency 2.052%		Consistency 0.8827%	
7.38	0.057	7.51	0.069
13.53	0.103	13.37	0.120
21.54	0.162	21.09	0.188
30.52	0.234	30.52	0.276
40.20	0.310	41.48	0.370
55.51	0.427	53.81	0.478
68.11	0.531	69.34	0.625
73.20	0.574	81.71	0.731
Consistency 1.265%		Consistency 0%	
7.40	0.062	7.51	0.074
13.34	0.112	10.22	0.099
21.17	0.178	13.34	0.130
30.48	0.260	16.77	0.163
41.48	0.352	21.08	0.202
54.17	0.459	25.46	0.244
67.82	0.578	30.24	0.292
81.19	0.700	35.80	0.346
		41.52	0.399
		47.26	0.456
		53.93	0.520
		60.51	0.585
		67.82	0.654
		74.47	0.727
		81.52	0.794

TABLE XVII

REPRESENTATIVE REPRODUCIBILITY DATA FOR TORQUE-ANGULAR VELOCITY RELATIONSHIP OF FIBER SLURRIES
(See Fig. 31)

Sample 260-1-17-Z-300: Fiber Length 2.53 mm.; Fiber Diameter 44.85 μ

Torque, dyne-cm.	Bob Angular Velocity, radians/sec.	Torque, dyne-cm.	Bob Angular Velocity, radians/sec.
Consistency 0.985%		Consistency 0.654%	
Run 1		Run 1	
7.51	0.055	5.18	0.045
13.47	0.106	7.32	0.066
21.08	0.172	13.31	0.120
29.84	0.251	21.09	0.191
42.32	0.353	30.29	0.282
53.93	0.452	41.75	0.384
66.90	0.568	53.93	0.491
73.20	0.616	67.97	0.616
Run 2		Run 2	
5.18	0.039	5.29	0.045
10.34	0.085	10.04	0.089
16.85	0.142	16.59	0.150
25.21	0.214	25.46	0.229
35.75	0.305	35.75	0.323
41.48	0.361	47.02	0.426
47.36	0.408	60.12	0.541
59.87	0.513	72.32	0.653
72.60	0.620		
Run 3			
11.37	0.098		
28.24	0.238		
50.00	0.426		
75.66	0.656		

TABLE XVIII

REPRESENTATIVE DATA ON THE NON-NEWTONIAN FLOW BEHAVIOR OF FIBER SLURRIES
(See Fig. 33)

Consistency 2.78%
Av. Fiber Length 1.69 mm.
Av. Fiber Diameter 44.85 μ

Torque, dyne-cm.	Bob Angular Velocity, radians/sec.	Torque, dyne-cm.	Bob Angular Velocity, radians/sec.
Run 1		Run 2	
7.67	0.020	10.64	0.031
13.49	0.047	16.89	0.062
21.13	0.093	25.96	0.109
30.88	0.152	36.48	0.171
40.69	0.215	47.78	0.239
53.99	0.296	59.68	0.321
67.68	0.391	75.94	0.436
79.15	0.478		

TABLE XIX

REPRESENTATIVE DATA FOR THE DETERMINATION OF THE RELATIONSHIP BETWEEN APPARENT VISCOSITY AND THE SUSPENSION HEIGHT
(See Fig. 36)

Fiber Sample 680: Fiber Length 1.70 mm.; Fiber Diameter 16.79 μ

Concentration, %	Bob Submersion Depth, cm.	Apparent Viscosity, T/ω_b, dyne-cm.-sec. per radian
0.838	15.28	174.44
	13.74	151.49
	11.88	129.51
	9.94	111.37
	7.82	93.28
0.460	15.28	137.57
	13.32	122.57
	10.78	97.17
	8.77	84.13
	6.41	68.90
0.086	15.28	116.64
	13.54	107.05
	11.10	88.50
	8.77	71.78
	6.69	56.37
0	15.28	102.96
	12.78	87.45
	9.88	69.08
	6.87	51.26

TABLE XX

END EFFECT DATA

Fiber Sample	Consistency, volume %	Axis Ratio	Apparent Viscosity dyne-cm.-sec.	End Effect Correction per radian
680-.4	C_1	22.0	160.0	16.0
	C_2		152.0	12.0
	C_3		140.0	7.5
	C_4		128.4	6.0
	C_5		121.0	3.7
	C_6		119.6	3.5
680-2.0	0.838	101.3	174.4	20.0
	0.460		137.6	8.4
	0.086		116.6	3.8
	0		103.0	3.0
680-2.5	0.165	162.5	125.0	5.0
	0.075		109.0	2.3
	0.035		104.0	2.0
	0		100.0	1.9
Pure solution	0	--	120.0	4.4
			85.0	1.1
			105.9	2.2

TABLE XXI

RELATIVE VISCOSITIES OF SUSPENSIONS OF FIBERS IN ORGANIC FLUIDS

Sample 680-2.5

Concentration, vol. %	Relative Viscosity
0.0186	1.006
0.0354	1.023, 1.002
0.0540	1.034, 1.039, 1.039
0.0753	1.049, 1.047
0.122	1.113, 1.107
0.165	1.186, 1.185
0.215	1.314, 1.311
0.266	1.448
0.309	1.576, 1.586
0.371	1.808, 1.808
0.427	2.108

Sample 680-1.2

Concentration, vol. %	Relative Viscosity
0.265	1.029
0.445	1.053, 1.043
0.630	1.077, 1.077
0.818	1.109, 1.106
1.114	1.159, 1.163
1.357	1.207, 1.210
1.739	1.297, 1.300
2.100	1.378, 1.365
2.541	1.473, 1.528, 1.572

Sample 680-.4

Concentration, vol. %	Relative Viscosity
0.232	1.010
0.429	1.016
0.606	1.031
0.793	1.044, 1.041
0.974	1.049, 1.048
1.160	1.057
1.358	1.065, 1.068
1.559	1.082
1.753	1.090

Sample 260-1.5

Concentration, vol. %	Relative Viscosity
0.215	1.017
0.450	1.047
0.647	1.063
0.863	1.107, 1.089
1.399	1.138
1.811	1.255, 1.225, 1.216
2.318	1.408
2.778	1.446, 1.506, 1.538

Sample 680-2.0

Concentration, vol. %	Relative Viscosity
0.041	1.007
0.0859	1.016
0.181	1.047, 1.046
0.268	1.080, 1.093
0.460	1.190
0.644	1.278
0.838	1.500
1.211	1.999
1.438	2.400
1.630	2.836

Sample 680-.6

Concentration, vol. %	Relative Viscosity
0.218	1.015
0.420	1.029
0.614	1.042
0.785	1.057
0.974	1.068
1.155	1.083, 1.082
1.335	1.096, 1.091
1.553	1.110, 1.109

Sample 260-.9

Concentration, vol. %	Relative Viscosity
0.502	1.035
0.883	1.061
1.265	1.107
1.638	1.149
2.052	1.202

Sample 260-2.42

Concentration, vol. %	Relative Viscosity
0.205	1.021
0.279	1.033, 1.033
0.383	1.057, 1.051, 1.044
0.446	1.045, 1.061
0.439	1.062, 1.065
0.509	1.073, 1.074
0.518	1.068, 1.063, 1.098, 1.065
0.654	1.091, 1.101
0.764	1.124, 1.112
0.985	1.173, 1.154, 1.149

TABLE XXI (Continued)

Concentration, vol. %	Relative Viscosity
Sample 260-4.0	
0.239	1.048
0.450	1.103
0.625	1.159, 1.150
0.796	1.230
1.045	1.327
Sample (P-1643-6)-1.5	
0.149	1.009, 1.014
0.311	1.028, 1.023
0.510	1.050, 1.040
0.725	1.051, 1.058
0.927	1.062, 1.060
O.C. 13.35	
0.177	1.017
0.322	1.035
0.458	1.057
0.587	1.076
0.736	1.106
0.880	1.112
1.024	1.129
1.175	1.141
Sample (P-1643-67-2)	
0.0287	1.009
0.0614	1.027, 1.039, 1.023
0.0963	1.049
0.1287	1.086
0.224	1.143
0.305	1.226
0.394	1.309, 1.349
0.494	1.395

Concentration, vol. %	Relative Viscosity
Sample 260-6.0	
0.060	1.013
0.129	1.039
0.205	1.069
0.281	1.111, 1.097
0.339	1.153, 1.137
0.402	1.189, 1.186, 1.179
Sample (P-1643-6)-2.5	
0.163	1.014
0.380	1.024
0.688	1.050
0.968	1.094, 1.094
Sample 11925-2.5	
0.0713	1.331
0.0469	1.212, 1.212
0.0247	1.062
Sample 11925-2.0	
0.0162	1.028
0.0334	1.051
0.0697	1.131, 1.132
0.1099	1.278, 1.272
0.1519	1.428, 1.390
Sample (P-1643-67-3)	
0.196	1.029, 1.028
0.393	1.049, 1.045
0.605	1.065, 1.058
0.797	1.089, 1.087
1.000	1.134, 1.130

TABLE XXII

RELATIVE VISCOSITIES OF A SUSPENSION OF FIBERS IN A SUCROSE SOLUTION
Sample 260-2.42

Concentration, volume %	Relative Viscosity
0.0866	1.035, 1.025, 1.028
0.139	1.160, 1.165
0.171	1.178, 1.200
0.216	1.342
0.258	1.516
0.344	1.555
0.517	1.695
0.606	1.856, 1.880

TABLE XXIII[a]

SHEAR STRESS-STRAIN DATA FOR A NYLON FIBER SLURRY
(See Fig. 47)

Fiber Suspension Concentration = 0.534%
Average Fiber Length = 2.42 mm.; Fiber Diameter = 44.85 μ

	Torque	Deflection	Torque	Deflection	Torque	Deflection
	Run 1		Run 2		Run 3	
Strain						
	1.30	0.0612	0.45	0.0612	1.30	0.0336
	2.05	0.134	0.75	0.071	1.75	0.1065
	2.48	0.227	1.00	0.081	2.25	0.165
	2.90	0.31	2.05	0.163	2.60	0.292
	3.40	0.434	2.48	0.21	3.10	0.454
	3.90	0.589	2.70	0.268	3.65	0.560
			3.00	0.304		
			3.40	0.41		
			3.90	0.58		
			4.40	0.87		
			4.65	Yield		
Recovery						
	3.40	0.508			3.30	0.485
	2.90	0.434			0	0.1065
	2.40	0.361				
	2.05	0.276				
	1.5	0.217				
	0	0.128				

[a] The units of torque in this table are dyne-cm., while the units of deflection are radians.

TABLE XXIII (Continued)

(See Fig. 48)

Fiber Suspension Concentration = 0.766%
Average Fiber Length = 2.42 mm.; Fiber Diameter = 44.85 μ

Strain

Torque	Deflection	Torque	Deflection	Torque	Deflection
Run 1		Run 2		Run 3	
0.8	0.00079	1.30	0.118	1.31	0.0077
1.3	0.00138	2.43	0.0207	2.42	0.0104
1.75	0.00197	3.65	0.0231	3.65	0.0157
2.25	0.00295	4.85	0.0256	4.85	0.0186
2.60	0.00394	8.35	0.0280	6.35	0.0204
3.10	0.00493	11.50	0.0298	8.35	0.0248
3.65	0.00590	15.80	0.0313	11.50	0.0260
4.20	0.00689	20.50	0.0382		
3.10	0.0102	27.1	0.0857		
3.60	0.0207				
6.35	0.0297				
7.05	0.0364				
7.90	0.0410				
8.80	0.0463				
10.02	0.0489				
14.95	0.0555				
19.00	0.0709				
22.00	0.135				

TABLE XXIII (Continued)

(See Fig. 50)

Fiber Suspension Concentration = 0.222%
Average Fiber Length = 10.8 mm.; Fiber Diameter = 44.8 μ

Strain

Torque	Deflection	Torque	Deflection	Torque	Deflection
Run 1		Run 2		Run 3	
2.5	0.00019	8.35	0.0019	8.35	0.00019
4.95	0.00039	25.30	0.00039	25.30	0.00019
8.3	0.00049	34.50	0.00078	34.50	0.00039
15.8	0.00078	44.50	0.00097	44.53	0.00058
25.3	0.00145	59.00	0.00126	59.00	0.00087
29.8	0.00174	69.00	0.00165	69.00	0.00106
34.4	0.00204	88.60	0.00204	88.62	0.00155
39.1	0.00262				
44.5	0.0032				
51.5	0.0043				
58.9	0.0057				
63.8	0.0069				
69.0	0.0104				

Recovery

Torque	Deflection	Torque	Deflection	Torque	Deflection
22.0	0.0065	41.2	0.00184	48.6	0.00116
15.8	0.0061	33.8	0.00155	27.5	0.00087
11.5	0.0058	25.7	0.00135	11.5	0.00058
8.3	0.0055	15.3	0.00106	4.65	0.00049
0	0.0038	3.9	0.00078	0	0.00019
		0	0.00019		

TABLE XXIII (Continued)

(See Fig. 53)

Fiber Type = Spruce
Fiber Suspension Concentration = ca. 0.15%
Average Fiber Length = 3.3 mm.; Fiber Diameter = 30-35 μ

Torque, dyne-cm.	Deflection, rad.	Recovery, rad.
1.00	0.00019	0.00716
9.5	0.00029	
15.0	0.00058	
23.0	0.00097	0.0097
32.0	0.00145	0.0106
43.0	0.0021	0.0116
51.0	0.0031	0.0124
67.0	0.0043	0.0132
82.0	0.0064	0.0139
98.0	0.00815	0.0145
116.0	0.0110	0.0151
135.0	0.0137	0.0158
153.0	0.0161	0.0158

TABLE XXIV

DATA FOR CHANGE IN STRAIN ACROSS THE ANNULUS
FOR AN INCREASE IN STRESS
(See Fig. 51)

Fiber Suspension Consistency = 0.534%
Fiber Length = 2.42 mm.; Fiber Diameter = 44.85 μ

Torque Change 2.05 to 2.48 dyne-cm.

Radius in Annulus, in.	Change in Strain, rad.
1.00	0.092
1.30	0.042
1.61	0.017
1.69	0.0115
1.94	0.0056

Torque Change 3.40 to 3.90 dyne-cm.

Radius in Annulus, in.	Change in Strain, rad.
1.00	0.153
1.40	0.144
1.49	0.061
1.72	0.014